Performance Investigation of Large-Scale Solar Water Heating System Using Solar Tower Technology: A Case of Bishoftu General Hospital

Mikias Demissie Borena

A Thesis Submitted to the Department of Mechanical Engineering,

School of Mechanical, Chemical, and Materials Engineering

Presented in Partial Fulfillment of the Requirement for the Degree of

Master of Science in Thermal Engineering

Office of Graduate Studies

Adama Science and Technology University

February, 2025

Adama, Ethiopia

Performance Investigation of Large-Scale Solar Water Heating System Using Solar Tower Technology: A Case of Bishoftu General Hospital

Mikias Demissie Borena

Advisor Dr. Addisu Bekele (Associate Professor)

A Thesis Submitted to the Department of Mechanical Engineering,

School of Mechanical, Chemical and Materials Engineering

Presented in Partial Fulfillment of the Requirement for the Degree of

Master of Science in Thermal Engineering

Office of Graduate Studies

Adama Science and Technology University

February, 2025

Adama, Ethiopia

DECLARATION

I hereby declare that this Master's thesis entitled "**Performance Investigation of Large-Scale Solar Water Heating System Using Solar Tower Technology: A Case of Bishoftu General Hospital**" is my original work. That is, it has been submitted for the award of any academic degree, diploma or certificate in any other university. All sources of materials that are used for this thesis have been duly acknowledged through citations.

Mikias Demissie Borena	__________________	_________
Name of student	Signature	Date

RECOMMENDATION OF ADVISORS

I the advisor of this thesis, hereby certify that I have closely advised the student while developing this thesis and read the draft thesis entitled **“Performance Investigation of Large-Scale Solar Water Heating System Using Solar Tower Technology: A Case of Bishoftu General Hospital ’’** prepared under my guidance by Mikias Demissie. Therefore, I recommend the submission of the thesis to the department for further review and evaluation.

Dr. Addisu Bekele	_______________	____________________
Advisor	Signature	Date

APPROVAL PAGE

I, the advisor of the thesis entitled hereby *"Performance Investigation of Large-Scale Solar Water Heating System Using Solar Tower Technology: A Case of Bishoftu General Hospital"* and developed by Mikias Demissie Borena, hereby certify that the recommendation and suggestions made by the board of examiners are appropriately incorporated into the final version of the thesis.

Dr. Addisu Bekele	______________	________________
Advisor	Signature	Date

We, the undersigned members of the Board of Examiners of the thesis by Mikias Demissie Borena have read and evaluated the thesis entitled "Performance Investigation of Large-Scale Solar Water Heating System Using Solar Tower Technology: A Case of Bishoftu General Hospital" and examined the candidate during open defense. Therefore, this is to certify that the thesis is accepted for partial fulfillment of the requirement of the degree of Master of Science in Thermal Engineering.

______________________	_____________	_________________
Chairperson	Signature	Date
______________________	_____________	_________________
Internal Examiner	Signature	Date
______________________	_____________	_________________
External Examiner	Signature	Date

Final approval and acceptance of the thesis is contingent upon submission of its final copy to the Office of Postgraduate Studies (OPGS) through the Department Graduate Council (DGC) and School Graduate Committee (SGC).

______________________	_____________	_________________
Department Head	Signature	Date
______________________	_____________	_________________
School Dean	Signature	Date
______________________	_____________	____________
Office of Postgraduate Studies, Dean	Signature	Date

ACKNOWLEDGEMENT

My utmost gratitude is to God Almighty, the Creator and the Sustainer of the heavens and the earth and all that exists in between. Secondly, I take this opportunity to place on record my profound sense of recognition and deep appreciation to my advisor, Dr. Addisu Bekele for his personal encouragement, valuable suggestions, unending benevolence, stimulating discussions and able guidance right from the beginning to date as a result of which the present study reached fruition. My gratitude to him knows no bounds.

Next, I express my sincere thanks to my instructors Dr. Dawit Gudeta and Dr. Gezahegn Habtamu for their invaluable encouragement, constructive suggestions, inspiration throughout my academic life, and support from the early stage of this thesis and for providing me with extraordinary experiences through the work. Then, I would like to thank all my well-wishers, colleagues and friends for making this thesis more valuable and aids an appreciated contributions for my research work.

A special gratitude goes to my beloved parents for their encouragement, support, love and affection which keeps me going always. I would like to show my deepest gratitude to people who made my time fruitful at Adama Science and Technology University (ASTU) which I will remember and treasure for long. Last but not the least I am also grateful to ASTU for their provision in providing me all necessary support.

ABSTRACT

Located 47 kilometers southeast of Addis Ababa, Ethiopia, in the town of Bishoftu, which is part of the Oromia region, is one of the first general hospitals. It was established in 1941G. C the current overall number of available beds in healthcare facilities is 216. In a hospital, the need for hot water is typically met by fitting consumers at a temperature of 40℃ to 70℃, while the kitchen, shower, and laundry for sterilization temperatures exceeding 85℃ are frequently needed to meet hygienic standards. It is challenging to reliably supply hot water in hospitals in developing nations like Ethiopia, where we know that there is a shortage of fuel and electricity in addition to other problems. This makes it possible for us to offer sustainable energy sources. Other solar collector techniques, such as concentrated and non-concentrated collectors, have been studied in the past for the production of hot water for hospitals. However, this has not been studied on a large scale because the visibility and potential of solar tower collectors to store temperature is higher than after reducing excess temperature by using different sizes of mixing chambers for end use as required temperature. the Ethiopian Meteorology Agency provided the work data for this thesis, that is global horizontal irradiance (GHI) data, but this data is not relevant for concentrated-type solar collectors. As a result, this data was substantially transformed, and the Hellas 1 type heliostat was chosen by taking into account the reflectivity of the glass. 322 heliostats are required to provide the 616.2 m^2 of hot water required by that institution. However, this project will require 3,801.1m^2 in total the output of a numerical simulation using weather information from the Bishoftu Agricultural Research Metrology Center, which was calculated to be 22.4 m^3 daily total hot water demand and required two storage tanks of 25m^3 each. This will be done through theoretical analysis and numerical using ANSYS software. This study will be conducted using a solar tower (ST) numerically supply of hot water.

Keywords: - *Solar tower, Solar Water Heater, Hospital, large-scale SWH*

Table of Content

LIST OF TABLES

LIST OF FIGURES

LIST OF ABBREVIATION AND ACRONYMS

ACRONYMS

ST…………………………………………….... Solar Tower

BGH……………………………………...... Bishoftu General Hospital

CSP………………………………………… Concentrated Solar Tower

SWHS……………………………………… Solar Water Heating System

ICS…………………………………………... Integrated Collector Storage

PV…………………………………………… Photovoltaic

SAM………………………………………… System Advisor Model

FPC……………………………………..... Flat Plate Collector

ETC…………………………………….... Evacuated-Tube Collectors

DSWHs …………………………………...... Domestic Solar Water Heating systems

GHI.…………………………………...... Global Horizontal Irradiance

DNI…………………………………….... Direct Normal Irradiance

HS... Horizontal Surface

SEE…………………………………….... Solar to-Electric Efficiency

NPV ………………………………………… Net Present Value

LCoE ………………………………………... Levelized Costs of Electricity

EES …………………………………...... Engineering Equation Solver

LHS ……………………………………..... Latent Heat Storage

HP …………………………………….... Heat Pump

CRT.. Central Receiver Tower Design

CSP.. Concentrating Solar Power

HWD... Hot water demand

TDHWD.. Total Daily Hot Water Demand

HWDK... Hot Water Demand for Kitchen

HWDL.. Hot Water Demand for Laundry

HWDS.. Hot Water Demand for Showering

LEAP……………………………… Long-range Energy Alternatives Planning

CSTEM …………………………… Concentrated Solar Techno-Economic Model

HCE .... Heat Collecting Element

NOMENCLATURE

V_{St}..Volume of the Storage Tank

Q_S..Energy Capacity of a Storage Unit

E ....Equation of Time

L_{St}..Standard Meridian for the Local Time Zone

L_{Loc}..Longitude of the Location

N_S..Sun Shine Hours

N...Day of The Year

G_b..Direct(Beam) Solar Radiation

G_d ....Diffuse Solar Radiation

G..Global Solar Radiation

I_{Sc} ....Solar Radiation Constant

N.. Average Days for the Month

H_H..Heliostat Efficiency

η_{rec}..Receiver Efficiency

A_{rec} ....Area of the Receiver

D_{rec} ....Diameter of the Receiver

H_{rec} ....Height of the Receiver

A_T..Heliostat Area

N..Number of Heliostats

A_h...Area of Each Heliostat

$H_{T,Min}$ .... Minimum Tower Height

$H_{T,Max}$ .... Maximum Tower Height

H_T...Tower Height

$\overline{H}_O$ ....Extraterrestrial (ETR) Daily Solar Radiation on a Horizontal Surface

$\overline{N}_s$.............................Monthly Average of the Maximum Possible Daily Hours of Sunshine

$\overline{H}_D$ ....Monthly Average Daily Diffuse Radiation on HS

$\overline{I}$ ....Monthly Average Hourly Global Radiation on A HS

$\overline{I}_D$ ....Monthly Average Hourly Diffuse Radiation on A HS

Q_{ref} ....Reflected Solar Radiation Per Square Meter from the Heliostats

Q_{rec}.........................Power Received on the Surface of the Receiver from the Heliostats

Q_{In} ....Average Annual Direct Normal Irradiation Per Square Meter

$\overline{\mathrm{H}}$................................ Monthly Average Daily Radiation on Horizontal Surface

$\bar{n}_s$................................Monthly Average Daily Hours of Bright Sunshine

$\mathrm{Q}_{\mathrm{fluid}}$ ....Required Thermal Output Power by the Water/Steam Fluid

$\mathrm{C}_{\mathrm{max}}$ ....Maximum Concentration Ratio

L ....Distance Between the Tower and the First Heliostat

A_{f} ....Total Area of the Field

R ....Radial Spacing

A ....Azimuth Spacing

h ....Height

w ....Width

$\mathrm{q}_{\mathrm{avg,flux}}$ ....Allowable Average Flux of the Receiver

$d_{o,tube}$ ....Tube Outer Diameter

$\mathrm{n}_{\mathrm{tube,rec}}$ ....Total Number of Receiver Tubes

$\mathrm{n}_{\mathrm{tube,panel}}$ ....Number of Tubes Per Panel

$\mathrm{A}_{\mathrm{sec}}$ ....Cross-sectional Area of the Fluid Path

$\mathrm{m}_{\mathrm{fluid}}$ ....Mass Flow Rate of the Receiver Fluid

ρ_{fluid} ....Density of the Fluid

ν_{fluid} ....Velocity of the Fluid

$T_{s,avg}$ ....Average Temperature of the Receiver Fluid

R_{cond} ....Resistance Due to Conduction

R_{conv} ....Resistance Due to Convection

$\mathrm{r}_{\mathrm{i,tube}}$ ....Radius of the Receiver Inner Tube

$\mathrm{r}_{\mathrm{o,tube}}$ ....Radius of the Receiver Outer Tube

$\mathrm{K}_{\mathrm{tube}}$ ....Thermal conductivity of the tube

$\mathrm{K}_{\mathrm{fluid}}$ ....Thermal conductivity of the fluid

n_{tube} ....Total number of tubes in the receiver

L_{c} ....Characteristic length

Nu ....Nusselt Number

Re ....Reynolds Number

$\mathrm{h}_{\mathrm{inner}}$ ....Heat Transfer Coefficient of Internal Convection

Pr ....Pradntl Number

$\mathrm{Q}_{\mathrm{loss,conv}}$ ....Convection Heat Loss

$Q_{loss,ref}$ ....Reflected Heat Loss from the Receiver Surface

h_{mix} ....Mixed Heat Transfer coefficient

h_{nat} ....Heat Transfer Coefficient Due to Natural Convection

H_{For} ....Heat Transfer Coefficient Due to Forced Convection

Nu_{nat} ....Nusselt Number for Natural Convection

K_{rec} ....Thermal Conductivity of the Receiver

Gr ....Grashof Number

V_{air} ....Wind Speed

L ....Length of Collector

T_{amb} ....Ambient Temperature

$h_{cv,ext}$ ....Convective Heat Transfer Coefficient Between the External Surface

$h_{r,ext}$ ....Radiation Heat Transfer Coefficient Between the External Surface

Q_u .... Heat Flow Transmitted to the Fluid

Cp_f ....Specific Heat of Fluid

$Q_r(t)$ ....Heat Quantity Received by the Receiver Tube

I_d ....Direct Normal Irradiation

A_r..................................Inner Surface and the Outer Surface of the Receiver Tube

A_c ....Collector Aperture Area

Q_{ext} ....External Heat Power (By Convection and Radiation)

GREEEK SYMBOL	DESCRIPTION	UNIT
δ	Declination angle	(°)
ω	Solar Hour angle	(°)
ω_{ss}	Sunset hour angle	(°)
φ	latitude angle	(°)
β	Tilt angle	(°)
θ_z	zenith angle	(°)
ε	emittance	
Ψ	fraction	_
ϕ_r	rim angle	(°)
θ_z	zenith angle	(°)
α_t	tower altitude angle	(°)
μ	dynamic viscosity	kg/m.s
ρ	density	kg/m^3
α_{eff}	effective absorptance	-
σ	Stefan–Boltzmann constant	-
ε_{go}	emittance of the external surface of the heliostat glass	-
ε_{eff}	Emissivity of the receiver	

CHAPTER ONE

INTRODUCTION

1.1 Background of the Study

In our country a lot of hospitals used electrical power and fuel energy for heating water ,and different functions. Not least, Bishoftu General Hospital is one of the first general Hospital in Bishoftu city founded in Oromia region, 47km to southeast of Addis Ababa Ethiopia. BGH was established in 1941G.C. At that time, it was serving as a prison camp for the Italian military. It was renovated by the government of the previous Soviet Union in 1988G.C. Since then, it became a primary level (district) hospital until 2003G.C. at that time it had 42 number of beds. Then in 2003G.C, it was expanded to a zonal hospital by the Regional Health Bureau. Now the Hospital is giving health services for three towns and five districts to 2.2 million people. The current total number of Beds 216. Its catchment area is around 5,600 Square km Since July 2007G.C the hospital has implemented new reforms and led by a Hospital Manager & governing board.

Nowadays, regarded as a low-tech, well-established system with great energy production potential are solar thermal systems. Globally, solar thermal technology can be applied in both hot and cold climates for low-to-high-temperature applications. A large variety of solar-thermal components and systems, mostly for residential, hospital, hotel, commercial building, and industrial applications, are available on the market. The products are reliable and have a high technical standard in the low-temperature regime (below 100°C). Solar thermal systems in larger buildings, multi-family houses and apartment blocks as well as in district heating plants are now emerging onto the market(Liu et al., 2014).

Solar water heating systems harness solar energy to warm water by utilizing a reservoir of water inside a hot water cylinder. Frequently, a boiler or electric immersion heater is employed to further heat the stored water for immediate usage. By utilizing solar energy to "pre-heat" the stored water, it results in reduced consumption of gas, oil, or electricity, leading to cost savings and a decrease in carbon emissions. In other words, solar water heating systems utilize the sun's energy to heat water, minimizing reliance on conventional fuel sources and thereby promoting financial savings and environmental sustainability.

A low-temperature solar water heating system plays a crucial role in various settings such as hospitals, residential buildings, hotels, industries, and domestic services. It serves as a vital component for numerous applications within hospitals, including sterilization through autoclaves, the cleaning and boiling of medical equipment, laundry services, bathing facilities, and kitchen operations. By utilizing solar energy to heat water, this system effectively caters to the diverse hot water and steam water requirements of these establishments. It ensures a reliable supply of hot water for essential processes, promoting cleanliness, hygiene, and efficient operations across different departments in a hospital or other related settings etc. The minimum-temperature hot water supply system represents a process that demands significant energy input. Particularly in the context of hospitals, the production of hot water relies heavily on the consumption of electrical and fossil fuel energy. The escalating concerns related to global environmental pollution, adverse impacts on human health, rising costs, and the depletion of fossil fuel resources have amplified the present and future reliance of the world on electricity. Consequently, there is a growing global pursuit for an energy solution that is both efficient and effective, while also being environmentally friendly and sustainable. In other words, there is a pressing need to develop alternative energy sources that minimize environmental harm, promote energy efficiency, and ensure long-term sustainability, given the increasing demand for hot water and the challenges associated with conventional energy consumption. (Liu et al., 2014; Turchi et al., 2013a, 2013b).

1.2 Working Principle of Solar Tower

A single receiver is mounted atop a tower in a solar central tower system, which is encircled by thousands of mirrors (heliostats) that track the sun's apparent motion in the atmosphere and targeted the sunlight onto the receiver. These plants are most suitable for utility-scale uses between 30 and 400 MW. Similar to how it is done when other types of collectors are utilized, system design is carried out for a central receiver application.

Each of those focused mirrors tracks the sun's location on two axes as it shines down on a field of heliostats a top solar tower. Over the course of a day, the heliostats are configured to effectively focus the light towards a receiver atop the tower. Solar towers' original design heated water with the sun's concentrated beams, and the steam that resulted operated a turbine to generate electricity. The liquid salts used in more recent models include 60% sodium nitrate and 40% potassium nitrate. Since these salts can hold more heat energy than water, some of the heat energy generated during the boiling of the water used to power the turbines can be stored.

Because of the higher operating temperatures, efficiency is increased and some electricity can be produced even on overcast days. This implies that solar towers can supply dependable energy continuously when coupled with some sort of energy storage system (JARED SAMUEL & O THANGGARAJ, 2012).

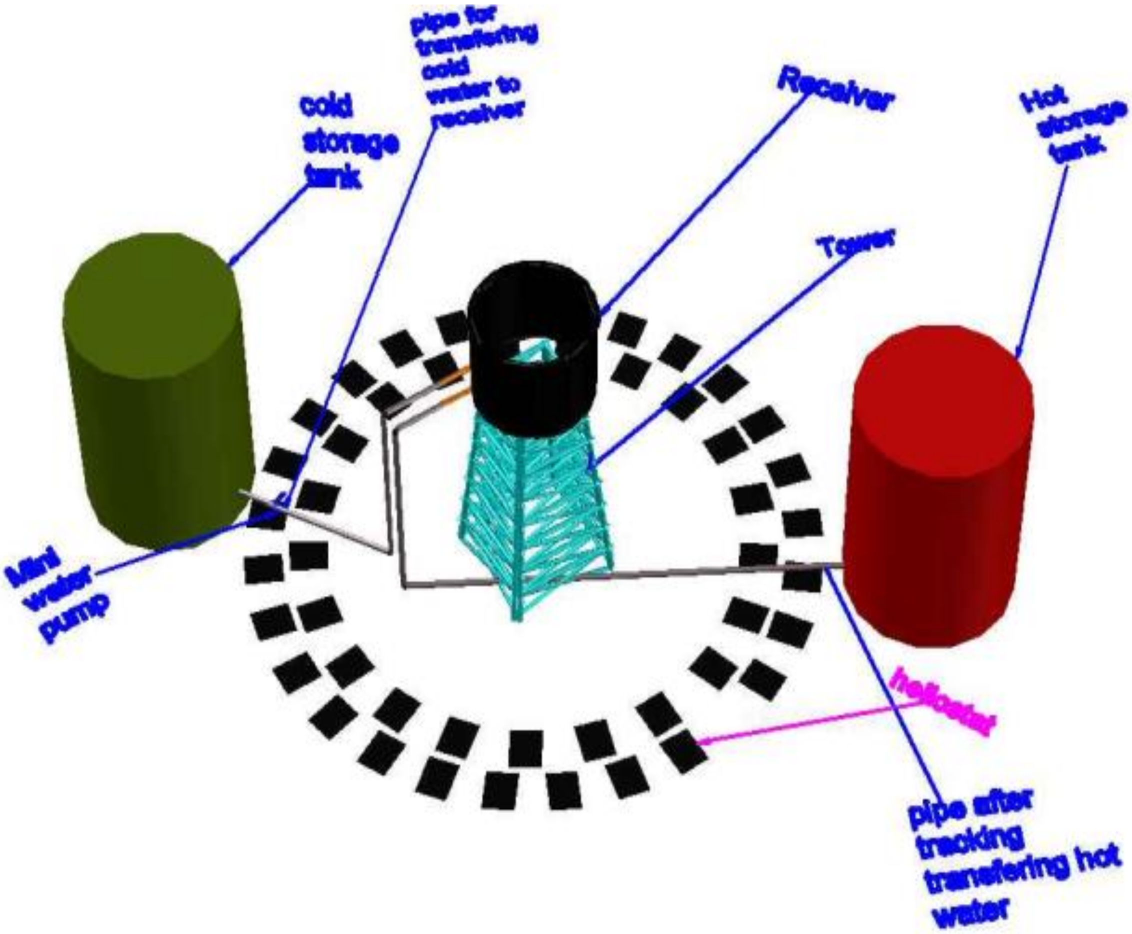

Figure 1.1 Conceptual Drawing of Solar Tower Through AUTO-CAD

1.3 Statement of the Problem

In the hospital, thermal energy applications account for more than 50–60% of energy use. They used a lot of hot water and steamed water in the hospital because, as all know, producing hot water using an electricity or fuel boiler is challenging to do so continuously due to energy shortage. Among them, Bishoftu General Hospital is one of the largest public hospitals, serving an average of 800-1000 patients each day. As a result, the country must implement alternative renewable energy sources for thermal hot water production systems. The greatest alternative is a solar heating system, which is a sustainable and environmentally acceptable source of energy in a country like Ethiopia with 13 months of sunshine. Ethiopia has a significant potential for solar energy due to its high levels of solar irradiation and average sunlight length of more than 10 hours per day all over the year-round with the potential of producing 5-6KWh/m^2/day(Hailu & Kumsa, 2021a, 2021b; Tiruye et al., 2021).

Therefore, it is important to will help design and investigate the Performance Investigation of Large-Scale Solar Water Heating System Using Solar Tower Technology.

1.4 Objectives of the Study

1.4.1 General Objectives

The primary goals of this thesis are Analytical and Numerical Performance Investigation of Large Scale Solar Heating System with Solar Tower Technology: A Case of Bishoftu General Hospital.

1.4.2 Specific Objectives

The specific objectives are, therefore:

- Estimate the solar energy potential of Bishoftu city.
- Estimate the hot water demand of Bishoftu General Hospital, the required temperature, and the corresponding temperature.
- Design a solar tower system all-inclusive size of the solar system (collector area and heliostat number.
- Analyze the performance of the solar tower system.
- Hot water temperature reduction system for end use.
- Perform a Cost-benefit analysis for the whole system.

1.5 Scope of the Study

This research will utilize the solar energy data obtained from Bishoftu General Hospital in Ethiopia as the foundation for analysis and design. The study aims to examine and develop various aspects related to solar energy utilization within the hospital context, incorporating the available data to inform decision-making processes and optimize the design of solar energy systems. The analysis of solar thermal systems encompasses a diverse array of applications, including but not limited to residential, hotel, hospital, and industrial settings. Here, "encompasses" can be replaced with envelopes, covers, or incorporates. etc. but this study focuses on The study will conduct an analysis and design of a solar thermal system intended for the low-temperature hot water supply system in the new building of Bishoftu Hospital. The research will focus on identifying the distinctive features and consequences of this investigation, and a variety of methodologies will be employed to carry out the design and analysis of the solar thermal system for the hot water supply system. The study will scrutinize the applied analysis procedures to assess their efficacy in developing and evaluating the solar thermal system design. Finally proposing optimal techniques to perform the analysis and design of the solar thermal system for hot water supply to bishoftu general hospital new building is the scope of this research.

1.6 Significance of the Study

In the BGH, the water heating system was powered by electricity or diesel boiler. In contrast to electric or boiler technology, this thesis advocates for hospitals to employ solar technology. Reduced electricity and gasoline costs, as well as a reduction in environmental pollutants, will all benefit hospitals more if they employ the study's output. Both day and night operations are possible with the solar thermal energy storage technology that is suggested for this facility. Solar energy is a cost-effective energy source that promotes physical health, minimizes reliance on electricity, and helps power the hospital's energy-hungry hot water supply system. Surely this study's findings will provide a platform for further Solar thermal accumulator system applications for a hot water production

CHAPTER TWO
LITERATURE REVIEW

2.1 Introduction

The first solar water heaters were created in California in the 1890s. Florida had more than 100,000 solar hot water systems by 1954. In the 1970s, the industry was widely popular, but by the 1980s, it had lost its shine. The demand for alternative energy sources is currently reviving the market. Modern technology is advanced and tightly controlled. Solar energy is widely used as a key source of thermal energy for hot water supply in several nations worldwide. Only 1% of the $4 billion worldwide solar thermal market is based in the United States(Homola, 2014, 2018; Tian & Zhao, 2013).

In this section, an extensive examination of the existing body of work relevant to the present research is provided. A comprehensive survey of the literature pertaining to solar-assisted water heating systems is conducted, encompassing various aspects such as the different types of solar water heaters, the optimal configuration of storage tanks, solar collectors, the impact of thermal-physical properties on system performance, and the overall dimensions and geometry of these systems. The review delves into detailed discussions on each of these topics, exploring the findings and insights derived from previous studies in the field.

2.2 Solar Collector

Solar energy collectors are special kind of heat exchangers that transform solar radiation energy to internal energy of the transport medium. The major component of any solar system is the solar collector. This is a device which absorbs the incoming solar radiation, converts it into heat, and transfers this heat to a fluid (usually air, water, or oil) flowing through the collector. The solar energy thus collected is carried from the circulating fluid either directly to the hot water or space conditioning equipment or to a thermal energy storage tank from which can be drawn for use at night and/or on cloudy days. There are two types of solar collectors: non-concentrating and concentrating collectors or stationary collectors.

2.2.1 Concentrated or Stationary Solar Collector

It is a type of collector, which has concave reflecting surfaces to intercept and focus the sunbeam radiation to a small receiving area. In this system working fluid can receive high temperature, and high thermal efficiency, reflecting surfaces require less material and are structurally simple. Also, the tracking system is required to get high thermal efficiency using either one tracking system or two tracking systems.

2.2.2 Non-Concentrated Solar Collector

These collectors are permanently fixed in position or the same area is used for both interception and absorption of incident radiation.

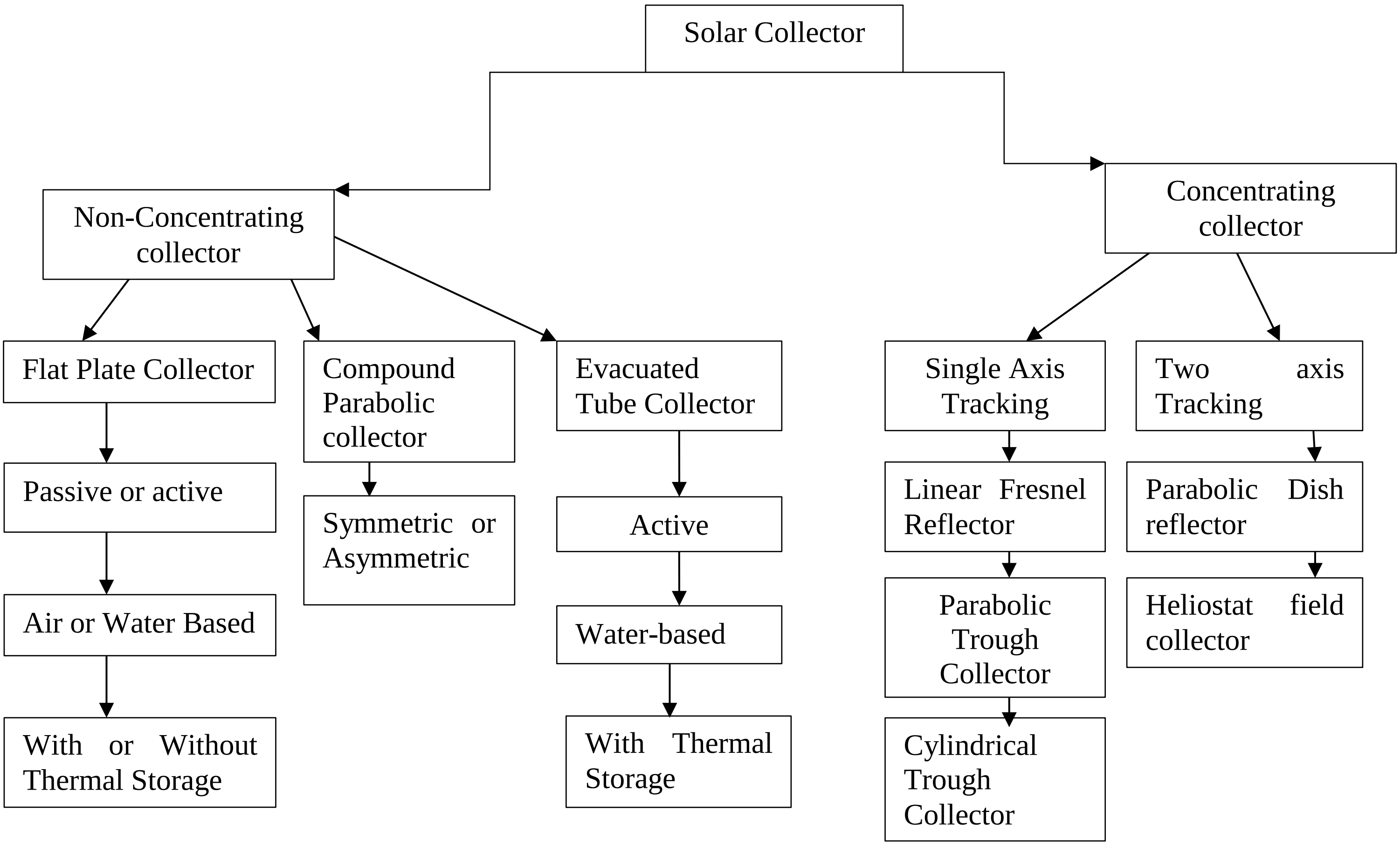

Figure 2.1 Classification of Solar Collector

2.2.3 Concentrated Solar Tower

Concentrated solar power systems generate solar power by using mirrors or lenses to focus a large area of sunlight onto a small area. In CSP with a tower, a central receiver system uses sun-tracking mirrors (known as heliostats) to concentrate the sun's energy onto a receiver at the top of a tower. The receiver heats a fluid that drives a steam turbine connected to an electrical power generator.

The operation of solar energy systems is necessarily transient. Over the lifetime of a concentrating solar power plant, the system operates at design conditions only occasionally, with the bulk of operation occurring under part-load conditions depending on solar resource availability. Credible economic analyses of solar-electric systems require versatile models capable of predicting system performance at both design and off-design conditions. The design process for solar power tower systems differs from that for other concentrating solar power (CSP) technologies such as the parabolic trough or parabolic dish systems that are nearly modular in their design. The design of an optimum power tower system requires a determination of the heliostat field layout and receiver geometry that results in the greatest long-term energy collection per unit cost(Wagner et al., 2009).

2.3 Solar Water Heating System

One of the most economical ways to heat water in homes, businesses, and healthcare facilities is through solar water heating, which is a respectable technology that uses solar radiation. It is also being used in the paper, textile, and food processing industries for dairy and edible oil. The household solar water heating system is particularly promising due to the abundance of solar energy. The demand for renewable energy sources has led to a reemerging market for this technology, which transforms sun energy converted to heat and can take the place of any type of traditional heating method or fuel (Homola, 2014). Domestic hot water supply at temperatures between 50^0C and 60^0C is regarded as appropriate.

2.4 Types of Solar Water Heating Systems (SWHS)

There are two types of solar water heating systems; active and passive solar heating systems. The active system consists of the open loop system and closed loop system; whereas the passive system contains a thermosiphon and integrated collector storage (ICS) (Jamar et al., 2016).

2.4.1 Passive Systems

In passive systems, a thermosiphon is used to move hot water from the collector to a storage tank situated above the collector, or the collector itself stores the heat. Pumps are not used in passive systems to move water or collect fluid. Because of this, they are typically more dependable, simpler to operate, and possibly more durable than active systems. Passive systems come in two varieties: integral collector storage systems and thermosiphon systems.(Dimitrios, 2001; Panapakidis, 2009).

a. Batch Systems Using Integral Collector Storage (ICS)

The storage tank functions as the solar collector in batch or integrated collector storage systems, which heat water directly from the sun. Almost always, batch water heaters are passive systems that use the home's water pressure to transfer hot water from a solar-heated tank to a backup tank or the point of usage. To circulate water in the collector, most designs use the local main water pressure. Additionally, water may flow because of buoyancy forces created by the collector's differential heating, with flow direction controlled by valves. The bottom of the container receives replacement water as the warmest water is extracted from the top. Compared to thermosyphon systems, these systems are often less expensive. (Dimitrios, 2001; Panapakidis, 2009).

b. Thermosyphon

Systems as the sun shines on the collector, the water inside the collector flow-tubes is heated. As it heats up, this water expands slightly and becomes lighter than the cold water in the solar storage tank mounted above the collector. Gravity then pulls heavier (cold water) down from the tank and into the collector inlet. The cold water pushes the heated water through the collector outlet and into the top of the tank, thus heating the water in the tank. a thermosiphon system requires neither pump nor controller(Dimitrios, 2001; Panapakidis, 2009).

Figure 2. 2 Thermosyphon SWH system (Dimitrios, 2001; Panapakidis, 2009)

2.4.2 Active Systems

Pumps, valves, and controllers are used in active systems to move fluids that transfer heat, such as water, through the collectors. Although they are more costly than passive systems, they are typically more effective. Since storage tanks for active systems do not need to be positioned above or close to the collectors, they are typically easier to retrofit than passive systems. However, in the event of a power loss, they will not operate as they rely on energy for pumping.(Dimitrios, 2001; Gong & Sumathy, 2016; Panapakidis, 2009).

A. Direct Active Systems (Open Loop)

In that they are direct systems that use a solar collector apart from the storage tank, direct (open loop) active systems resemble thermosyphon systems. The way direct active systems differ is that water is circulated from the storage tank to the collector and back again using an electric pump. The most often used method in tropical and sub-tropical regions, where it rarely gets below 0°C, is the Direct method.(Gong & Sumathy, 2016).

Recirculation: Systems These are a particular kind of freeze-protective open-loop system. When the temperature gets close to freezing, they circulate warm water from storage tanks via collectors and exposed pipework using the system pump.(Gong & Sumathy, 2016).

Photovoltaic Operated Systems: The energy source for the pump in this system is supplied by a photovoltaic (PV) panel, which is the primary difference between it and a recirculation system. (Gong & Sumathy, 2016).

B. Closed-loop, indirect active systems (such as glycol antifreeze systems)

The purpose of indirect systems, or active systems with sealed loops, is to be used in areas where freezing weather may happen on a regular basis. These arrangements, sometimes referred to as closed-loop systems, the majority of frequently employed in frigid locations everywhere it frequently gets below zero degrees. The thermal energy in sunshine is captured using a solar collector that is loaded with anti-freeze fluid (heat-transfer fluids). Typically, a combination of water and propylene glycol or ethylene glycol is employed. Systems for a heat exchanger is a part of glycol antifreeze's indirect, active systems. (Gong & Sumathy, 2016).

Drain Back System: In cold locations systems with drain back are employed to dependable guarantee the gatherers and the pipework never go cold. When the system stands not producing heat, the fluid within the gatherers and pipework is all emptied once more into a tank of insulated reservoir. The collector's solution flows into the storage tank when the pump stops, and the reservoir tank has an indicator that lets you know when the collector is full.(Dimitrios, 2001; Gong & Sumathy, 2016; Panapakidis, 2009).

2.5 Reviews Related on Large Scale Water Heating

Endale (2019) Used the System Advisor Model (SAM) and Long-range Energy Alternatives Planning System (LEAP) for analysis. In 2025, it will be predicted that 5.474 million m^2 of flat plate collector (FPC) areas will be able to save 1,480 GWH of electricity, 1,698,116 tonnes of firewood, and 47,730 tonnes of kerosene. The amount that can be saved is equal to 5% of the industry's demand for diesel, 50% of the demand for kerosene from urban families, and 50% of the demand for power and firewood from urban households, commercial sectors, and the industrial sector. This energy is equivalent to installed power generation capacities of 691 MW wind, 429 MW hydropower, or 1,045 MW grid-connected PV.

Hazami et al. (2013) Studied the energetic and financial potential of employing Domestic Solar Water Heating systems (DSWHs) instead of electric, gas, or town gas water heaters is the major objective of the current effort. The two most common DSWHs in recent years were assessed in this scenario for performance and life cycle perspectives DSWHs with evacuated-tube solar collectors (ETC) and flat-plate solar collectors (FPC), TRNSYS simulation was used to achieve the dynamic behavior of DSWHs in accordance with Tunisian weather data. According to the findings, the FPC and ETC produce roughly 8118kWh and 12032kWh of thermal energy annually. results showed that the annual savings in electrical energy relative to the FPC and ETC are about 1316- and 1459-kW h/year.

Arekete (2013) The design, construction, and testing of a solar water heater took place at Akure, South West, Nigeria (Latitude 7.30^0N and Longitude 5.25^0E) A flat plate collector covered with double glazing layers at 20^0 angle of tilt to the horizontal was employed. Six days' number of readings were taken. A maximum hot water temperature of 73^0C was measured during the experiment at an ambient temperature of 36^0C.

Bekele et al. (2013) Large-scale water heating systems at many possible locations around the nation that could be powered by solar energy are investigated. Numerical formulae are used to anticipate global and diffuse radiations over the collector surfaces for each of the chosen sites. The total number of collectors required to heat the daily hot water up to 50◦C is, 261 for Addis Ababa tannery, 149 for Dire tannery, 1667 for Ethiopian tannery and 795 for Jimma hospital. The solar contribution to the annual heating load obtained for Addis Ababa tannery (80.9%), Dire tannery (76.2%), Ethiopia tannery (81.6%) and Jimma hospital (81.8%) After further economic study, they came to the conclusion that solar energy can be employed in Ethiopia as a substitute energy source for large-scale water heating systems.

Ben Taher et al. (2021) Model was created with the intention of examining and comparing the energy effectiveness of flat-plated collectors and evacuate collectors in the African continent. each had a 300-L hot water tank.43 countries were included in the study, which was separated into 5 regions: North Africa, West Africa, Central Africa, East Africa, and Southern Africa. According to the energy study, the solar-derived domestic hot water output varies between 25 and 88% for evacuated tubes and between 10 and 60% for fat plat collectors. The TRNSYS computer program is used to investigate the annual energy potential of SWH.

Yang et al. (2018) In order to examine the performance of the solar hot water system, this research develops a simulation model. TRNSYS software is used as the simulation platform to simulate the annual thermal performance of a solar hot water system. In the same way, in normal weather circumstances, the variation in water temperature in the storage tank, the temperature at the collector's inlet and outflow, the total solar radiation, and the change in heat collection efficiency are all examined. they arrived at a decision. The following results are reached following the analysis of the solar hot water system using simulation: The amount of solar radiation received directly relates to how much the collector heats the water, as a result, the collector's outlet temperature will depend on how much solar radiation it can absorb. Additionally, when the system is forced to circulate, the water will circulate within the system. As a result, the amount of solar radiation will also, to some extent, affect the collector's inlet temperature.

Saleem et al. (2020) Using TRNSYS software, a Solar Water Heater (SWH) with an Evacuated Glass Tube Collector (EGTC) is modelled The system was developed with the highest possible efficiency using efficiency parameters and a parametric optimization technique under the seasonal climate conditions of Karachi, Pakistan, a Solar Water Heating system was modelled year-round Specific heat (kJ/kg.K), fluid density (kg/m^3), fluid thermal conductivity (kJ/hr-m-K), fluid viscosity (kg/m/hr.), and thermal expansion (1/K) were the input properties for these refrigerants.

Zeghib and Chaker (2011) In this work, a household solar water heating installation was modeled. The results of daily simulations for a solar system in Constantine, Algeria, which produces hot water for heating and has a collector with a surface area of 2 m^2 and a 200-liter storage tank Radiators, a water storage tank, a source of supplemental energy, and a solar flat collector make up the system. The month of February was selected for the simulation in the current study since it was thought to be the coldest one based on weather data from Constantine. A simulation program written in Fortran programming was used to model the systems.

Mongibello et al. (2015) A solar domestic hot water (DHW) system made up of two flat plate collectors, a water tank for storing heat, and a coil heat exchanger was subjected to an unsteady numerical simulation in this work, the basic operational characteristics of a solar DHW system made up of two non-concentrating flat plate solar collectors, a vertical cylindrical water tank for heat storage, and an immersed coil heat exchanger have been numerically simulated and discussed in this study. The simulations were run using two separate solvers, TRNSYS 17 and a custom MATLAB program that was created at home. A time-step of 60 s has been employed, and the HTF flow rate has been set to 3.10^{-5} m3/s. The outcomes of the simulations, which used the ENEA Portici Research Center's measurements of irradiance, ambient temperature, and wind speed as input data, have been presented and analyzed.

Abdunnabi et al. (2014) The goal of this research is to verify the TRNSYS simulation program's accuracy in simulating various forced circulation solar water heating system configurations and to examine the key factors that influence the disparity between simulation and experiment. On a forced circulation solar water heating system with four vacuum tube collectors connected in series and a 200-liter storage tank outfitted with the necessary equipment, experimental work lasting six days is being conducted. There was no heat exchanger in the open loop system. In order to validate the software and assess its accuracy, the TRNSYS simulation program uses the identical system parameters, weather, and operational conditions. The results indicate that when compared to the experiment, the TRNSYS simulation tool provides reliable predictions.

2.6 Review Related to Solar Tower

Elbeh and Sleiti (2021) Examined the technology of concentrated solar power (CSP) for constructing and enhancing a CSP tower plant for places with a dry climate like Qatar. Database and spreadsheet models for calculating solar irradiance were created. SolarPILOT and System Advisor Model (SAM), two software programs, were utilized to analyze and optimize the entire solar thermal plant and cost. The solar field parameters of a suggested CSP plant, such as the tower optical height, heliostat structure width and height, number of heliostats, horizontal and vertical panel height and diameter, water consumption, cleaning schedule, maintenance, and overall cost, were optimized using a thorough iterative optimization process that was developed and put to use. An 8 MW CSP power tower plant with a 10-hour thermal energy storage capacity and a hybrid steam condensing system was the result of the optimization procedure. A 0.45 km^2 solar field with 2,736 heliostats was intended for the facility. The receiver was 3m high and 5m in diameter, while the solar tower was 140 meters high. The annual water requirement for the plant's operation, heliostat cleaning tasks, steam cycle makeup, and hybrid cooling system augmentation was calculated to be 95,579 m^3. Finally compared with conventional power systems, the Levelized cost of energy was still high.

Ashour et al. (2021) Designed a short-scope concentrating solar power tower (CSP) model that had been constructed at King Abdul-Aziz University in Jeddah, Saudi Arabia. Solar energy is used to produce electricity in this prototype. Ten heliostats were used to redirect incident solar sun rays to a tower that was elevated at 7m in the investigation to focus solar energy on a solar receiver. molten salt that was 40% $KNO3$ and 60% $NaNO3$ was used. The condensed theory of the solar tower examined the theoretical, experimental, and economic features of solar towers. the receiver's temperature using analytical division calculated, finite element research using ANSYS was carried out. The simulation's maximum temperature was 521^0C.

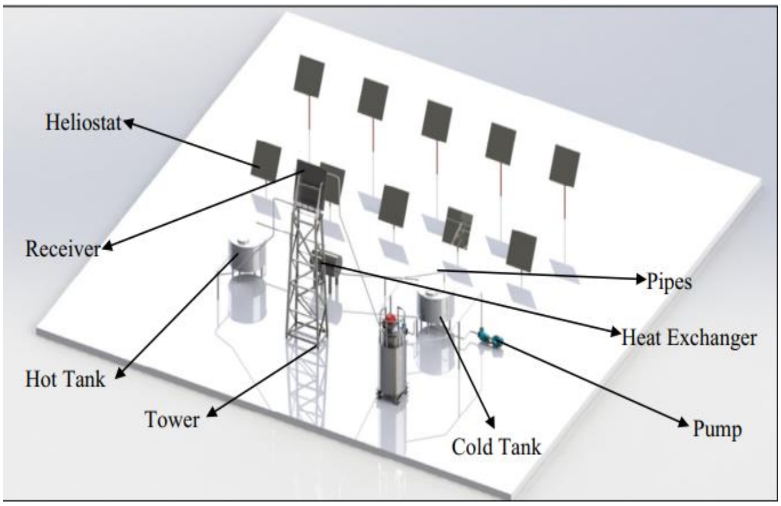

Figure 2.3 Solar Tower Power Plant Prototype for the Current Study in Saudi (Ashour et al., 2021)

Ashour et al. (2021) Studied the solar tower (ST) and photovoltaic (PV) technologies the two primary solar to-electrical energy conversion methods were compared. For an accurate comparison, 100 MW ST and PV facilities of the same size were planned for an area with excellent global horizontal irradiance (GHI) and direct normal irradiance (DNI). a thorough comparison of ST and PV technology's energy and economic impacts were made. Compared to the PV plant, the proposed ST produces 89.5% more energy annually. Declared Throughout its lifetime, the ST plant produces 96.4% more energy than a PV plant. PV plants have a higher performance ratio than ST plants, compared to ST plants, PV plant SEE is 20.42%, while ST plant SEE is 17.28%. Compared to 1475484m^2 for a PV plant, the planned ST plant needs 6755094 m^2 of land. Compared to the PV plant's 0.39 land use factor, the ST plant's is 0.173. The ST plant's NCC is 5.58 times greater than that of the PV plant. The ST plant's LCoE is 2.83 times greater than the PV plants. While the NPV of the ST plant is negative, that of the PV plant is positive. It was determined that PV, which had excellent DNI and GHI, was the standout technology for the suggested location.

Srilakshmi et al. (2017) Designed an approach for estimating the performance of a tower plant with storage and hybridization utilizing an external cylindrical receiver. The Gemasolar plant in Spain and the Crescent Dunes plant in the United States of America served as validation sites for the methodology. For the Gemasolar project 20 MW and 15 hours of storage, the optimal efficiency was 16%, and for the Crescent Dunes facility 110 MW and 10 hours of storage, it was 18.3%. It was mentioned that the CSTEM tool for solar towers may be used to analyze plant performance in the same way as the CSTEM tool for parabolic troughs.

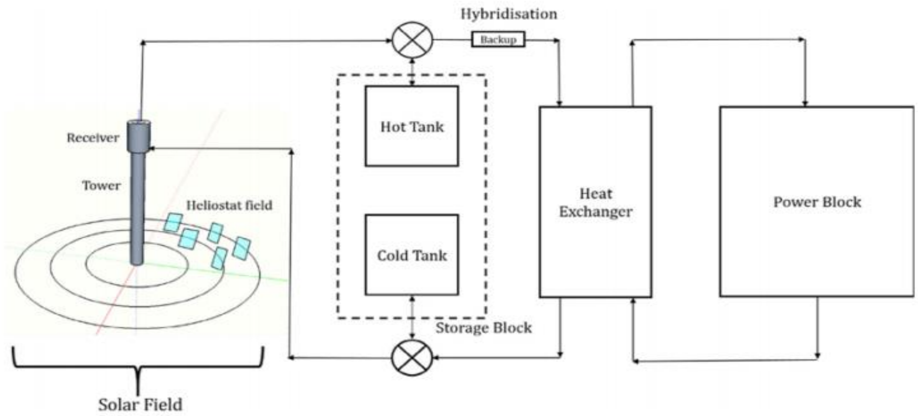

Figure 2.4 Schematic Diagram of Solar Power Plant with Storage and Hybridization (Srilakshmi et al., 2017)

Boretti et al. (2020) Offered a methodology for designing the key elements of solar power tower plants and for estimating the precise investment costs and economic indices. Through a comparison with the design data of two functioning commercial power tower plants, the Gemasolar medium-scale plant with a capacity of 19.9 MW and the Crescent Dunes big plant with a capacity of 110 MW, the design approach employed in this work was effectively validated. An operational power tower plant's design has an 8.75% average degree of uncertainty. Six solar power tower plants with a capacity of between 10 and 100 MW were designed using this technology to be integrated into Chile mining operations.

Ozturk and Dincer (2013) Studied the thermodynamic evaluation of a solar-based multi-generation system with coal gasification which produces hot water, hydrogen, oxygen, and power was examined. To use the concentrating solar energy, a solar power tower is combined with the coal gasification system. There were six separate subsystems in this multigenerational system. According to the findings, the sub-systems' energy and exergy efficiencies fluctuate between 19.43 and 46.05% and 14.4 and 36.14%, respectively, while the multi-generation system has the highest energy and exergy efficiencies at 54.04% and 57.72%. Engineering

Equation Solver (EES) software was used to calculate the working fluids' thermodynamic characteristics. they succeeded.

N'Tsoukpoe et al. (2016) Proposed a concept for a 10 kW micro-central tower power plant for Sahelian nations. The project that was the subject of this article was a Burkina Faso micro-concentrating solar and power facility. Using central tower technology, addressed the problems with electricity availability in rural areas of the Sub-Saharan region. The power plant's important features had been established, identified, and designed. Used locally accessible mirrors for the heliostats and acquire experience with small-scale solar tower technology, a solar tower technology had been kept. The solar field that could supply 100 kW to the thermodynamic cycle was made up of 20 multifaceted heliostats with a total mirror area of 180m^2. The usable volume of the storage tanks was around 4 m^3. A galvanized steel coil heat exchanger served as the solar receiver. Below 250°C was the maximum operational temperature that had been established. Finally, announced that the design for the following generation of μ-CSP will be modified and installed in rural regions for decentralized electricity generation. The maximum operating temperature has been set below 250 °C in order to avoid dealing with more complex high temperature level processes, which are not commonly locally managed.

Al-Madani (2006) Developed and produced a cylindrical solar water heater in the University of Bahrain's mechanical engineering department. It comprises a cylindrical, high-quality glass tube measuring 0.8m. long, 0.14m. in diameter, and 6 mm. thick. The incident solar energy on the cylinder wall is collected by a copper coil tube in the form of spiral rings with an outside diameter of 3.175 mm and an inner diameter of 2 mm. The copper coil tube is painted black. the maximum temperature difference of 27.8^{0}C between the inlet and outlet of the solar water heater at a mass flow rate of 9 kg/h was achieved. 41.8% was found to be the highest result over the testing period. This demonstrates the system's effective ability to transform solar energy into heat that can be utilized to warm water. claimed that an economic investigation had shown that the cylindrical solar water heater was more cost-effective than the flat plate collector.

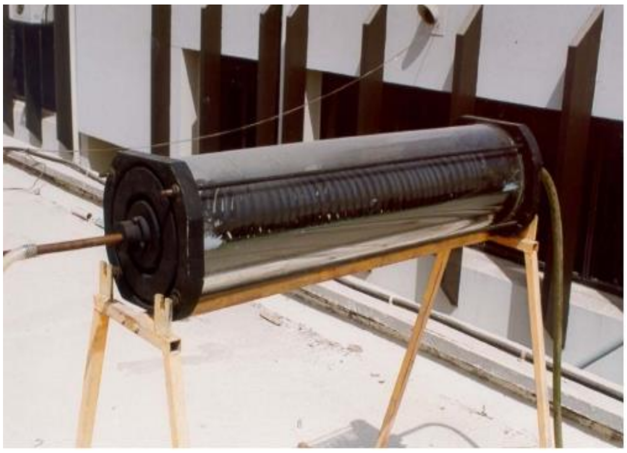

Figure 2.5 Cylindrical Solar Water Heater (Al-Madani, 2006)

Allouhi et al. (2019) Presented a promising alternative to traditional systems. By incorporating heat pipes into commonly used flat plate collectors as a way of heat extraction devices, A complete forced circulation solar water heating system using a heat pipe flat plate collector underwent transient performance investigation (HPFPC). To analyze the energetic performance, a simulation platform was created for this purpose using MATLAB. Due to the glass cover's poor absorbance and high transmittance as well as significant heat losses to the outside, simulation results revealed a pronounced difference between the temperature of the glass cover and absorber surface of up to 45^0C. The evaporator and condenser sections' maximum temperature differential were measured to be about 2.7^0C. On a typical winter day temperature at the maximum outflow reached 57^0C, with maximum instantaneous thermal efficiency reaching up to 55%. The instantaneous energetic efficiency was found to be greater than 6.9% on the same day.

Sadhishkumar and Balusamy (2014) Summarized the previous research on solar water heating systems with various heat transfer enhancement techniques. These techniques include collector design, collector tilt angle, coating of pipes, fluid flow rate, thermal insulation, integrated collector storage, thermal energy storage, use of phase change materials, and insertion of twisted tapes. To comprehend the flow and thermal behavior in solar collectors, which would increase the thermal performance of solar collectors, this research also examined approaches to optimize and simulate solar water heating systems. The majority of research projects have simply used forced circulation. The study on solar water heating systems with natural circulation had to be improved. Thermal energy storage systems offer a less expensive and more efficient alternative to the current solar water heating technology. With more research in this area, latent heat thermal energy systems could be an economically feasible solution for storing solar heat energy.

Naghavi et al. (2017) Discussed the charging-only and discharging-only modes' designs, operational concepts, and experimental thermal operations. The supply water is then heated by the heat that was previously stored, thanks to a system of finned pipes inside the LHS tank. Reports also cover supply water flow rates, hot water draw-off times, and the effects of tropical weather conditions. In this arrangement, a heat pipe with fins connecting to the condenser ends within the LHS tank was used to collect and store solar energy incidents on the HPSC. The system's thermal efficiency varies between 38% and 42% on sunny days and 34% to 36% on overcast or rainy days, indicating a range of around 8% variability depending on the circumstances. An entire design of the suggested system was constructed and put to the test in the experimental phase. The conceptual design of the theoretical model is simpler than the design of the LHS tank in the experimental test. The heat transmission from the collector to the LHS tank by HP is fast and efficient.

Boukelia et al. (2014) Studied to evaluate the performance of solar gas turbine power plant with a capacity of 20.5 MW in south west Algeria. The objective of this project is to calculate the energetic and exergetic efficiency of hybrid and solar electric cycle of two operating system of the installation first without regenerator then with regenerator and evaluate their feasibility in this area.

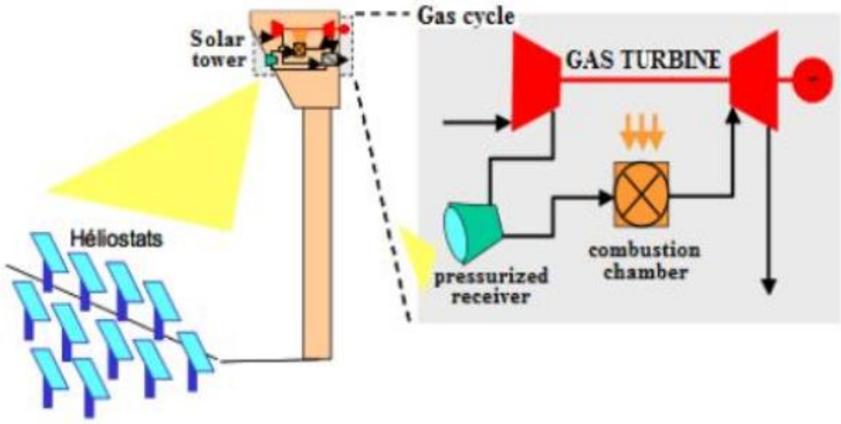

Figure 2.6 Solar Tower Power Plant with Brayton Cycle (Boukelia et al., 2014)

Mahdi and Khudheyer (2021) Evaluated numerically and experimentally a new receiver design to increase both the thermal and the optical efficiency of CRT to compensate for the efficiency drop of the traditional old cylindrical central receiver design, which has been accrued by increasing the design temperature from 560 °C to more than 700 °C. The central receiver tower (CRT) design for concentrating solar power (CSP) technology has undergone substantial component studies over the past ten years to increase the quantity of solar heat that is absorbed. To reduce the losses of the reflected solar energy from the receiver body to the environment through reabsorption method, they used a receiver with a fin-like form. For a different situation, the fin-like receivers produced better efficiency. However, compared to the standard cylindrical receiver, the fin-like receiver experienced a 38.6% reduction in peak solar output.

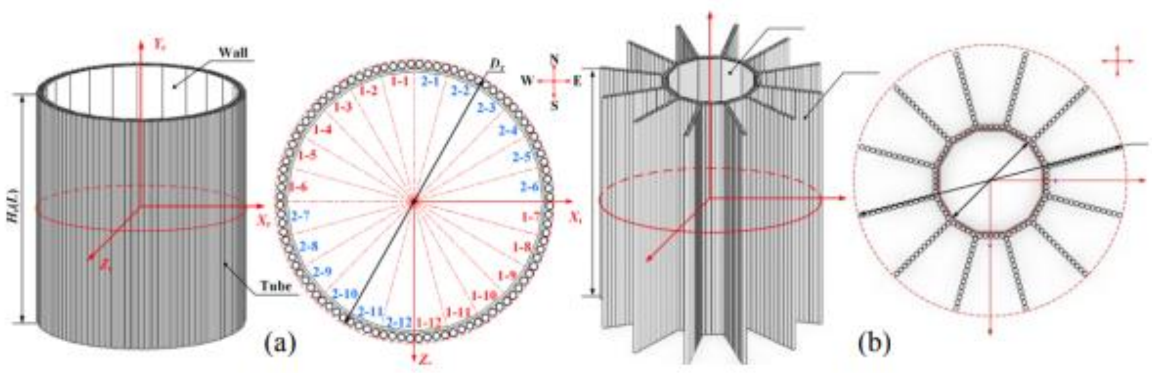

Figure 2.7 Schematic diagram: (a) Three-dimensional structure and top view of the cylindrical receiver, (b) Three-dimensional structure and top view of the cylindrical receiver of the fin-like receiver.

Zhang et al. (2017) Examined the thermal performance of the three-dimensional (3-D) molten salt cavity models in steady state, a modified mixed computational method was presented. The Molten-Salt Subsystem/ Component Test Experiment (MSS/CTE) in the United States also used this computational method to determine the thermal performance of the receiver, and the results were in accordance with published data. The study involved molten salt cavity receivers of various heights. The findings indicate that a receiver's thermal efficiency will suffer from either a too-low or too-high height. Therefore, adequate heights must be chosen to allow receivers to achieve relatively high efficiency and low temperatures. Smaller cavity heights do not necessarily have great thermal efficiency, and a smaller cavity height of 2 m causes thermal efficiency to decrease. However, a bigger cavity height (6 m) results in worse thermal efficiency. The tube panel temperature can be kept within an acceptable range while achieving a comparatively high efficiency at a reasonable height of 3.96 m.

Zhou and Zhao (2014) In this study, a ray tracing program based on graphics processing unit (GPU) is created to compute the annual optical efficiency in precise physical account of cosine effects, shadowing and blocking (S&B) factor, spillage, atmospheric attenuation, and mirror reflectivity excluding mirror flaws. As the outcome, on the basis of the quick computation on GPU, two typical heliostat field layout patterns are built and optimized. Locating the receiver and the mirrors in a specific land area is the main goal of the heliostat field layout design.

based on this study the number of mirrors in each row and column may be calculated with ease once the column space and line spacing between the mirrors are known. In order to be consistent with the Monte Carlo ray tracing approach, the solar model is constructed taking the divergence of the sunlight into account.

Mahboob et al. (2018) In this study, a solar tower construction for a 50MW solar thermal power plant is designed. The tower structure design method begins by creating a tower structure based on the necessary height discovered through ray trace analysis. Then, using angles with various cross sections, three variations of this structure are created. Deformation is computed after CAE software analyzes each variant Shear force, bending moments, and deformation plots are all present.

2.7 Summary of Literature Review

A solar water heater is a long-term investment that will save money and energy for many years. Like other renewable energy systems, solar water heaters minimize the environmental effects. In addition, they provide insurance against energy price increases, help reduce our dependence on imported oil, and are investments in everyone's future. These different pervious works are summarized as follows:

- Studied the energetic and financial potential of employing Domestic Solar Water Heating systems (DSWHs) instead of electric, gas, or town gas water heaters, they did DSWHs with evacuated-tube solar collectors (ETC) and flat-plate solar collectors (FPC) they did the simulation using TRNSYS (Hazami et al., 2013).
- A flat plate collector covered with double glazing layers at 20^0 angles of tilt to the horizontal was employed. A maximum hot water temperature of 73^0C was measured during the experiment at an ambient temperature of 36^0C (Arekete, 2013).
- Solar energy for massive water heating systems at various prospective locations across the country is examined. They used flat plate collector the conclusion that solar energy can be employed in Ethiopia as a substitute energy source for large-scale water heating systems (Bekele et al., 2013).
- Examining and comparing the energy performance of evacuated and flat plate collectors in the African continent. According to the energy study, the solar-derived domestic hot water output varies between 25 and 88% for evacuated tubes and between 10 and 60% for fat plat collectors. The TRNSYS computer program is used (Boretti et al., 2020)

- Database and spreadsheet models for calculating solar irradiance were created. SolarPILOT and System Advisor Model (SAM), two software programs, were utilized to analyze and optimize the entire solar thermal plant and cost. An 8 MW CSP power tower plant with a 10-hour thermal energy storage capacity (Elbeh & Sleiti, 2021).

2.8 Research Gap

Many researchers have been working on Flat Plate, Evacuated Tube, and Parabolic Trough collectors that are utilized to produce hot water utilizing solar energy as the power source according to the literature examined. However, due to the intermittent and unpredictable nature of solar energy, the power generated by those solar collectors does not function effectively. Due to the enormous amount of temperature that solar towers collect, about 1000^0C, this makes them unsuitable for water heating, but by utilizing a mixing chamber to manage the temperature of steamed water created by a solar tower, this study aims to provide hot water for large-scale applications like hospitals. Previously, solar towers were used to generate energy.

CHAPTER THREE

3. MATERIAL AND METHODOLGY

3.1 Materials

Purchasing items from the local market provides the materials, measuring tools, and system components needed for creating the trial prototype and determining the system characteristics. According to local availability and cost-effectiveness, materials utilized to build the experimental setup were chosen. There is a presentation of the principal tools and materials utilized in the experiment. The main materials and measuring devices used in the experiment are presented.

Materials;

- Reflective Glass Mirror Used for Heliostat
- Aluminum sheet metal used as frame for heliostat Receiver
- Tower used for holding receiver.
- Pipe used for transferring fluid through them pipe made from mild sheet metal.
- Storage tank
- Mini pump will use for pumping cold water to the receiver.

3.2 Methodology

Analytical and Numerical approaches will be used as a methodology in this study. The analytical approach uses governing equations to size and designs the components in the system. Performance analysis of the system in the storage tank. The numerical approach means validating the theoretical analysis to supply hot water at the required temperature and performance enhancement due to increase duration of time. Finally, validation of both theoretical and numerical simulation has been done. To achieve the objective of this study the following methodology has been followed.

Methodology

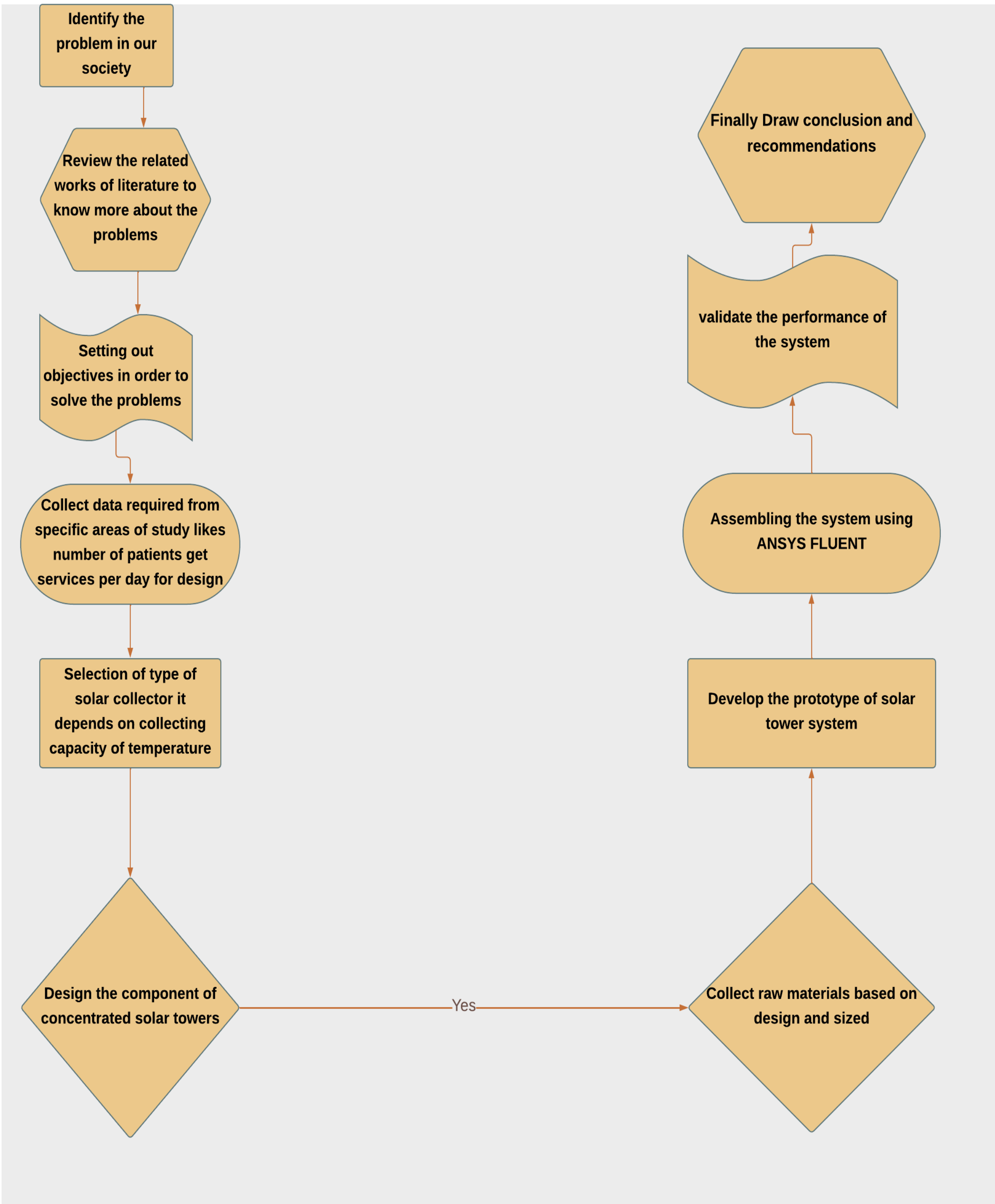

Figure 3.1 Methodology Using Lucid Flow Chart of the Study

3.3 Estimation of Hot Water Demand

Water is typically needed in hospitals across worldwide for various devices that Hospitals require different amounts of water for different purposes. For example, sterile processing and radiology require 15% of the water used for non-domestic use, and operating rooms, laundry facilities, kitchen equipment, sinks, tubs, and showers, washing machines, and toilets require 85% of the water used for domestic use.

About 90% of the hospital's daily water consumption is used for hot water, while 10% is used for cold water (https://edurev.in/question/1470462/Water-requirement-per-day-per-bed-in-250-beds-hospital-according-to-IS-11721992-is-a-340-litersb-450).

Every day, health clinics typically need 160 liters for per resident. A hospital may turn harmful lacking sufficient hot water, and it is difficult to clean with no proper hot water. This is a significant amount of water for a large hospital. Each person needs 50 liters each hour on average during peak situations (Homola, 2018) In addition to using hot water, the hospital needs to be heated or cooled throughout specific seasons of the year to keep staff and patients at comfortable temperatures. Thus, hot water is the most important prerequisite for many appliances in the health services. In order to meet the daily need for hot water, the Bishoftu General Hospital employs electrical power fuel as a source of energy.

3.3.1 Demand for Hot Water

Determining the requirement for hot water accurately in hospitals crucial because it varies from one facility to another. This accurate assessment helps prevent wasteful use of energy to heat the water. By reducing power usage and minimizing emissions of greenhouse gases, hospitals can contribute to environmental sustainability. The healthcare sector seeks energy-efficient solutions that operate at a low cost and minimize pollution, enabling them to meet their goals of reducing environmental impact while maintaining optimal patient care. In hospitals worldwide, water is required for various purposes. The distribution of water usage varies based on the kind and dimensions of the building. Typically, hospitals allocate approximately 15% of the water used for non-domestic purposes., which includes activities like sterile processing and radiology. The remaining 85% of water is utilized for domestic purposes within the hospital.

Domestic water usage in hospitals encompasses several areas and services. This includes water consumption for boilers, which are used to provide heating and hot water throughout the facility. Additionally, chillers, which are responsible for cooling systems, also require water. Water is also used in food services provided to patients and pantry services for guests. This includes activities related to meal preparation, dishwashing, and other kitchen equipment. Furthermore, water is necessary for specific areas within the hospital, such as operating rooms, laundry facilities, and various sanitary facilities. This includes sinks, tubs, showers, washing basins, and toilets. By clearly understanding the distribution of water usage in hospitals, facilities can effectively manage their water resources and implement strategies to optimize water conservation and efficiency in each area of operation.

3.3.2 Estimate Hot Water Demand of Bishoftu General Hospital

Each resident of a health center needs about 160 liters of water per day on average. A hospital could become dangerous without adequate hot water, also that can difficult for tidying up without enough heated water. This is significant quantity of water for a large hospital. Each occupant needs 50 liters of water per hour on average at peak demand rates. In addition to using hot water to keep the hospital's patients at comfortable temperatures, it sometimes has to be heated or cooled. Therefore, the essential necessity in health services for many appliances is hot water (Homola, 2014). In order to meet the daily need for hot water, the Bishoftu general hospital uses electricity and fuel as a source of energy for water heating.

3.3.3 Data Collected from Bishoftu General Hospital

Reliable information about the hospital is difficult to find in impoverished nations like Ethiopia since there aren't enough measurement devices and there's a lack of accurate information regarding the hot water system in hospitals. Assumptions and estimates are according to the hospital's conventional mechanism for delivering hot water because there aren't many credible sources of data about the hospital's hot water system.

Table 3.1 Gathered Statistics from Bishoftu General Hospital

	Utilization				
Specifications	**Kitchen**		**Shower**		**Laundry**
	For Dish washing	For cooking	Patient	Medical staff	
Number of rooms	1	2	54	12	2
Person per room	2	2	4	6	4
Energy Source	Fuel and Electric				

3.3.4 Calculating the Hospital's Hot Water Requirement

The desire for hot water determines size of domestic solar water heating system The behaviors of the users, nevertheless, will determine this. The daily demand for hot water is, for instance, much lower if a person prefers to take showers versus bathing than it would be otherwise. It is better to assume that the daily hot water requirement for industrialized countries is based on their requirements.

When sizing or designing a residential water heating solar system, the amount of hot water required is an important consideration. The formula provided in **IS 1172:1992** for calculating the water requirement per day per bed in a hospital is as follows:

Water Requirement = (Person Water Requirement + Hospital Water Requirement) * Number of Beds.

Person Water Needed: This concerns the estimated volume of water consumed by an individual in a hospital setting. It takes into account the water used for drinking, cooking, personal hygiene, and other related activities. The specific value for a person water requirement may vary depending on factors such as climate, local regulations, and the type of hospital.

Hospital Water Requirement: This component represents the additional water demand arising from the hospital's specific activities and operations. It includes water used for medical purposes, such as sterilization, washing medical equipment, maintaining cleanliness in healthcare facilities, and other non-patient-related uses.

Number of Beds: This indicates the overall quantity of beds present within the hospital. It is a crucial factor in estimating the overall water requirement, as each bed represents a potential water user. By multiplying the sum of person water requirement and hospital water requirement by the number of beds, the formula provides an estimate of the total water demand for a given hospital. This calculation helps in determining the quantity of water required on a daily basis to meet the needs of both patients and hospital operations, as per the guidelines provided by **IS 1172:1992.**

The water requirement of 315 liters per day is calculated based on the guidelines provided by IS 1172:1992. According to the formula mentioned earlier, the water requirement per day per bed is the sum of the person water requirement and the hospital water requirement, multiplied by the number of beds. In this case, let's assume that the person water requirement is 200 liters per bed per day and the hospital water requirement is 115 liters per bed per day.

Person Water Requirement:

The person water requirement represents the estimated amount of water consumed by an individual in a hospital setting. It includes water used for drinking, cooking, personal hygiene, and other related activities. In this study, we assume it to be 200 liters per bed per day.

Hospital Water Requirement:

The hospital water requirement represents the additional water demand arising from the hospital's specific activities and operations. It includes water used for medical purposes, such as shower, washing medical equipment, maintaining cleanliness in healthcare facilities, laundry and other non-patient-related uses. In this study, we assume it to be 115 liters per bed per day.

Number of Beds: The number of beds in Bishoftu General hospital is 216. Now, let's calculate the total water requirement for the hospital:

Total Water Requirement = (Person Water Requirement + Hospital Water Requirement) * Number of Beds

Therefore, for a hospital with 216 beds, the total water requirement is **18,644** liters per day. This estimation takes into account both the individual water needs of patients and the additional water demands of hospital operations, as per the guidelines provided by IS **1172:1992.**

Hot water is commonly used in hospitals for various purposes, including kitchen activities, patient showers, and laundry. The specific hot water requirements may vary depending on the hospital's size, patient load, and other factors. It is important to consider the guidelines and regulations provided by local authorities or healthcare standards when estimating the hot water requirement for a hospital.

To accommodate the hot water needs in your study, you would need to determine the portion of the total water requirement that should be allocated for hot water purposes. This allocation can be based on factors such as the number of staff, patients, and the expected usage patterns for kitchen, shower, and laundry facilities.

Once you have determined the allocation, you can calculate the hot water requirement by multiplying the allocated portion of the total water requirement by an estimated temperature rise, which is the increase in temperature required to achieve the desired hot water temperature. This will give you an estimate of the hot water demand specifically for kitchen, shower, and laundry purposes in Bishoftu General Hospital.

It is worth noting that hot water systems in hospitals typically involve the use of water heaters or boilers to provide a continuous supply of hot water. These systems should be designed and maintained by local regulations and safety standards to ensure the efficient and safe delivery of hot water throughout the hospital.

Please keep in mind that the specific calculations and requirements for hot water may vary depending on the hospital's infrastructure, local regulations, and other factors. It is recommended to consult with experts or professionals in the field of plumbing and building services to ensure accurate and appropriate estimations for the hot water requirements in your study on Bishoftu General Hospital. The temperature distribution for hot water in areas such as the laundry, kitchen, and shower in a hospital can vary depending on the specific requirements and regulations. Typically, different temperature ranges are recommended for each area to ensure safety and hygiene standards are met. Here are some general guidelines:

a. **Laundry:** The hot water temperature for laundry facilities in hospitals is usually set at a higher range to ensure effective cleaning and disinfection of linens and other textile materials. The recommended temperature for laundry hot water is typically between 65°C (149°F) to 71°C (160°F). This higher temperature helps to kill bacteria and remove stains effectively.
b. **Kitchen:** In the kitchen area, hot water is essential for food preparation, dishwashing, and general cleaning. The recommended temperature for hot water in kitchens is typically between 60°C (140°F) to 65°C (149°F). This temperature range is considered safe for handwashing, cleaning dishes, and other kitchen-related activities.
c. **Shower:** For patient showers and personal hygiene purposes, the hot water temperature should be comfortable and safe. The recommended temperature for hot water in showers is around 40°C (104°F) to 43°C (110°F). This temperature range provides a pleasant and soothing shower experience while minimizing the risk of scalding or burns.

It's important to note that these temperature ranges are general guidelines, and specific regulations or standards may vary based on local codes, healthcare regulations, and safety guidelines. It is crucial to adhere to the specific regulations and recommendations provided by local authorities or healthcare governing bodies to ensure the safety and well-being of patients, staff, and visitors. Additionally, hospitals may implement temperature control measures, such as the use of thermostatic mixing valves or temperature limiters, to maintain consistent and safe hot water temperatures throughout the different areas. These measures help prevent scalding accidents and ensure adequate temperature distribution for various purposes within the hospital.

When conducting your study on temperature distribution in Bishoftu General Hospital, it is essential to consider local regulations, safety standards, and best practices specific to the region and healthcare industry. Consulting with experts in the field, such as plumbing engineers or hospital facility managers, can provide valuable insights and guidance for ensuring appropriate temperature distribution in the laundry, kitchen, and shower areas of the hospital(Katsanis et al., 2006).

If you have determined that 50% of the total hot water requirement is allocated for laundry, 35% for the kitchen, and 15% for the shower, we can calculate the distribution of water for each purpose based on the 315 liters of water required in Bishoftu General Hospital.

Water allocated for laundry 50% of total hot water requirement 50% of 315 liters Water allocated for the kitchen is 35% of total hot water requirement Water allocated for the shower is 15% of total hot water required.

Therefore, based on the given allocation percentages, the distribution of water for the three purposes would be approximately: 157.5 liters for laundry, 110.25 liters for the kitchen, and 47.25 liters for the shower(https://edurev.in/question/1470462/Water-requirement-per-day-per-bed-in-250-beds-hospital-according-to-IS-11721992-is-a-340-litersb-450).

It is important to note that these calculations are based on the allocated percentages you provided, and they may be subject to adjustment based on specific requirements, regulations, and the operational needs of Bishoftu General Hospital. It is always recommended to consult with professionals and consider local guidelines to ensure accurate water distribution for different purposes within the hospital.

For this study, a daily calculation of the hospital's hot water consumption is done based on assumptions. It is sensible to presume that, given Ethiopia's circumstances, the amount of hot water needed each day for showering is calculated by multiplying the ratio (3:4) by the hot water necessary for showering in developed nations.

Table 3.2 Requirements for Hot Water with Per Hospital Equipment

Demand	Hospital Equipment		
	Cooking Area	Bath	Washing
Hot Water(lt/day)	110.25	47.25	157.5
Temperature (°C)	65	43	71
Energy Source	Fuel and Electric		

Only the hospital's hot water needs are taken into account when calculating the need for hot water for various appliances. The daily use of hot water system, which is used to determine the best location for the storage tank and collector area of the solar thermal water heating system, is one of the hospital's hot water consumption systems.

Hot water demand for each appliance is given by:

$$\mathrm{HWD} = (\text{Number of room}) * (\text{Water per appliance}) \quad (3.1)$$

Hot water demand for showering service is given by:

$$\mathrm{HWDS} = (\text{Number of rooms}) * \left(\frac{\text{person}}{\text{room}}\right) * \left(\frac{\text{water}}{\text{person}}\right) \quad (3.2)$$

The total daily hot water demand of the hospital is determined as:

$$\mathrm{TDHWD} = \mathrm{HWDK} + \mathrm{HWDL} + \mathrm{HWDS} \quad (3.3)$$

3.3.4.1 Kitchen Needs Hot Water

For cleaning meals and appliances and providing hot water for showers, hot water is necessary in the kitchen. Using equation (3.1), the kitchen's daily hot water requirement is:

$$\mathrm{HWDK} = \mathbf{330.75\ liter\ per\ day}$$

3.3.4.2 Laundry Service Requires Hot Water.

Hot water is necessary for the hospital's laundry service, cleaning clothing, and providing showers for hospital staff. The requirement for hot water in a washing service can be calculated using equation (3.1).

$$\mathrm{HWDL} = \mathbf{315\ liter\ per\ day}$$

3.3.4.3 Showering Requires Hot Water

Both hospital staff and patients must have access to shower facilities. The hot water demand for shower services is calculated using equation (3.2), and shower services are categorized into four categories based on this.

shower facilities for cooks who work in kitchens:

$$\mathrm{HWDS1} = \mathbf{94.5\ liter\ per\ day}$$

Kitchen staff members who also wash dishes have access to showers:

$$\mathrm{HWDS2} = \mathbf{189\ liter\ per\ day}$$

Shower service for patients is:

$$\mathrm{HWDS2} = \mathbf{10,206\ liter\ per\ day}$$

Shower service for medical staff is:

$$\mathrm{HWDS3} = \mathbf{3,402\ liter\ per\ day}$$

Shower service for laundry workers:

$$\mathrm{HWDLs} = \mathbf{378\ liter\ per\ day}$$

The entire daily demand for hot water in showers is calculated utilizing using equation (3.3):

$$\mathrm{TDHWDS} = 94.5\mathrm{lt} + 189\mathrm{lt} + 10{,}206\mathrm{lt} + 3{,}402\mathrm{lt} + 378\mathrm{lt} = \mathbf{14{,}269.5\ liter\ per\ day}$$

3.3.4.4 Hospital's Overall Need for Hot Water

Therefore, the hospital's overall hot water consumption is:

$$\mathrm{THWD} = 330.75\mathrm{lt} + 315\mathrm{lt} + 14{,}269.5\mathrm{lt} = \mathbf{14{,}915.25\ liter\ per\ day}$$

Table 3.3 Hospital's Need for Hot Water Per Service

Mandate	**Facilities**			**Total**
	Cooking Area	**Bath**	**Washing**	**14,915.25**
Hot Water(lt/day)	330.75	14,269.5	315	

The hospital's daily and weekly heated water usage may differ from the estimated amount; therefore, the computed number may need to be multiplied by the same factor 1.25 in order to account for the error. The component represents one-fourth of the hospital's total estimated daily and weekly hot water usage.(Alemu, 1998).

Total Hot Water Should be supplied ($THWS$) is:

$$THWS = \left(Daily\ hot\ water\ consumption\ \frac{liter}{day}\right) * 1.25 \qquad (3.4)$$

Table 3.4 Hospital's Need for Hot Water Per Service

Mandate	**Facilities**			**Total**
	Cooking Area	Bath	Washing	
Hot Water(liter/day)	413.44	17,836.88	393.75	**18,644**

Each Appliance's Daily Hot Water Consumption

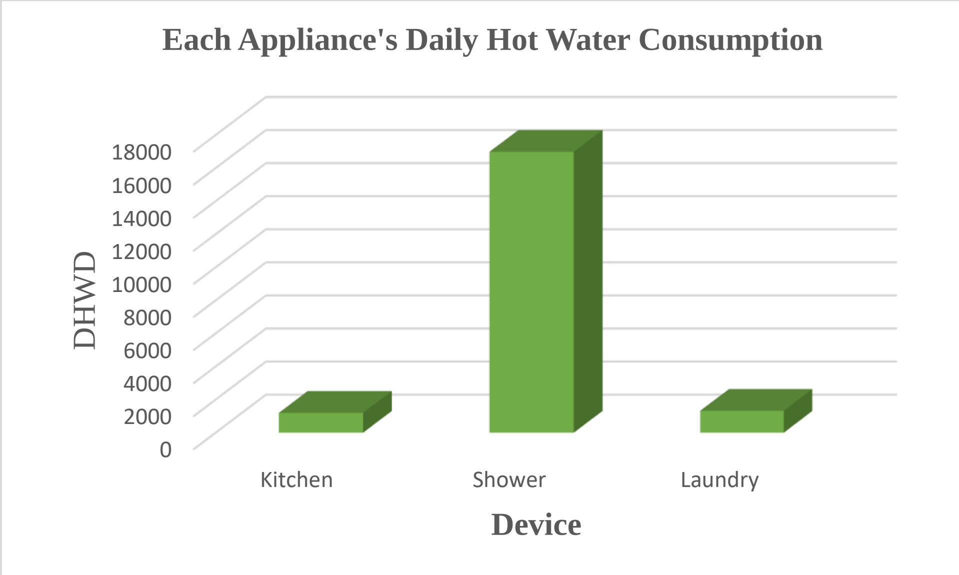

Figure 3.2 Each Appliance's Daily Hot Water Consumption

3.3.5 Pattern of Hot Water Usage

The total daily need for hot water for Bishoftu General Hospital has been scheduled to 18,644 liters daily. It is possible to distribute this daily hot water usage as 60 % morning, 23% afternoon, and 17% evening will be distributed over the daytime as gathered data from the hospital.

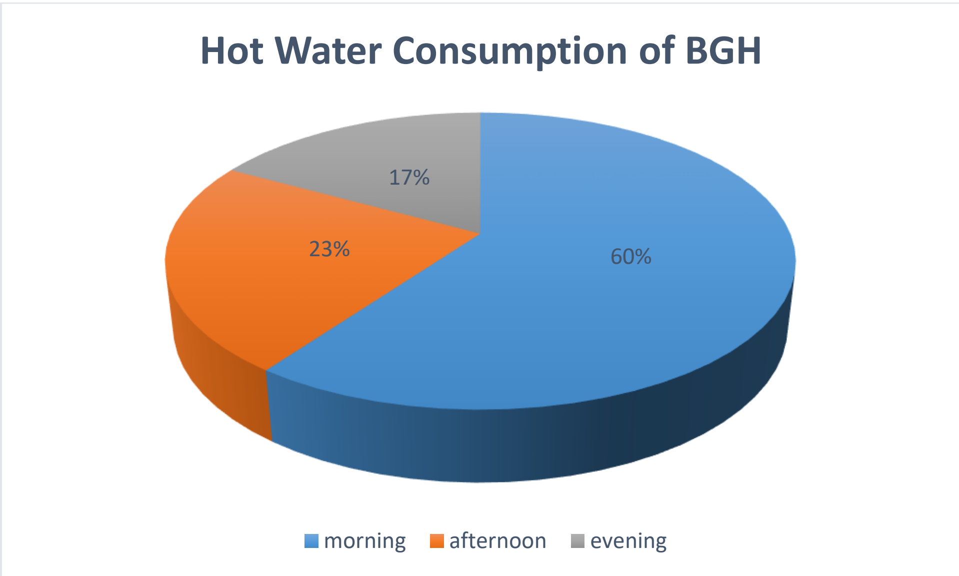

Figure 3.3 Spreading of Hot Water Usage Throughout the Day

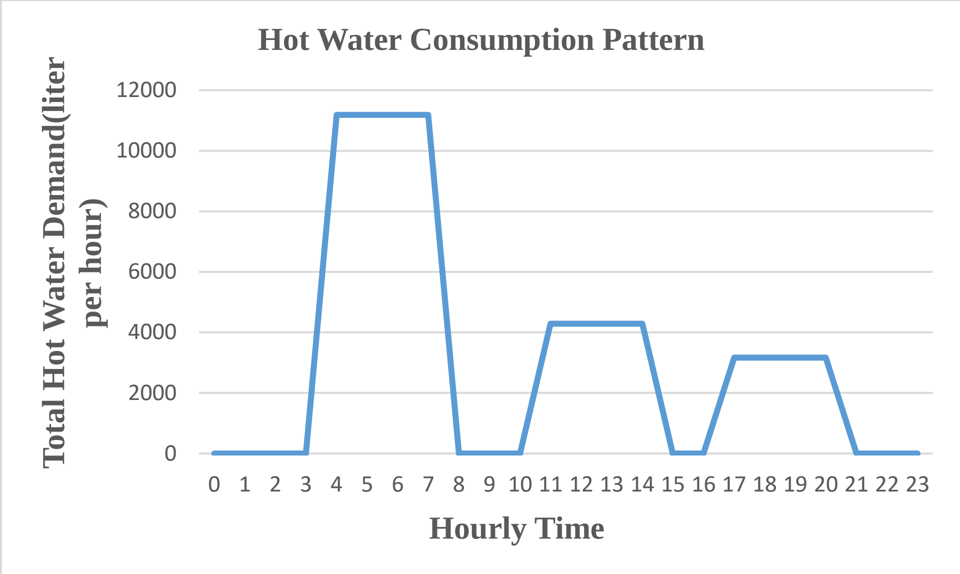

Figure 3.4 Hot Water consumption of bishoftu general hospital

3.3.6 Tank for Heating Water Storage Capacity

The capacity of the storage container can be decided once the daily hot water requirement has been established. So that consumption peaks can be adequately met and cloudy days can be made up for, Ideally, it would be approximately A daily requirement that is 0.8–1.2 times greater in locations with high sun radiation and 2–2.5 times greater in areas that have fewer solar radiation (Betseha, 2020).

Thus, the following formula is used to determine the storage tank's volume ($\mathrm{V_{st}}$):

$$\mathrm{V_{st}} = \mathrm{THWD} * 1.2 \tag{3.5}$$

For total daily hot water demand volume of the storage tank (V_{st}) is:

$$V_{st} = \mathbf{22,372.8}\ \boldsymbol{liter}$$

Since the manufacturers do not sell tanks in all potential sizes, a decision must be made from among those that are commonly offered available for purchase. Therefore, The storage tank capacity should be at least 90% and not more than 120% of the estimated volume, according to recommendations. (Betseha, 2020; Homola, 2014).

3.3.7 Energy Storage Device Capacity

A water storage device's energy storage capability at constant temperature is determined by (Duffie & Beckman, 2013)

$$\mathrm{Q}_T = (m * \mathrm{C_p})\Delta\mathrm{T} \tag{3.6}$$

Where: Q_T = total heat capacity of storage tank [KWH]

m = volume of the storage tank [$\mathrm{m^3}$]

$$C_p = 4.2 \frac{KW}{m^3K} \text{ heat capacity of water}$$

$$\Delta T = \text{temperature difference hot and cold water temperature(K)}$$

Since ambient temperature equal to cold water temperature is 20^0C and hot water taken as averagely 60^0C.

Table 3.5 Overviews of Required Energy Capacity, Storage Tank, and Hot Water

Overviews of Required Energy Capacity, Storage Tank, and Hot Water			
Overall Desire	**Utilization of Hot Water Everyday**	**Storage Container**	**Power output**
Daily	18,644 lt	$22.4m^3$	3.76MWH

CHAPTER FOUR

CALCULATING SOLAR RADIATION DATA

4.1 Calculating the Availability of Solar Energy

There is solar energy available everywhere, although it is most abundant in tropical regions. Its strength changes dramatically depending on where on Earth's surface it is located, as well as depending on the time of day and the local weather circumstances. Parameters of solar radiation and sunny-earth angles are crucial for estimating the amount of energy that reaches the surface of the planet since solar radiation is a significant renewable energy source. The most renewable and sustainable energy source is solar thermal, which is ideal for developing nations like Ethiopia, where the sun shines for twelve months of the year. Ethiopia has a great potential for solar irradiation, with an annual mean average solar radiation of roughly 5.2 kwh/$m2$, and a range of 4 to 6 kwh/m^2. The country also has an average daily sunshine duration of more than 10 hours(Tiruye et al., 2021).

4.1.1 Considering Sunshine Duration to Estimate the Amount of Solar Radiation in the World

The most crucial and prerequisite information for calculating sunlight is the location of the site, the amount of sunshine hours, and the weather. Merely, Sunshine duration, which is a measure of how long the sun's rays is present on the ground, can be employed to describe the climate of a location. location-specific coordinates of Bishoftu station: - Latitude: 8°45′8″N, Longitude: 38°58′42″E, Altitude: 1978m = 6489ft above sea level Temperature min/max: 12.2℃ and 26.67℃.

Table 4.1 Sunshine's Duration Per Hour for Five Seasons (Source; Bishoftu Agricultural Research Metrology Center)

Month	Jan	Feb	March	Apr	May	June	July	Aug	Sept	Oct	Nov	Dec
2015	9.87	8.5	8.6	8.12	8.35	7.89	5.3	6.9	7.7	8.3	8.78	10.1
2016	8.9	8.7	8.4	9.0	8.6	8.6	6.4	6.8	6.6	8.7	9.1	8.9
2017	9.46	10.1	9.5	8.7	8.8	7.5	9.3	8.0	8.3	9.0	9.07	8.8
2018	7.9	10.05	9.3	6.7	7.6	7.8	6.4	6.7	7.2	9.8	10.05	9.7
2019	7.7	8.9	9.2	9.5	7.8	8.0	6.6	5.9	6.8	8.7	9.9	9.4

Table 4.2 Five-Year Mean Sunshine Period Estimation

Months	Jan	Feb	Mar	Apr	May	June	July	Aug	Sept	Oct	Nov	Dec
Avg (2015-2019)	8.73	9.25	9.0	8.4	8.23	7.96	6.8	6.86	7.32	8.9	9.38	9.35

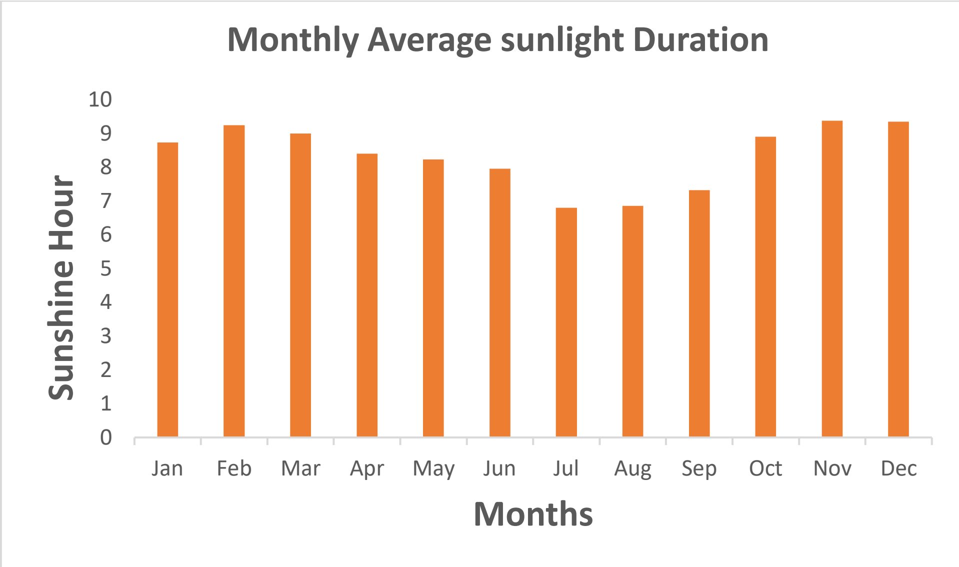

Figure 4.1 The mean Monthly Sunlight Duration per Every Month of Bishoftu

4.1.2 Fundamental Sign Standards and Terms in Solar Energy Estimation

A. Solar Time

Solar noon is the moment at which the sun passes the observer's axis. Time is based upon the sun's perceived angular velocity across the sky. The time frame utilized in all sun-angle connections is called solar time. Consequently, the equation of time must be used to convert standard time to solar time, accounting for variations in the earth's rotational speed that impact when sunlight crosses the viewer's meridian.

$$\text{Solar time} - \text{standard time} = 4(L_{st} - L_{loc}) + E \qquad (4.1)$$

Where, L_{st}-is the standard meridian for the local time zone;

L_{loc}-is the longitude of the location in question, and longitudes are in (°) West, that is, 0< L < 360◦.

The parameter E is the equation of time, sited(Kalogirou, 2012).

$$E = 9.78\sin(2B) - 7.53\cos(2B) - 1.5\sin(2B)\,[min] \qquad (4.2)$$

$$B = (N - 81)\frac{360}{365}$$

N denotes a particular day of given year.,$1 \leq N \leq 360$.

B. Declination angle (δ): - the sun's angle compared to our equator's axis at solar noon, plus north (−23.45° ≤δ ≤23.45°). The formula can be used to determine the declination angle in degrees for any given day of a given year (N) (Duffie & Beckman, 2013)

$$\delta = 23.45\sin[\frac{360}{365} * (284 + N)] \qquad (4.3)$$

C. Solar Hour angle (ω): -The solar system's angular displacement owing to the earth's rotating on its axis, which occurs at a rate of 15 degrees each hour (morning negative and afternoon positive), east or west of the local meridian. and cited from (Duffie & Beckman, 2013).

$$\omega = 15 * (Solar\ Time - 12) \quad (4.4)$$

D. Day duration, timings of sunrise and sunset

When a solar elevation angle (α) is a value of zero the position of the sun is considered to be rising and sets. Therefore, the hour angle at dusk, h can be originated by

$$\omega_{ss} = \cos^{-1}(-\tan\delta * \tan\varphi) \quad (4.5)$$

Where ω_{ss} is taken as positive for sunset and is negative for sunrise.

The length of sunshine hours (N_S) is computed from: -

$$N_S = \frac{2}{15}\ \omega_{ss} \quad (4.6)$$

E. Collector Tilt: - The angle formed by a collector plus the surrounding horizontal is known as the collector's tilt. For the majority of sunlight-to-heat water programs, a tilt of roughly 10° to 15° above latitude is almost ideal. (Duffie & Beckman, 2013).

Slope, $\beta = \varphi + (10°\ to\ 15°)$.

For the latitude of Bishoftu = 8.7347; the slope of the collector is:- $\beta = \varphi + 12.5°$

$$\beta = 8.7347 + 12.5 \cong 22°$$

4.1.3 Calculating Hourly Sun Radiation across a Horizontal Surface

4.1.3.1 Extra-terrestrial (ETR) Sun Radiation Per Day on a Horizontal Plane

Given by the Klein connection Equation, the normal direct solar energy at any given time is the radiation that strikes on a horizontal surface outside of the environment.: -

$$\overline{H}_O = \frac{24 * 3600}{\pi} I_{SC}(1 + 0.033\cos(\frac{360n}{365})) * (\cos\varphi\cos\delta\cos\omega_s + \frac{\pi}{180}\omega_s\sin\delta\sin\varphi) \quad (4.7)$$

Where, ω_s = sunset hour angle

$\overline{H}_O$ – in Wh/m^2

$I_{sc} = G_{sc} = 1367\ {}^{W}/_{m^2}$

n = average days for the month or the day of the year under consideration (1 to 365).

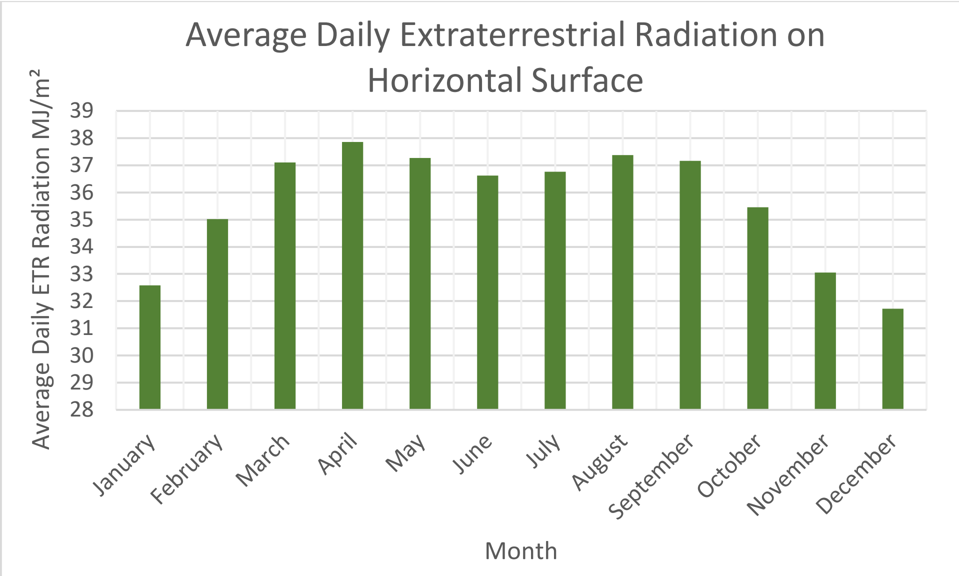

Figure 4.2 The Solar Radiation on Horizontal Plane Outside of the Atmosphere Extraterrestrial (ETR) Daily Solar Radiation

4.1.3.2 Forecast of Monthly Mean Every Day Radiation Worldwide on an HS ($\overline{H}$)

Angstrom proposed the first empirical correlation utilizing sunshine hours as a means of estimating global solar radiation. Prescott and Page made modifications to the Angstrom relationship.

The well-known Angstrom equation is the most basic model used to determine monthly average daily sun radiation on a horizontal plane. (Kalogiour & Soteris, 2014).

$$\frac{\overline{H}}{\overline{\mathrm{H}}_o} = a + b\left(\frac{\overline{n}_s}{\overline{N}_s}\right) \quad (4.8)$$

Where $\overline{\mathrm{H}}$= Global radiation is the monthly mean of everyday radiation across a horizontal plane.

$\overline{\mathrm{H}}_{\mathrm{o}}$= Monthly average radiation outside of the atmosphere (extraterrestrial, ETR on the horizontal surface) for the same location ($^{W}/_{m^2}$).

a, b – empirical constants.

$\overline{n}_s$ − Monthly average daily hours of bright sunshine (sunshine hour).

$\overline{N}_s$ −Monthly average of the maximum possible daily hours of bright sunshine.

The regression parameters “a” and “b” can be determined from; -

$$a = -0.11 + 0.235\cos\varphi + 0.323(\frac{\overline{n}_s}{\overline{N}_s})$$

$$b = 1.449 - 0533\cos\varphi - 0.694(\frac{\overline{n}_s}{\overline{N}_s})$$

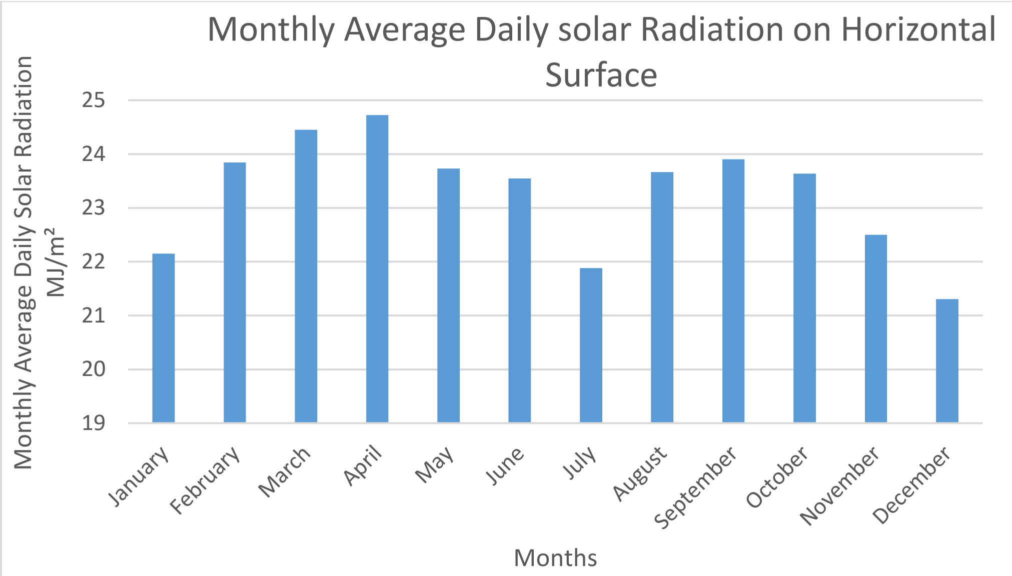

Figure 4.3 Graph of Monthly Average Daily Global Radiation on a Horizontal Surface

4.1.3.3 Forecast of Mean Daily Diffuse Radiation for a Month on HS($\overline{H}_d$)

The number of brilliant sunshine hours and the monthly average daily global radiation on a horizontal surface can be used to calculate the monthly mean daily diffuse rays on a horizontal plane. by (Duffie et al., 2020).

$$\frac{\overline{H}_d}{\overline{H}} = 0.931 + 0.814\left(\frac{\overline{n}_s}{\overline{N}_s}\right) \tag{4.9}$$

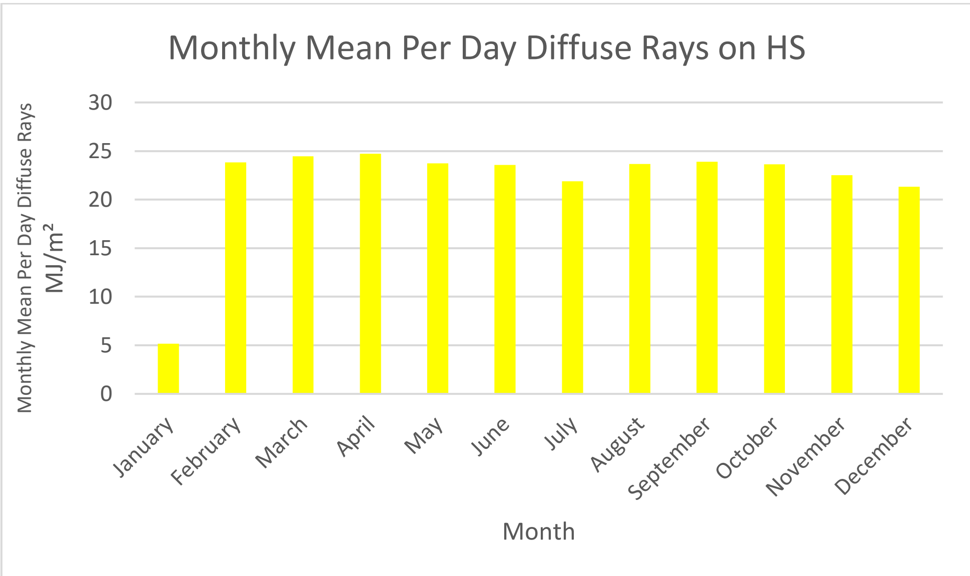

Figure 4.4 Horizontal Surface Displays the Monthly Mean Daily Diffuse Rays on Graph.

4.1.3.4 Forecast of Mean Per hour Global Radiation for Each Month on a HS ($\overline{I}$)

If the monthly mean daily global energy on a horizontal plane is known, it is possible to compute the monthly mean hourly global energy on that surface. The entire solar radiation received per hour on a horizontal plane, I in ${Wh}/{m^2}$ could be calculated using the daily radiation exposure worldwide, H (in ${KJ}/{m^2}$ per day) in harmony with (Duffie et al., 2020).

$$\frac{\bar{\mathrm{I}}}{\bar{\bar{\mathrm{H}}}} = \frac{\pi}{24}(a + b\cos\omega)\frac{\cos\omega - \cos\omega_s}{\sin\omega_s - \frac{\pi}{180}\omega_s\cos\omega_s} \tag{4.10}$$

a= $0.409 + 0.5016\sin(\omega_s - 60)$

$b = 0.6609 - 0.4767\sin(\omega_s - 60)$

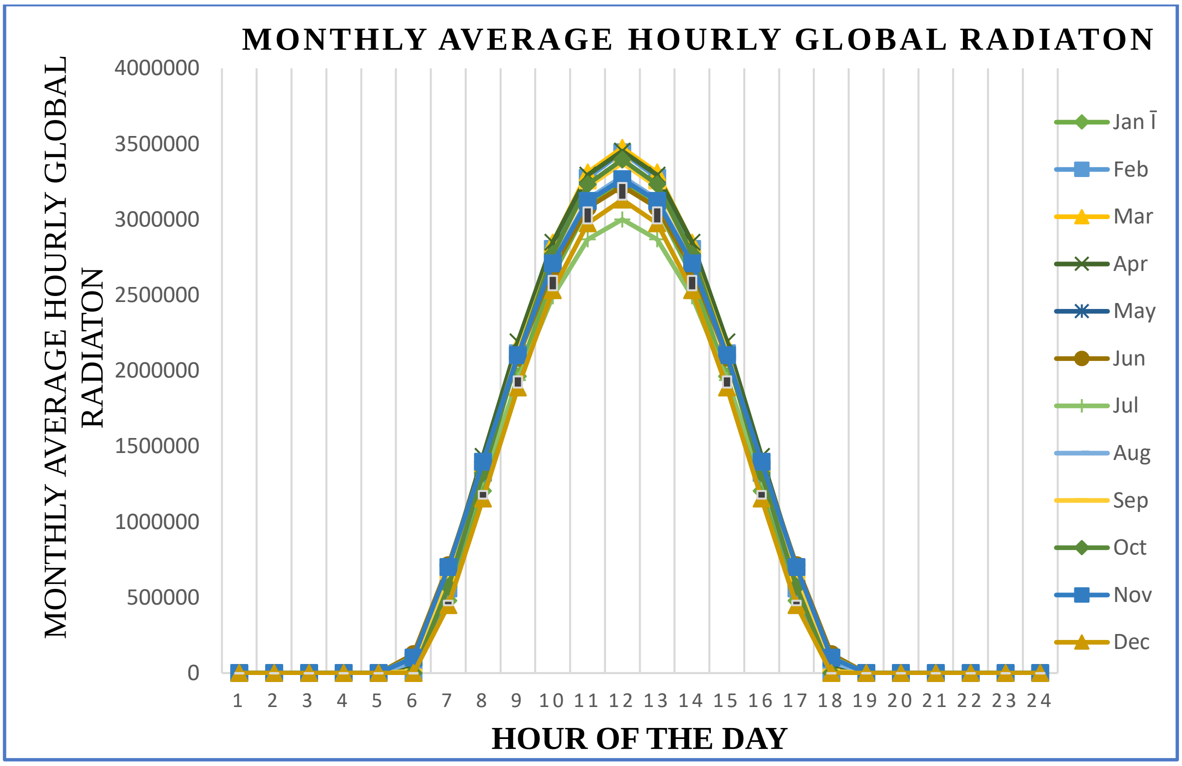

Figure 4.5 Graph of Monthly Average Hourly Global Radiation on a HS ($\bar{\boldsymbol{I}}$)

4.1.3.5 Forecast for the Monthly Mean Diffuse The Radiation Per Hour on a HS ($\bar{I}_d$)

The formula can be used to estimate the hourly amounts of diffuse solar radiation from the equation 4.10.

$$\frac{\bar{I}_d}{\bar{\bar{H}}_d} = \frac{\pi}{24}\frac{\cos\omega - \cos\omega_s}{\sin\omega_s - \frac{\pi}{180}\omega_s\cos\omega_s} \tag{4.11}$$

The direct (beam) component of the solar radiation on a horizontal surface is then obtained from:

$$G_b = G - G_d \tag{4.12}$$

Where: $\mathrm{G_b}$ is direct(beam) solar radiation

$\mathrm{G_d}$ diffuse solar radiation

G global solar radiation

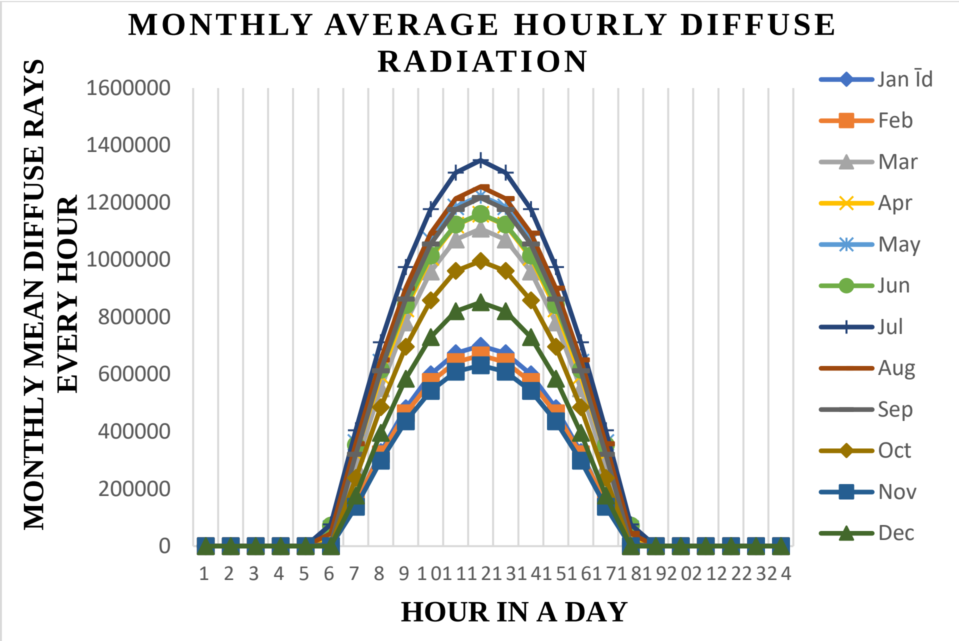

Figure 4.6 Graph of Monthly Mean Diffuse Rays Every Hour on a HS ($\bar{I}_d$)

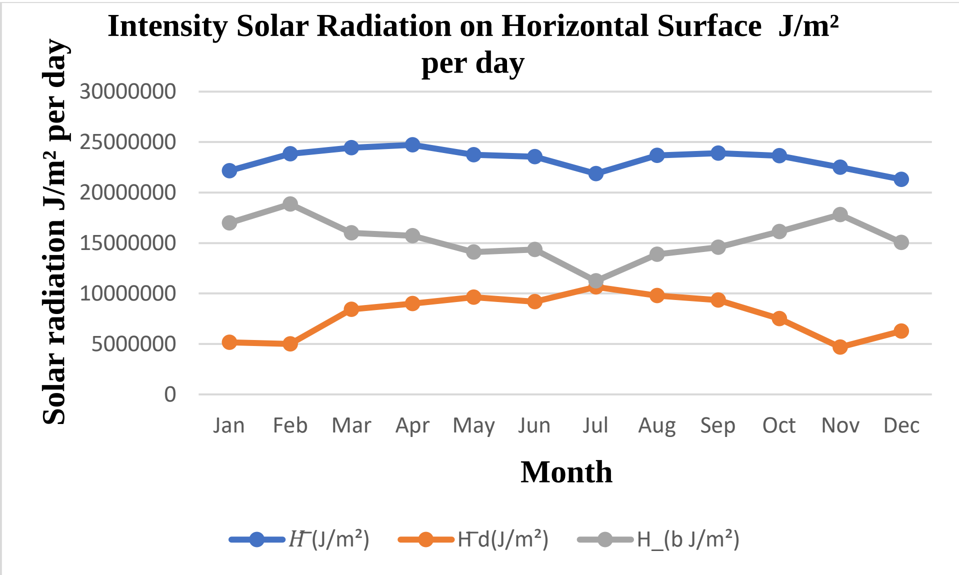

Figure 4.7 Monthly standard deviation of sun radiation (global, diffuse, and direct) graph.

CHAPTER FIVE

5. DESIGN SOLAR TOWER SYSTEM OVER ALL DIMENSION OF THE SOLAR SYSTEM

5.1 Solar Tower System

Heliostats focus the sun's beams onto a solar receiver in central receiver systems (CRSs), where they generate extremely high temperatures. A heliostat is made to use actuators to follow the sun's motion in two dimensions throughout the day. The heliostat field is defined by the total number of heliostats. The heliostat field, solar receiver, and power block make up the entire plant. The solar component of the power plant is made up of the receiver and the heliostat field.

The receiver absorbs the concentrated solar radiation and transforms the solar energy to thermal energy. The heat is then transferred to a conventional thermal cycle with a heat-transfer fluid (HTF). In the heat exchanger, steam is produced, which drives a steam turbine, transforming heat first to mechanical energy and then to electricity in a generator. Different working fluids may be used as HTF, with the common ones being salt, water/steam, and air (Alexopoulos & Hoffschmidt, 2017)

5.2 Solar Tower Selection

5.2.1 Heliostat Selection

The purpose of a heliostat is to follow the sun and maintain the sun's radiation being reflected into the center of the receiver by using a big mirror or group of mirrors coupled to a tracking control system that travels along two axes throughout the day. The reflecting surface is usually a thin, low-iron glass mirror. The heliostat is capable of rotating up and down (tilt) and left to right (surface azimuth adjustments). Another main purpose of the tracking control system uses motors controlled by a central computer that accurately points the heliostats in a way that bisects the angle between the vector coming from the sun and a vector pointing from the heliostat origin to the receiver. This bisection is done by analyzing the astronomical equations for the positioning of the sun, as well as the coordinates for the known position of the individual heliostat and the tower. This process minimizes the incident angle of the radiation beam and thereby maximizes the reflected radiation(Masters, 2011; Stine, 2001).

Heliostats are also used in small-scale applications, either to provide natural lighting or modest water heating.

5.2.2 Receivers

The receiver transfers the energy from the incoming reflected solar radiation to a heat transfer fluid that runs a turbine. Receivers are positioned at the top of the tower and high above the level of the heliostats on the tower in order to minimize the effect of shadowing and blocking among neighboring heliostats. The reflected energy from the heliostats is efficiently captured in this way. The size of the receiver apertures (absorbers) is chosen to roughly match the size of the sun's picture from the furthest heliostat. Additionally, since heat loss from convection and radiation is directly proportional to the aperture area, the aperture size must also be kept to a minimum.

In general, two main types of receivers are used: external and cavity receivers.

- External receiver
- Cavity receiver

External receiver: - typically consist of cylindrical panels of tubes joined by welding the tubes supply heat transfer fluid that is heated and collected for use in a turbine. External receivers usually have a height to diameter ratio of 1:1 to 2:1. Heat transfer fluids are typically those with high thermal conductivities, such as water/steam, liquid sodium, or molten nitrate salt.(Stine, 2001). For water/steam and molten nitrate salt, the surface area must be larger to compensate for the relatively low heat capacity of these fluids.

Cavity (Internal) Receivers: - The primary benefit of cavity receivers is the reduction in heat loss to the surroundings due to the placement of the heat-absorbing surface inside an insulated cavity. Cavity receivers generally have a structure between the aperture and the ambient called a secondary concentrator, which serves to further concentrate the incoming reflected radiation from the heliostats (Battleson, 1981). Therefore, the external receiver is preferred over the cavity receiver in this study because it is more effective and allows for development across the tower whereas the cavity receiver only tracks in one direction, north and south.

5.2.3 Towers

The tower should be constructed sufficiently high to reduce interference between nearby heliostats. However, the tower's height is often constrained by its price. Wind, receiver weight, and seismic loads are the three most important factors considered when designing a tower. Receiver weight loads are variable, but many towers have been designed to withstand wind and seismic loads of 90 mph and 0.25 g, respectively(Stine, 2001). Beam characterization targets are structures that are frequently present on the tower, just below the receiver. These are used for periodic beam radiation measurements and heliostat calibration. They are not intended to receive radiation from more than one or two heliostats at a time(Stine, 2001). Towers are mainly constructed from either reinforced concrete or free-standing steel. Free-standing steel towers are generally more cost-effective at tower heights below 120 m (400 feet). Reinforced concrete towers have proven more cost-effective at tower heights greater than 120 m(Falcone, 1986).

5.3 Heliostat Field Calculation

Choose the best heliostat first, then figure out how many are required. The "HELLAS 01" type heliostat has been selected out of the several heliostat types by taking into account the cost, size, and reflectivity.

Table 5.1 Properties of **HELLAS "01"** type heliostat

Name/model number	HELLAS 01
Manufacturer	GHER S. A
Area (Height, Width)	$2\ \mathrm{m}^2\ \ (2\mathrm{m}, 1\mathrm{m})$
Reflectivity	94%
Mirror Thickness	4mm
Control type	Microprocessor, Self-Sufficient

5.3.1 Number of Heliostat

A heliostat is a large mirror or set of mirrors attached to a tracking control system that moves about two axes throughout the day to track the sun and keep the sun's radiation reflected onto the center of the receiver.

The method used to estimate the number of heliostats was as follows:

$$\mathrm{Q_{ref}} = \mathrm{Q_{in}} * \eta_\mathrm{h} \tag{5.1}$$

Where " $\mathrm{Q_{ref}}$ " is the reflected solar radiation per square meter from the heliostats towards the receiver (W/m^2)

" $\mathrm{Q_{in}}$ " is the average annual direct normal irradiation per square meter (W/m^2). And

" η_h " is the heliostat efficiency.

In the converted data (GHI to DNI) the average direct normal irradiation of Bishoftu is $750.6\ ^{\mathrm{W}}/_{\mathrm{m}^2}$. Additionally, as seen in the above table, the "HELLAS 01" type heliostat has an efficiency of 94%.

$$\mathrm{Q_{ref}} = \mathrm{Q_{in}} * \eta_\mathrm{h} \tag{5.2}$$

$$\mathbf{Q_{ref}} = \mathbf{750.56}\ ^{\mathbf{W}}/_{\mathbf{m^2}}$$

Now that the DNI and heliostat efficiency values have been substituted, the reflected solar radiation to the receiver will be $750.56\,{}^{W}/_{m^2}$.

The power transmitted to the water/steam in the receiver can be calculated by

$$Q_{rec} = \frac{Q_f}{\eta_{rec}} \tag{5.3}$$

Where,

"Q_{rec}" is the power received on the surface of the receiver from the heliostats (W)

"Q_f" is the required thermal output power by the water/steam fluid(W) and

"η_{rec}" is the receiver efficiency.

The total heat capacity of the power input into the storage tank is the thermal output power by steam water. To determine the power input to the storage tank.

The hospital uses $\mathbf{3763.2KW}$ of power in total, and an average receiver efficiency is $\mathbf{85\%}$(Stalin Maria Jebamalai, 2016).

The power received on the surface of the receiver that is reflected from the heliostats will be

$$Q_{rec} = \frac{Q_f}{\eta_{rec}} = \mathbf{4427.3KW}$$

The total area of the heliostats " A_T" can be calculated from:

$$\text{Heliostat Area} = \frac{Q_{receiver}}{\text{Average DNI}} \tag{5.4}$$

$$A_T = \frac{Q_{rec}}{Q_{ref}} \tag{5.5}$$

$$A_T = \mathbf{616.2m^2}$$

The number "N" of heliostats is now determined by:

$$N = \frac{A_T}{A_h} \tag{5.6}$$

Where "A_h" is the area of each heliostat (m^2).

"**HELLAS 01**" type heliostat has a dimension of **2 $\mathbf{m^2}$ (2 m, 1 m)**. Substituting a value of "Ah" in equation (5.5) and then 322 heliostats are needed to gate that amount of power.

5.3.2 Tower Height

Usually, the tower's price determines how high it may go. The three main aspects that go into tower design are wind, receiver weight, and seismic stresses. However, several towers have been built to handle wind loads of 90 mph and seismic (earthquake) loads of 0.25 g. Receiver weight loads might vary. Usually, free-standing steel or reinforced concrete is used to build towers. Free-standing steel towers are generally more cost-effective at tower heights below

120m. Reinforced concrete towers have proven more cost-effective at tower heights greater than 120 m. The foundation of the tower is most often constructed from reinforced concrete to transfer loads to the underlying soil(Murray, 2012). The optimum tower height is generally about 1/6 the length of the farthest heliostat in the field to the tower. To calculate the height of the tower, take these two equations that shown below from Joseph correlation(Stalin Maria Jebamalai, 2016; Wah et al., 2019).

$$H_{t,min} = 36.30075 + (0.3013896Q_{rec}) - \left(0.1004369 * 10^{-3}Q_{rec}{}^{2}\right) \tag{5.7}$$

$$H_{t,max} = 54.91579 + (0.3070526Q_{rec}) - \left(0.1039793 * 10^{-3}Q_{rec}{}^{2}\right) \tag{5.8}$$

$$H_t = \frac{H_{t,min+H_{t,max}}}{2} \tag{5.9}$$

Where " Q_{rec} " is Receiver thermal power (MW); $H_{t,min}$ is minimum tower height (m); $H_{t,max}$ is maximum tower height (m); and H_t is Tower height (m) Now, by changing the receiver thermal power value **(4.427 MW)** in equations (5.7) and (5.8) and averaging those values, the tower's height is **14.5 m.**

5.3.3 Heliostat Field Layout

If all reflected beam radiation is to be absorbed by a spherical receiver, the maximum concentration ratio for a three-dimensional concentrator system with radiation on the plane of the heliostat array $\theta_i = \theta_z$, a rim angle of " ϕ_r", and a declination angle of "δ" is

$$C_{max} = \frac{\psi \sin^2 \phi_r}{4\sin^2(0.267 + {}^{\delta}/_{2})} - 1 \tag{5.10}$$

The heliostats are spaced apart, and only a fraction of the ground area ψ is covered by mirrors. A "ψ" of about 0.3 to 0.5 has been suggested as a practical value(Duffie et al., 2020). In this design the rim angel is 45° and taking the maximum value of declination angle (23°) when substitute these values is equation (5.10) the value of the maximum concentration ratio will be **0.287**.

Then to get the distance between the tower and the first heliostat (L) is

$$L = \frac{H_t}{\tan(\alpha_t)} \tag{5.11}$$

$$\alpha_t = 90 - \theta_z \tag{5.12}$$

$$\theta_z = \cos\phi\cos\delta\cos\omega + \sin\delta\sin\phi \tag{5.13}$$

Where, θ_z is zenith angle, δ declination angle, ω is hour angle considered the effective sunshine hour and α_t is the tower altitude angle measured from the center of the front heliostat, and ϕ is latitude of location.

Table 5.2 Monthly Calculated Value of Tower Altitude Angle

Months	N	δ	ϕ	θ_z	α_t
Jan	17	-20.917	8.7347	33.85	56.15
Feb	47	-12.9546	8.7347	28.59	61.41
Mar	75	-2.41773	8.7347	22.93	67.07
Apr	105	9.414893	8.7347	19.56	70.44
May	135	18.79192	8.7347	19.8	70.2
Jun	162	23.08591	8.7347	20.79	69.21
Jul	198	21.18369	8.7347	20.29	69.71
Aug	228	13.45496	8.7347	19.33	70.67
Sep	258	2.216887	8.7347	21.18	68.82
Oct	288	-9.5994	8.7347	26.45	63.55
Nov	318	-18.912	8.7347	32.45	57.55
Dec	344	-23.0496	8.7347	35.35	54.65

By taking the maximum value of declination angle (-23°) and gate the minimum value of tower altitude angle of 54.65°(Grigoriev et al., 2021). Then substitute this value in equation (5.11) and finally the maximum distance between the first heliostat and tower will be **6.23 m**. Then the total area of the field (A_f) will be

$$A_f = \frac{\pi[(5H_t)^2 - L^2]}{4} \tag{5.14}$$

Now substitute the values of tower height and the distance between tower and the first heliostat the area of the field is **3,801.1 m^2**. In order to minimize shading of heliostats and blocking of the reflected light on optimized layout of the heliostat field was developed by Lipps and Vant-Hull. The layout as shown in figure (5.8) is called a radial stagger layout. The radial (R) and azimuthal (A) spacing are given below (Goswami, 2022; Wagner, 2008).

$$R = h(1.44\cot\alpha_t - 1.094 + 3.068\alpha_t - 1.256{\alpha_t}^2) \tag{5.15}$$

$$A = w\left(1.749 + 0.639\alpha_t + \frac{0.2873}{\alpha_t - 0.04902}\right) \tag{5.16}$$

The HELLAS 01 type heliostat has the following dimensions: height "h" is2 m and width "W" is 1 m when these values are substituted in equations (5.15) and (5.16). The radial separation (R) is **0.9688 m** and the azimuthal spacing (A) is **1.66 m**.

5.3.4 Selection of Working Fluid

Water has good physical properties to be used as a heat transfer fluid (HTF) due to its high specific heat (4185.5 J/kg·K), availability, low viscosity, non-toxicity, and low cost. Since it is readily available, has great thermos physical characteristics, and is environmentally acceptable, water is one of the fluids utilized as HTF. The usage of alternative HTFs with a greater working temperature is recommended when a high operating temperature is required. However, as the primary goal of this study is to provide hot water to the hospital, employing water as HTF is the most suitable option for this research.

Table 5.3 Thermo-physical properties of water/steam

Physical Property	**Value**
Specific Heat (577-300K)($^{J}/_{Kg.K}$)	4185.5
The efficiency of the receiver (%)	85
Temperature of HTF at the Outlet (K)	577
Temperature of HTF at the Inlet (k)	300
Density of Water ($^{Kg}/_{m^3}$)	1000
Velocity of Fluid ($^{m}/_{s}$)	4

5.3.5 Receiver

The energy from the incoming reflected solar radiation is transferred from the receiver to a heat-transfer fluid that powers a turbine. The primary goal of this project is to give hot water to the hospital after heliostats track the sun and reflect its rays to heat the water. Receivers are positioned at the top of the tower and high above the level of the heliostats on the tower in order to minimize the effect of blocking and shading between heliostats. The reflected energy from the heliostats is collected as efficiently as possible.

5.3.5.1 Receiver sizing

The size of the sun's picture as it is reflected off the heliostats is about equivalent to the size of the receiver. For cavity receivers, the enclosed construction exposes the inside surfaces to re-radiation, which might cause overheating. For the same incident receiver thermal power, the cavity receiver size is 25% greater than the external receiver(Stalin Maria Jebamalai, 2016). Receiver size is done based on the allowable flux on the receiver. The allowable flux on the receiver is depends on the receiver material and the type of heat transfer fluid. Generally, the allowable peak flux from water/steam receivers that built with 316 stainless steel material is 0.6MW/m^2 and for the receivers that built with in coloy 800H is 1MW/m^2(Stalin Maria Jebamalai, 2016).

The area of the receiver will be determined by utilizing the typical permitted flux.

$$A_{rec} = \frac{Q_{rec}}{q_{avg,flux}} \tag{5.17}$$

Where "$q_{avg,flux}$" is the allowable average flux of the receiver (W/m^2). This power plant is used water/steam as a heat transfer fluid and considering the strength and cost of the material the receiver tubes will be done by stainless steel, therefore the allowable average flux of the receiver is 0.6MW/m^2 and receiver thermal power output is 4.427MW/m^2. Then the area of the receiver will be $\mathbf{4.708m^2}$.

The parameter receiver aspect ratio (AR) is induced to construct outer geometry. The receiver's height-to-diameter ratio is known as the aspect ratio. The aspect ratio for an external receiver typically ranges from 1 to 2. The receiver aspect ratio will be in the range 1.2 to 1.5 and it should be selected for maximum receiver efficiency(Stalin Maria Jebamalai, 2016).

In this model, the default value of the receiver aspect ratio is set as 1.5. Then the area of the receiver "A_{rec}" can be calculated as(Stalin Maria Jebamalai, 2016)

$$A_{rec} = \pi D_{rec} H_{rec} \frac{\pi}{2} \tag{5.18}$$

The factor "$\frac{\pi}{2}$" is used to take into account the curvature of the tube in the receiver. Equation (5.18) can be reformulated in terms of the receiver aspect ratio. and the diameter of the receiver will be

$$D_{rec} = \sqrt{\frac{A_{rec}}{\pi . AR . \frac{\pi}{2}}} \tag{5.19}$$

$$H_{rec} = AR . D_{rec} \tag{5.20}$$

$D_{rec} = \mathbf{1.021m}$ Then the height of the receiver is $H_{rec} = \mathbf{1.5315m}$

5.3.5.2 Panel and Receiver Tube Design

In order to design receiver tubes and panels, the tube outer diameter, tube thickness, and number of flow channels in the receiver must be chosen. The range of the tube's outer diameter is typically 20 to 45 mm. The diameter of tube is related to receiver thermal power, because of the fact that the mass flow rate of the heat transfer fluid depends on the required receiver thermal power. Consequently, the fluid velocity is adapted to meet the required mass flow. The fluid velocity is maintained by the cross-sectional area of the tube within the allowable limits (Stalin Maria Jebamalai, 2016).

The scalability of the power plant is addressed by developing a linear correlation for the tube outer diameter with receiver thermal power. The developed linear correlation for tube outer diameter " $d_{o,tube}$ " is

$$\mathrm{d_{o,tube}} = (0.2682 * 10^{-4} * \mathrm{Q_{rec}}) + 0.02268 \qquad (5.21)$$

Substitute the value of thermal power output of the receiver, "Q_{rec}" 4624.94KW in equation (5.21) and the outer diameter of the receiver tube, "$d_{o,tube}$" will be 22.93 mm. Then to make the standard size it will be **23 mm**.

The fluid flow path is chosen in such a way that it can distribute the local peak flux on the receiver evenly. The number of fluid flow paths has an influence on the pressure drop.

For water/steam receivers, single flow path is needed to get high velocities and high wall heat transfer coefficients for water/steam receiver. Hence, single flow path in the water/steam receiver are suggested in order to obtain better overall efficiency of the plant(Stalin Maria Jebamalai, 2016).

For single flow path the total number of receiver tubes, "$\mathrm{n_{tube,rec}}$" can be calculated as:

$$\mathrm{n_{tube,rec}} = \frac{\pi * \mathrm{D_{rec}}}{2 * \mathrm{d_{o,tube}}} = 40 \qquad (5.22)$$

Tube thickness depends on the pressure exerted by the fluid onto the tube. In case of water/steam receivers, it can be as low as 1 mm (Wagner, 2008). The default value of tube thickness is selected as 1.5 mm in this model.

The number of tubes per panel, " $n_{tube,panel}$" can be calculated with the cross-sectional area of the fluid path:

$$\mathrm{n_{tube,panel}} = \frac{\mathrm{A_{sec}}}{\pi(\frac{\mathrm{d_{i,tube}}}{2})^2 * \mathrm{n_{flow,path}}} \qquad (5.23)$$

It is necessary to first determine the total cross-sectional area of the fluid path, A_{sec} before determining the number of tubes per panel.

$$\mathrm{A_{sec}} = \frac{\mathrm{m_{fluid}}}{\rho_{\mathrm{fluid}} * \nu_{\mathrm{fluid}}} \qquad (5.24)$$

The absorbed receiver thermal power is used to compute the design mass flow rate of the receiver fluid. The requirement that the flow must be turbulent sets the minimal mass flow rate that may be transported without causing any harm. As a result, the Reynolds number needs to be at least 4000(Stalin Maria Jebamalai, 2016).

The mass flow rate “m_{fluid}” is calculated by;

$$m_{fluid} = \frac{Q_{rec} * \eta_{rec}}{C_p(T_{hf} - T_{cf})} \qquad (5.24)$$

Where, the thermal output of the receiver “ Q_{rec} ” is 4625 KW; the efficiency of the receiver ηrec is 85%; the specific heat of the receiver fluid “C_p” is 4185.5 $^{J}/_{Kg.K}$; and the change in temperature is 277K (Mahboob et al., 2021), then the mass flow rate of the fluid “m_{fluid}” is **3.391Kg/s**. Now substitute the values of density and mass flow rate of the fluid 1000$^{Kg}/_{m^3}$ and also assume the velocity of the fluid **4 m/s**, the cross-sectional area of the fluid path “A_{sec}” will be **8.478*$\boldsymbol{10^{-4} m^2}$**.

Finally, substitute equations (5.24) & (5.25) in equation (5.23) and the internal tube diameter is 20 mm where the tube thickness is **1.5 mm** and the number $n_{flow,path}$ is **2** for water/steam receiver HTF then a number of tubes per panel “ $n_{tube,the\ panel}$” is **3** in number.

The number of tubes per panel and the total number of tube receivers are already calculated, the number of panels “n_{panel}” can be calculated as;

$$n_{panel} = \frac{n_{tube,rec}}{n_{tube,panel}} \qquad (5.26)$$

Now substitute the number of tubes in the receiver and the number of tubes in a panel in equation (5.26) and then the number of panels for this receiver is **26**.

5.3.6 Surface Temperature of the Receiver

Calculating the heat transfer through the tube walls requires assuming that the receiver has a constant surface temperature. Conduction through the thickness of the tube wall is considered in the computation, followed by convection to the receiver fluid. By computing the resistance resulting from conduction and convection, the surface temperature of the receiver is determined. Calculations for the receiver surface temperature "$T_{s,avg}$" include;

$$T_{s,avg} = Q_{fluid}(R_{cond} + R_{conv}) + T_{htf,avg} \qquad (5.27)$$

Where “$T_{htf,avg}$” is average temperature of the receiver fluid in “K” and solar water heating system: between 40°C to 80°C. The resistance due to conduction through the tube walls “ R_{cond}” can be given by:

$$R_{cond} = \frac{\ln(^{r_{o,tube}}/_{r_{i,tube}})}{\pi * H_{rec} * K_{tube} * n_{tube}} \qquad (5.28)$$

Where $r_{o,tube}$= Radius of the receiver outer tube, m. $r_{i,tube}$= Radius of the receiver inner tube, m. K_{tube} = Thermal conductivity of the tube, 15.1W/m. k where the tube is stainless steel. n_{tube} = Total number of tubes in the receiver.

$$\mathbf{R_{cond} = 2.468 * 10^{-5}\ K/W}$$

The resistance due to the internal convection between tube wall and the receiver fluid R_{conv} can be given by:

$$R_{conv} = \frac{1}{h_{inner} * \pi * r_{i,tube} * H_{rec} * n_{tube}} \qquad (5.29)$$

The following equation can be used to get the heat transfer coefficient of internal convection between the tube wall and the receiver fluid "h_{inner}".

$$\mathbf{h_{inner} = Nu * K_{fluid}/L_c} \qquad (5.30)$$

Where $\mathbf{L_c}$ is the Characteristic length, which is the inner receiver tube diameter, "$d_{i,tube}$". Reynolds number and Pradntl number must be calculated before determining the Nusselt number, which determines whether the flow is turbulent or laminar.

The Nusselt correlation is;

$$Nu = 0.023Re^{0.8} * Pr^{0.4} \qquad (5.31)$$

$$Re = \frac{\rho DV}{\mu} = \mathbf{107.8 * 10^3} \qquad (5.32)$$

$$Pr = \frac{Cp * \mu}{K} = \mathbf{14.354} \qquad (5.33)$$

The above equation is valid for $0.7 < Pr < 120$ and $10^4 < Re < 1.2 \times 10^5$ (Shatnawi et al., 2021; Stalin Maria Jebamalai, 2016). Using these equations, the surface temperature of the receiver is calculated.

Nusselt number is 709 as determined by equations (5.32) and (5.33) and the heat transfer coefficient of internal convection between the tube wall and the receiver fluid, "$\boldsymbol{h_{inner}}$" is $\mathbf{21.5 * 10^3\ W/m^2.K}$. then substitute this value in equation (5.29). The resistance resulting from the internal convection between the receiver fluid and the tube wall will be;

$$\mathbf{R_{conv} = 1.24 * 10^{-5}\ K/W}$$

The surface temperature of the receiver will finally be determined using the previously discussed calculations. $\mathbf{T_{s,avg} = 498.77K}$

5.3.7 Heat Loss on The Receiver

The full absorber surface is exposed to the environment when using external receivers. Therefore, compared to cavity receivers, there are more heat losses from the receiver to the environment(Stalin Maria Jebamalai, 2016). The heat loss model takes into account heat loss from radiation, external convection, and reflection. Conduction to the back of the receiver panel results in minimal losses compared to other losses, hence it is neglected.

a) Convection Heat Loss

The only heat loss in the receiver that is directly related to the wind conditions is convective heat loss. Typically, a vertical cylinder is used to represent the external receiver. To use the receiver as a vertical plate for the heat transfer correlations, the following need must be satisfied. Given below is the equation for external convection heat loss along with the mixed convection heat transfer coefficient(Stalin Maria Jebamalai, 2016).

$$\mathrm{Q_{loss,conv}} = \mathrm{h_{mix}} * \mathrm{A_{rec}} * \left(\mathrm{T_{s,avg}} - \mathrm{T_{amb}}\right) \tag{5.35}$$

The majority of the outdoor solar receivers will experience "$\mathrm{h_{mix}}$" convection. Both natural and forced convection have an impact on convective heat transfer for cylindrical receivers. Thus, mixed convection is typically taken into account.

$$\mathrm{h_{mix}} = (\mathrm{h_{nat}}^{\mathrm{m}} + \mathrm{h_{for}}^{\mathrm{m}})^{1/\mathrm{m}} \tag{5.36}$$

Where, $\mathrm{h_{nat}}$= Heat transfer coefficient due to natural convection, $\mathrm{W}/_{\mathrm{m^2.K}}$ and

$\mathrm{h_{for}}$ = Heat transfer coefficient due to forced convection, $\mathrm{W}/_{\mathrm{m^2.K}}$.

The number m falls between 3 and 4. According to Cengel(Cengel & Heat, 2003), the bigger numbers are appropriate for horizontal surfaces while the value nearer to 3 is better for vertical surfaces. The heat transfer coefficient for natural convection, “$\mathrm{h_{nat}}$” can be calculated with the following equation:

$$\mathrm{h_{nat}} = \frac{\mathrm{Nu_{nat}} * \mathrm{K_{rec}}}{\mathrm{H_{rec}}} \tag{5.37}$$

Where, $\mathrm{Nu_{nat}}$ = The Nusselt number for natural convection and $\mathrm{K_{rec}}$ = Thermal conductivity of the receiver.

For natural convection, the Nusselt number should be computed first.

$$\mathrm{Nu_{nat}} = 0.098 * \mathrm{Gr}^{1/3} * \left(\mathrm{T_s}/_{\mathrm{T_{amb}}}\right)^{-0.14} \tag{5.38}$$

All the fluid properties are calculated at the ambient temperature “$\mathrm{T_{amb}}$”. Where $\mathrm{T_s}$ is surface temperature of the receiver and Gr is The Grashof number.

The following equation can be used to determine the Grashof number, Gr;

$$\mathrm{Gr} = \mathrm{g} * \beta * \left(\mathrm{T_{s,avg}} - \mathrm{T_{amb}}\right) * {\mathrm{H_{rec}}^3}/{\nu_{\mathrm{fluid}}} \tag{5.39}$$

Where, g = Acceleration due to gravity, $m/_{s^2}$, β = Volumetric expansion coefficient, $1/_{\mathrm{K}}$ $\mathrm{T_{s,avg}}$ = Average surface temperature of the receiver, K, $\mathrm{T_{amb}}$= Ambient temperature, K

$\mathrm{H_{rec}}$ = Height of the receiver, ν_{fluid} = Kinematic viscosity, $\mathrm{m^2}/_{\mathrm{s}}$.

$@\mathrm{T_{amb}}\ is\ \beta = 2.45 * 10^3$ and $\nu_{\mathrm{fluid}} = 15.89 * 10^6$

Grashof number will be $108.6*10^{-3}$ if you now replace the values of the volumetric expansion coefficient and kinematic viscosity of air at ambient temperature in equation (5.39). Then, the natural convection Nusselt number will be 0.056.

After doing so, enter the values for the receiver's Nusselt number (0.056), thermal conductivity $15.1 * 10^3\ W/_{m.K}$, and receiver diameter (1.021 m) into equation (5.37), and the heat transfer coefficient for natural convection "$\mathrm{h_{nat}}$" will be $0.656 * 10^3\ \mathrm{W}/_{\mathrm{m^2}}$ K.

The heat transfer coefficient for forced convection, "$\mathrm{h_{for}}$" can be calculated in the following equation:

$$\mathrm{h_{for}} = \frac{\mathrm{Nu_{for}} * \mathrm{K_{rec}}}{\mathrm{D_{rec}}} \tag{5.40}$$

The Nusselt number for forced convection will be calculated as:

$$\mathrm{Nu_{for}} = 0.3 + \frac{0.62 * \mathrm{Re}^{1/2} * \mathrm{Pr}^{1/3}}{[1 + ({0.4}/_{\mathrm{Pr}})^{2/3}]^{1/4}} * \left[1 + \left(\frac{\mathrm{Re}}{282000}\right)^{5/8}\right]^{4/5} \tag{5.41}$$

Reynolds and Prandtl numbers should be calculated before calculating the Nusselt number. Reynolds number, "Re" is defined as the ratio of inertial and viscous forces. It can be calculated using the following equation:

$$\mathrm{Re} = \frac{\mathrm{V_{wind}} * \mathrm{D_{rec}}}{\nu_{\mathrm{air}}} \tag{5.42}$$

Where, $\mathrm{V_{wind}}$= wind velocity and $\mathrm{D_{rec}}$=diameter of receiver.

All the fluid properties are calculated at the film temperature, "$\mathrm{T_f}$".

$$\mathrm{T_f} = \frac{\mathrm{T_{amb}} + \mathrm{T_s}}{2} = \mathbf{399.385K}$$

Using the interpolation method, the fluid properties are calculated as follows

Table 5.4 air properties

T(K)	Cp ($^{KJ}/_{Kg.s}$)	$\mu(^{N.s}/_{m^2})$	K ($^{W}/_{m.s}$)	$\nu(^{m^2}/_{s})$
350	1.021	$250.7 * 10^7$	$37.3 * 10^3$	$32.39 * 10^6$
400	1.030	$270.1 * 10^7$	$40.7 * 10^3$	$38.79 * 10^6$

$$\frac{400-350}{399.385-350} = \left(\frac{@400 - @350}{x-350}\right) \quad (5.43)$$

By using the above relation, the properties of the fluid at temperature of 399.385 K will be

$$@T_f = 399.385K \begin{cases} Cp = 1.0225 \\ \mu = 254.56 * 10^7 \\ K = 37.98 * 10^3 \end{cases}$$

$$\nu = 33.105 * 10^6$$

Now using these properties and the diameter of the receiver the Reynolds number, “Re” will be $0.17 * 10^6$.

The proportion of thermal to viscous diffusion rate is known as the Prandtl number, or "Pr" The equation below can be used to compute it:

$$Pr = \frac{^{\mu}/_{\rho}}{^{K}/_{Cp * \rho}} = \frac{Cp * \mu}{K} \quad (5.44)$$

Where, μ = Dynamic viscosity, kg/m.s, K = Thermal conductivity, W/m.K and Cp = Specific heat, J/kg.K.

Now substitute Reynolds number ($0.17 * 10^6$) and Prandtl number ($7.025 * 10^3$) in equation (5.39) then the value of Nusselt number for forced convection will be 0.3024. Also, by substituting the value of the Nusselt number in equation (5.40), the heat transfer coefficient for forced convection will be $4.248 * 10^3 \, ^{W}/_{m^2}.K$.

Then the mixed convection will be

$$\mathbf{h_{mix} = 4.253 * 10^3 \, ^{W}/_{m^2} . k}$$

Finally, the convection heat loss will be $\mathbf{651.61 * 10^3 W}$ by substituting the value of mixed convection, the area of the receiver, and the temperature differential between the receiver surface and atmosphere.

b) Heat Loss from Long-wave Thermal Radiation

The Stefan-Boltzmann law can be used to compute the radiation heat loss, or "Q_{loss}" which is basic for external receiver. The black coating is applied to the exterior receiver to improve absorptivity.

$$Q_{loss} = \sigma * \varepsilon_{eff} * A_{proj} * \left(T_{s,avg}{}^{4} - T_{amb}{}^{4}\right) \tag{5.45}$$

Where σ = Stefan-Boltzmann constant, $5.67 * 10^{-8}\, {W}/{m^{2}}.K^{4}$ ε_{eff}= Emissivity of the receiver, A_{proj} = Projected area of the receiver,m^2 $T_{s,avg}$ = Average surface temperature, K T_{amb}= Ambient temperature, K.

The following equation provides the effective emittance.

$$\varepsilon_{eff} = \frac{\varepsilon}{\varepsilon + (1 - \varepsilon) * {2}/{\pi}} \tag{5.46}$$

The stainless-steel receiver's emissivity is 0.17 at 498.77K(Hunnewell et al., 2017; King et al., 2018). When this value is used in place of equation (5.46), the effective emittance value is equal to **0.2434**. Since the projected area and receiver area are almost similar, if the projected area, Stefan Boltzmann constant, average surface temperature, $T_{s,avg}$, and ambient temperature, T_{amb} are substituted in equation (5.45), the radiation heat loss, "Q_{loss}, rad," will be $5.26 * 10^3 W$.

c) Heat Loss from Reflection

Reflective heat loss refers to the portion of radiation that is reflected away from the receiver surface. The receiver coating's absorptance can be used to compute it. The reflected heat loss from the receiver surface, "$Q_{loss,ref}$," is given by the equation below:

$$Q_{loss,ref} = (1 - \alpha_{eff}) * Q_{rec} \tag{5.47}$$

Since receiver tubes are curved, "α_{eff}" stands for effective absorptance. When determining the absorptance, the tubes' curvature must be taken into consideration. It is possible to determine the effective absorptance, or "α_{eff}"

$$\alpha_{eff} = \frac{\alpha}{\alpha + (1 - \alpha) * {2}/{\pi}} \tag{5.48}$$

The receiver's absorptance for metal that has been coated black is 0.92. The effective absorptance of the receiver is 0.9475 as a result of replacing this value in equation (5.48). Since we now have the effective absorbance and thermal power output values for the receiver, we can substitute these values in equation (5.47), and the reflected heat loss will be equal to $\mathbf{242.8 * 10^{3} W}$.

5.3.7 Heat Transfer Interactions Analysis in HCE

- **Heat transfer between Heliostat Glass cover and the atmosphere**.

Due to the temperature difference, there is convectional heat transmission from the heliostat glass cover to the ambient air around it, as well as radiation heat transfer between the heliostat glass cover and sky.

a. Convection heat transfer

The following illustration uses Newton's equation of cooling to estimate the convection heat transfer(Padilla et al., 2011).

$$Q_{go-r} = h_{cv,ext}\pi D_{go}\left(T_{go} - T_r\right) \tag{5.49}$$

Where, $h_{cv,ext}$ is the convective heat transfer coefficient between the external surface of the heliostat glass cover and the ambient air(Tzivanidis et al., 2016).

$$h_{cv,ext} = \frac{8.6{V_{air}}^{0.6}}{L^{0.4}} \tag{5.50}$$

Where: V_{air} is wind speed in m/s and L is the length of a collector in m

b. Radiation heat transfer

Assume that the sky is represented as a big blackbody cavity, with the heliostat glass envelope acting as a little gray plate. Between the glass heliostat envelope and the sky, there is a radiation heat transfer caused by(Lamrani et al., 2018).

$$\mathrm{Q_{go-sky,rad}} = \pi \mathrm{D_{go} h_{r,ext}}\left(\mathrm{T_{go}} - \mathrm{T_{sky}}\right) \tag{5.51}$$

The glass envelope of the heliostat and the sky's heat transfer coefficient by radiation are given as follows:

$$\mathrm{h_{r,ext}} = \sigma\varepsilon_{\mathrm{go}}(\mathrm{T_{go}})^2 + \left(\mathrm{T_{sky}}\right)^2\left(\mathrm{T_{sky}} + \mathrm{T_{go}}\right) \tag{5.52}$$

Where σ is the Stefan–Boltzman constant (5.67 $*10^{-8}$) and ε_{go} is the emittance of the external surface of the heliostat glass envelope.

The effective sky temperature is assumed to be 12°C below the ambient temperature(Yılmaz & Mwesigye, 2018).

$$\mathrm{T_{sky}} = \mathrm{T_{amb}} - 12°\mathrm{C}$$

- **Heat transfer between the receiver tube and heliostat glass cover**

Heat transfer between the receiver tube and glass cover occurs by convection and radiation mechanism.

a. Convection heat transfer

The annulus pressure affects convection heat transmission. The convective heat transfer coefficient is taken to be zero for pressures below 0.013 Pa. Free convection is used for heat transmission at greater pressures. According to **Raith by and Holland's formula**, the convective heat transfer is computed as follows for pressures greater than 0.013 Pa(Lamrani et al., 2018).

$$\mathrm{Q_{go-r}} = \mathrm{h_{cv,int}}\left(\mathrm{T_g} - \mathrm{T_r}\right) \tag{5.53}$$

where $h_{cv,int}$ is calculated using the natural convection relationships between two horizontal, concentric cylinders, and, is provided by(Kalogirou, 2012).

$$h_{cv,int} = \frac{2\pi K_{eff}}{\ln(\frac{D_{gi}}{D_{ro}})} \tag{5.54}$$

$$K_{eff} = 0.36K_{air}(\frac{Pr_{air}}{0.861 + Pr_{air}})^{0.25}(R_{acc})^{0.25} \tag{5.55}$$

Where,

$$R_{acc} = \frac{\ln(\frac{D_{gi}}{D_{ro}})^4}{{L_{eff}}^3\left({D_{gi}}^{-0.6} + {D_{ro}}^{-0.6}\right)}(Gr_{air} * Pr_{air}) \tag{5.56}$$

The critical length is given by

$$L_{eff} = 0.5\left(D_{gi} - D_{ro}\right) \tag{5.57}$$

b. Radiation Heat Transfer

The radiation heat transfer between the heliostat glass cover and the receiver tube is computed by(Padilla et al., 2011).

$$Q_{ro-gi,rad} = \pi D_{go} h_{r,int}\left(T_r - T_g\right) \tag{5.58}$$

$$h_{r,int} = \frac{\sigma((T_r)^2 + (T_g)^2(T_r + T_g)}{\frac{1}{\varepsilon_r} + \frac{1 - \varepsilon_g}{\varepsilon_g}(\frac{D_{ro}}{D_{gi}})} \tag{5.59}$$

Pump Selection

An active system moves the hot water via a pump or circulation. from receiver to hot water storage tank and to heat up again it takes from cold storage A circulator is used in pressure systems, which are full of liquid, to transfer hot water or heat-exchange liquid from the collector to the thermal energy storage. Pumps are sized to satisfy specified system design and performance flow rate requirements by surpassing static and head pressure requirements.

Pump selection is based on different factors such as:

- The necessary delivery rate (capacity)
- Types of systems (both direct and indirect)
- Fluid for collecting heat
- Functioning temperature
- Mandatory fluid movement duties
- Head needed
- Distraction losses
- Accessibility and easy maintenance

5.3.8 Transient Analysis of Temperature in the Solar Tower Collector System

Modeling the concentrating solar tower collector system mathematically while taking into account the transient characteristics of each zone. The investigated control volume of the solar tower collector (heliostat, receiver, tower, fluid stream, and storage tank) in the suggested model is perpendicular to the direction of the liquid flow. The transient analysis of the solar tower collector temperature varies for each zone of the collector, having a maximum temperature on the receiver after tracking the ray and water stream zone, a minimum temperature before entering the receiver coil, and also varies over the day(Hachicha et al., 2019).

In the transient analysis of general Concentrated Solar Collector, Solar Tower Collector's different assumptions are considered(Bellos & Tzivanidis, 2018).

The following assumptions are applied in the present modeling:

- There are no contact thermal losses.
- The heat convection losses between the (receiver)absorber and heliostat glass cover are neglected.
- There is uniform heat flux over the receiver.
- The solar collector radiates thermally to the ambient.
- There is no great difference between heliostat glass(cover) and ambient temperature level.
- There is no great difference between the receiver and fluid temperature level
- The flow is fully developed and it can be characterized by a constant heat transfer coefficient along the tube.
- This model needs knowledge of the fluid thermal properties, as well as of the heat transfer coefficient.
- All the thermal properties, as well as the receiver emittance, can be estimated for the temperature level of the inlet temperature.

5.3.8.1 Energy Balance for the Fluid

The energy balance for the heat transfer fluid circulating in the receiver tube is expressed by the following relationship:

$$\rho_f * Cp_f * A_f \frac{\partial T_f(x,t)}{\partial t} = Q_u - \rho_f * Cp_f * \dot{V} \frac{\partial T_f(x,t)}{\partial X} \qquad (5.60)$$

Where Q_u − is the heat flow transmitted to the fluid [W] ρ_f - is the fluid density ($^{Kg}/_{m^3}$) Cp_f - is the specific heat of fluid ($^{J}/_{Kg.\,K}$), $\dot{V}$ - is the volume flow rate ($^{m^3}/_{s}$).

All thermos physical characteristics of the water are a function of its temperature. Initial and boundary conditions of the above heat transfer fluid (HTF) energy balance.

$$T_f(0,t) = T_{inlet}(t)$$

$$T_f(x,t) = T_{inlet}(0)$$

5.3.8.2 Energy Balance for the Receiver

The energy balance for the receiver is given by the following equation

$$\rho_{rec} * Cp_{rec} * A_r \frac{\partial T_f(x,t)}{\partial t} = Q_r(t) - Q_{exit}(x,t) - Q_u(x,t) \qquad (5.61)$$

$Q_r(t)$− is the heat quantity received by the receiver tube (W)

$$Q_r(t) = I_d * \gamma * \tau_g * \alpha_r * r_m * W_k(\theta)$$

$$\begin{aligned} \rho_{rec} * Cp_{rec} * A_r \frac{\partial T_f(x,t)}{\partial t} &\\ = I_d * \gamma * \tau_g * \alpha_r * r_m * W_k(\theta) - \pi D_{ro} * h_{rad,int}(T_r - T_c) - \pi D_{ro} &\\ * h_{cv,int}(T_r - T_c) - \pi D_{ro} * h_{conv,f}(T_r - T_f) & \end{aligned}$$

Where, I_d- is direct normal irradiation ($^{W}/_{m^2}$), A_r - is the difference between the inner surface and the outer surface of the receiver tube (m²), A_c – is the collector aperture area m².

The initial conditions for the equations.

$$T_{rec}(x,t) = T_{entry}(0)$$

5.3.8.3 Energy Balance for the Cover (Heliostat Glass Tube)

Energy balance for heliostat glass tube is

$$\rho_g * Cp_g * A_g \frac{\partial T_g(x,t)}{\partial t} = Q_{int}(x,t) - Q_{ext}(x,t) \qquad (5.62)$$

Q_{int}:- is the internal heat power (by convection and radiation) between the receiver and heliostat glass tubes (W).

Where,

$$Q_{int} = Q_{ro-ci,cv} + Q_{ro-ci,rad}$$

$$Q_{ro-gi,cv} = \pi D_{ro} * h_{cv,int}(T_r - T_g)$$

$$Q_{ro-gi,rad} = \pi D_{ro} * h_{rad,int}(T_r - T_g)$$

Q_{ext} is -the external heat power (by convection and radiation) between the heliostat glass tube and the atmosphere (W).

$$Q_{ext} = Q_{go-amb,cv} + Q_{go-sky,rad}$$

$$Q_{go-amb,cv} = A_{go} * h_{cv,int}(T_g - T_{amb})$$

$$Q_{go-sky,rad} = A_{go} * \sigma({T_g}^4 - {T_{sky}}^4)$$

$$\rho_g * Cp_g * A_g \frac{\partial T_g(x,t)}{\partial t} = [\pi D_{ro} * h_{cv,int}(T_r - T_g) + \pi D_{ro} * h_{rad,int}(T_r - T_g)] - [A_{go} * h_{out}(T_g - T_{am}) + A_{go} * \sigma({T_g}^4 - {T_{sky}}^4)]$$

The equation's initial location is,

$$T_g(x,t) = T_{g,initial}(t) = T_{amb}(0)$$

The above three differential Equations (5.60, 5.61, and 5.62) The following equations are obtained using a finite difference approach centered on space and forward time. $\frac{\partial T_f(x,t)}{\partial t} = \frac{{T_{f,n}}^{i+1} - {T_{f,n}}^{i}}{\Delta t}$

$$\frac{\partial T_g(x,t)}{\partial t} = \frac{{T_{g,n}}^{i+1} - {T_{g,n}}^{i}}{\Delta t}$$

$$\frac{\partial T_r(x,t)}{\partial t} = \frac{{T_{r,n}}^{i+1} - {T_{r,n}}^{i}}{\Delta t}$$

$$\frac{\partial T_f(x,t)}{\partial t} = \frac{{T_{f,n+1}}^{i} - {T_{f,n-1}}^{i}}{2\Delta X}$$

Following algebraic equations were produced by applying the previously discussed derivatives and some rearrangement.

For Heat Transfer Fluid

$${T_{f,n}}^{i+1} = \left(\left(\frac{1}{\Delta t} - B\right) * {T_{f,n}}^{i} + B * {T_{r,n}}^{i} - A\left({T_{f,n+1}}^{i} - {T_{f,n-1}}^{i}\right)\right) * \Delta t \qquad (5.63)$$

For Receiver

$${T_{r,n}}^{i+1} = \left(I_d * \gamma * \tau_g * \alpha_r * \frac{r_{m*W_k}(\theta)}{T} + \left(\frac{1}{\Delta t} - V\right) * {T_{r,n}}^{i} + Y * {T_{g,n}}^{i} + T * {T_{f,n}}^{i}\right) * \Delta t \quad (5.64)$$

Regarding the heliostat Glass Envelope

$${T_{g,n}}^{i+1} = \left(\left(\frac{1}{\Delta t} - R - P - S - Q\right) {T_{g,n}}^{i} + (R + P){T_{r,n}}^{i} + S{T_{amb}}^{i} + QT_{sky}\right) * \Delta t \qquad (5.65)$$

Whereas the coefficients in Equations 5.63, 5.64. and 5.65 are as follows:

$$R = \frac{h_{cv,int}}{\rho_g * Cp_g * A_g} \qquad S = \frac{\pi D_{g,e} h_{cv,ext}}{\rho_g * Cp_g * A_g} \qquad P = \frac{\pi D_{g,e} h_{cv,ext}}{\rho_g * Cp_g * A_g}$$

$$Z = R + P + S + Q \qquad X = R + P \qquad Q = \frac{\pi D_{g,e} h_{r,ext}}{\rho_g * Cp_g * A_g}$$

$$N = \frac{\pi D_{r,e} h_{cv,int}}{\rho_r * Cp_r * A_r} \qquad T = \frac{\pi D_{r,i} h_{cv,f}}{\rho_r * Cp_r * A_r} \qquad M = \frac{\pi D_{r,e} h_{r,int}}{\rho_r * Cp_r * A_r}$$

$$V = N + M + T \qquad Y = N + M \qquad U = \frac{1}{\rho_r * Cp_r * A_r}$$

$$B = \frac{\pi D_{r,i} h_{cv,f}}{\rho_f * Cp_f * A_f} \qquad A = \frac{\dot{m} * Cp_f}{2\rho_f * Cp_f * A_f * \Delta X}$$

Initial conditions

At $t = t_0$, for $0 \le x \le L$

The heliostat glass envelope is at ambient air temperature, $T_g(x, t_0) = T_{amb}(x, t_0)$

The receiver is expected to be 23^0C overhead the ambient air, $T_g(x, t_0) = T_{amb}(x, t_0) + 23^0$C.

The fluid is assumed to be at an initial temperature of 80°C.

Boundary conditions

At $> t_0$, For x = 0, the Temperature of fluid at the inlet of the receiver is equal to the exit fluid temperature of the storage tank, $T_f(0, t) = T_{inlet}$

At $t > t_0$ for x=L $\frac{\partial T_f}{\partial t} = 0$

5.4 Hot Water Temperature Reduction System for End Use

In the hospital, hot water is frequently needed for tasks like cooking, laundry, bathing, and cleaning that involve direct skin contact. Numerous health issues have been connected to excessive water temperature exposure in humans. Attention is momentarily directed to medical issues in order to better grasp the preferred water temperature at the bath, shower, and sinks (H.E. Jacobs 1 2018).

The thermal power requirement $\dot{Q}_e^{DHW}$ of a DHW end-use e is calculated considering its density ρ its heat capacity Cp, the hot water volumetric flow $\dot{V}_e^{hw}$ and the difference between hot and fresh water temperatures($T_{out,e}^{hw} - T_{in}^{fresh}$) Both volumetric flow and hot water temperature are specific to the considered end-use e.

$$\dot{Q}_e^{DHW} = \rho * Cp * \dot{V}_e * \left(T_{out,e}^{hw} - T_{in}^{fresh}\right) \tag{5.67}$$

In hospitals, some DHW end-uses (such as kitchen, showering, bathing, washing, and shaving) are connected to the activities of the patient o while other streams (such as dishwashing) are directly connected to the hospital h. By adding the daily energy use Q DHW e,o,t of the various DHW streams e of the occupier o for time t and the energy use Q DHW e,h,t necessary at hospital level h for time t, the overall DHW-related annual energy demand of the hospital Q DHW, hospital, expressed in kWh, is obtained(Bertranda et al., 2017).

$$Q^{DHW,hospital} = \sum_{t=1}^{365}\left(\sum_{e} Q_{e,h,t}^{DHW} + \sum_{o}\sum_{e} Q_{e,o,t}^{DHW}\right) \quad (5.68)$$

CHAPTER SIX

6. NUMERICAL SIMULATING SOLAR TOWER COLLECTOR USING ANSYS FLUENT

6.1 Numerical Simulation Procedure Draft Out Through Lucid Flow Chart

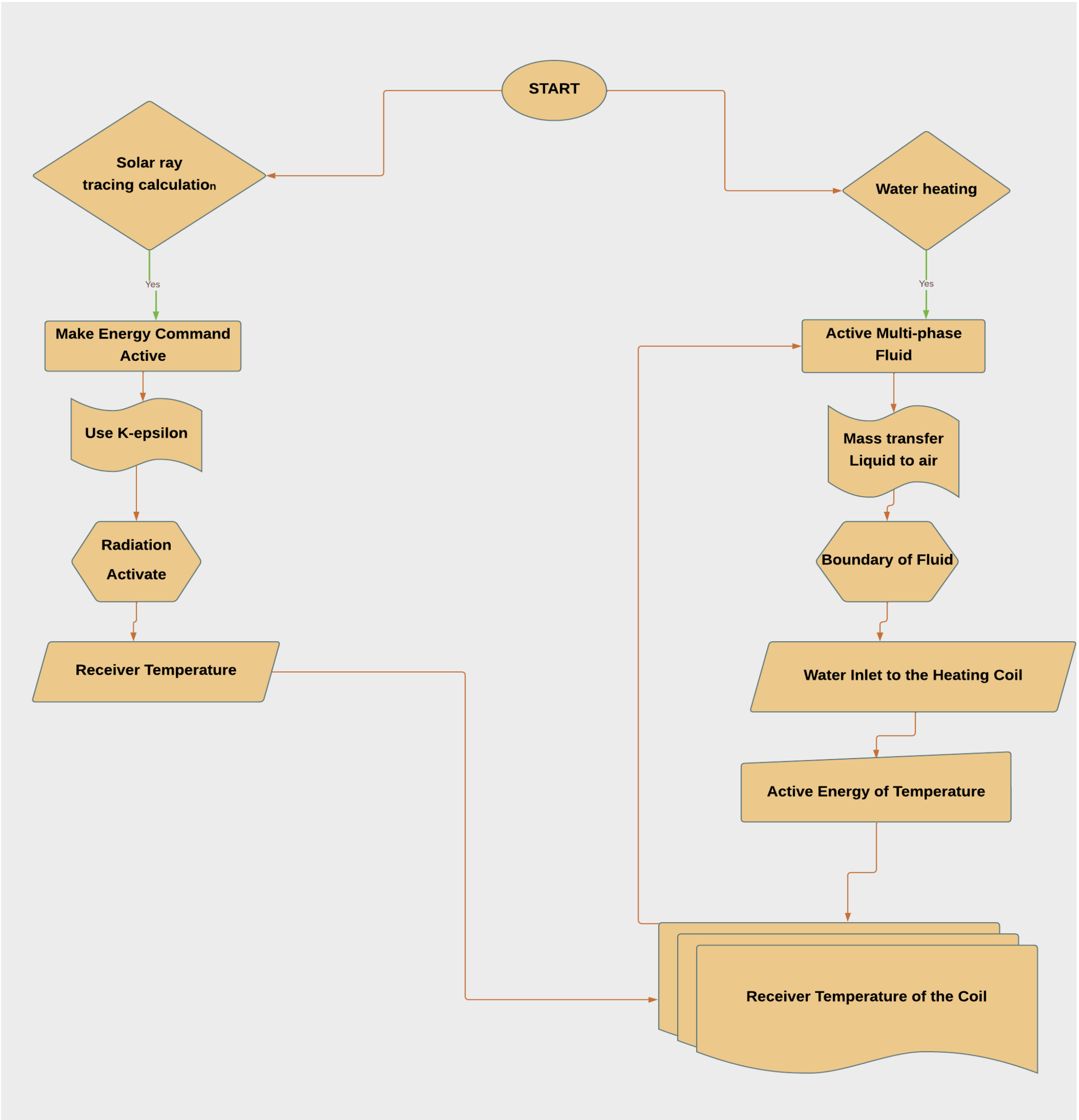

Figure 6.1 Procedure of Solar Tower Simulation Path Using Lucid Chart Diagram

6.1.1 Governing Equation

Several engineering applications involve in solar ray tracing numerical simulation. In ANSYS Fluent, Solar ray tracing is developed to satisfy this need. Therefore, the governing equations used to solve this type of numerical simulation are, to solve the incompressible flow; Naiver-

Stokes Equations for flow type is solved. The form of these equations based on the flow assumption follows(Xue et al., 2022)

Equation of Mass

$$\frac{\partial \rho u_x}{\partial x_x} = 0 \tag{6.1}$$

Equation of Momentum

$$\frac{\partial \rho u_x}{\partial t} + \frac{\partial u_y \rho u_x}{\partial x_y} = -\frac{\partial p}{\partial x_x} + \frac{\partial}{\partial x_y}\mu\left(\frac{\partial u_x}{\partial x_y} + \frac{\partial u_y}{\partial x_x}\right) - \rho g_x \beta (T - T_o) \tag{6.2}$$

$$\text{Where } \mu = \mu_1 + \mu_2$$

$$\mu_1 = \text{Laminar Coefficiet of Viscosity}$$

$$\mu_2 = \frac{C_t \rho k^2}{\varepsilon} = \text{Turbulent Coefficiet of Viscosity}$$

Equation of Energy

$$\frac{\partial \rho c_p T}{\partial t} + \frac{\partial u_y \rho c_p T}{\partial x_y} = \frac{\partial}{\partial x_x} K\left(\frac{\partial T}{\partial x_x}\right) + \dot{q} \tag{6.3}$$

6.1.2 The turbulence model is a standard k-ε equation

The results obtained using the k-epsilon model depend heavily on the wall Y-plus and it highly used to solve internal flow problems rather than external flow (Arniac, 2016; Parab et al., 2014).

$$\frac{\partial \rho u_x}{\partial t} + \frac{\partial u_y \rho u_x}{\partial x_x} = -\frac{\partial p}{\partial x_x} + \frac{\partial}{\partial x_y}\mu\left(\frac{\partial u_x}{\partial x_y} + \frac{\partial u_y}{\partial x_x}\right) - \rho g_x \beta (T - T_o) \tag{6.4}$$

$$\frac{\partial \rho k}{\partial t} + \frac{\partial u_y \rho k}{\partial x_y} = \frac{\partial}{\partial x_y}\left(\frac{\mu_t}{\sigma_k}\frac{\partial k}{\partial x_y}\right) + G_s + G_T - \rho\varepsilon \tag{6.5}$$

$$\frac{\partial \rho \varepsilon}{\partial t} + \frac{\partial u_y \rho \varepsilon}{\partial x_y} = \frac{\partial}{\partial x_y}\left(\frac{\mu_t}{\sigma_k}\frac{\partial \varepsilon}{\partial x_y}\right) + C_1 \frac{\varepsilon}{k}(G_s + G_T)(1 + C_3 R_f) - C_2 \frac{\rho \varepsilon^2}{k} \tag{6.6}$$

Where,

$$G_s = \mu_t\left(\frac{\partial u_x}{\partial x_y} + \frac{\partial u_y}{\partial x_x}\right)\frac{\partial u_x}{\partial x_y} G_T = g\beta\left(\frac{\mu_t}{\sigma_t} + \frac{\partial T}{\partial x_x}\right) R_f = -\frac{G_T}{G_s + G_T} \tag{6.7}$$

The equations comprise several experimental coefficients that are labeled as; for the governing equations used to solve this type of numerical simulation are obtained from a source of Peng KE,

(Pei et al., 2019), all empirical constants used as this of previous work $\sigma_k = 1.0, \sigma_\varepsilon = 1.30, \sigma_t = 0.90, C_t = 0.090$

$C_1 = 1.4\,, C_2 = 1.9, C_3 = 1.3$

Symbols used in the equalities signify their typical implications

Where,

ρ is density of fluid, T is fluid temperature , ε is epsilon which is energy dissipation, μ is fluid vicosity and u_j fluid flows speed

Table 6.1 Boundary and Initial Condition

Name of Boundary walls	Description	Value	Participating in Solar radiation
Sky	Stationary	Atmospheric	No
Ground	Stationary	-	No
Heliostat	Stationary	-	Yes
Water tank for supply	Stationary	-	No
Water tank for discharge	Stationary	-	No
Receiver	Stationary	-	No
supply pipe	Stationary	-	No
discharge pipe	Stationary		No
Fluid inlet	Velocity inlet	4 m/s	No
Fluid outlet	Pressure outlet	Atmospheric	No
Radiation Heat flux	-	750.6 w/m^2	No
Surface Temperature	-	498.77 K	No
Atmospheric Temperature	-	300	No
Fluid inlet Temprature	-	300	No

6.1.3 Polyhedral Grid (Mesh)

The main advantage of polyhedral mesh is that each individual cell has many neighbors, so gradients can be well approximated. Polyhedrons are also less sensitive to stretching than tetrahedrons which results in better mesh quality leading to improved numerical stability of the model. The mesh used in this numerical simulation is polyhedral mesh. The figure shows the numerical polyhedral grid used on solar ray tracing for solar towers.

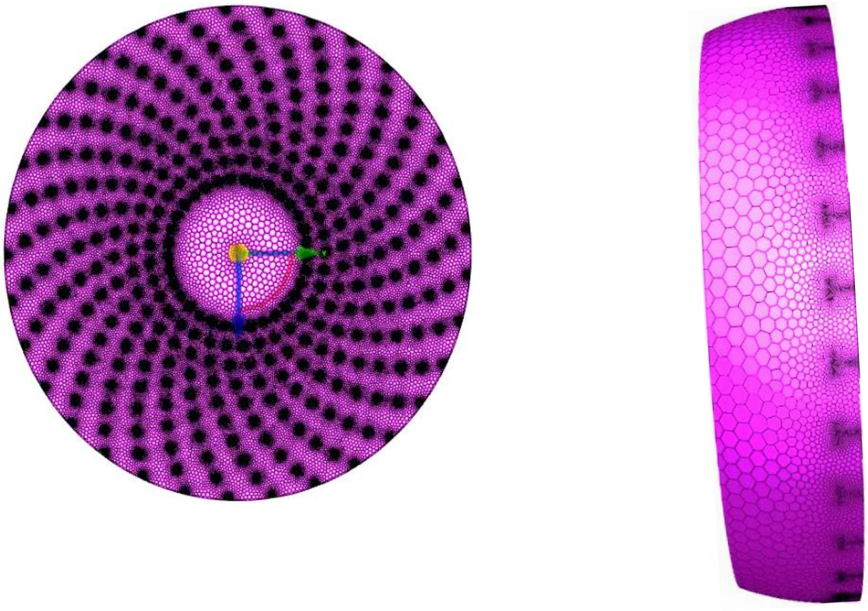

Figure 6.2 Solar Tower Poly-Hedral Grid Generation.

CHAPTER 7
RESULT AND DISCUSSION

a. Temperature Distribution on Heliostat

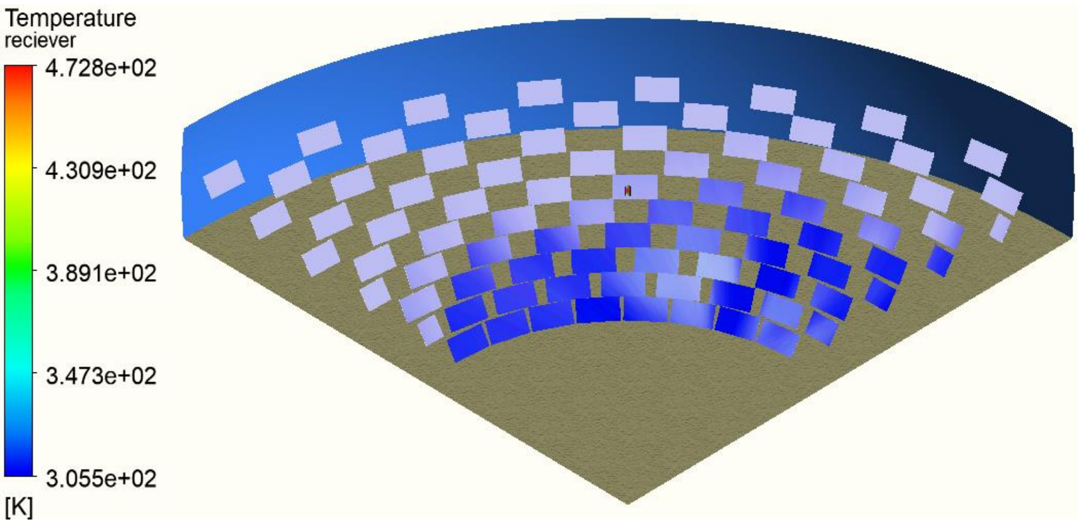

Figure 7.1 Temperature Distribution on Heliostat.

In a solar tower collector system, the temperature distribution refers to how heat energy is spread or radiated across the system. According to the statement, the temperature is said to be equally radiated on the heliostat mirror. A heliostat mirror is a component of the solar tower collector system that reflects and concentrates sunlight onto a central receiver. Additionally, the statement mentions that the ambient temperature is equal to the temperature of the heliostat mirror. The ambient temperature refers to the temperature of the surrounding environment. In this case, it suggests that the temperature of the heliostat mirror, which is exposed to the ambient conditions, is in equilibrium with the surrounding temperature. Overall, the description suggests that in the solar tower collector system, the temperature is evenly radiated on the heliostat mirror, which is in equilibrium with the ambient temperature. Additionally, the temperature in the environment remains relatively constant over specific time intervals

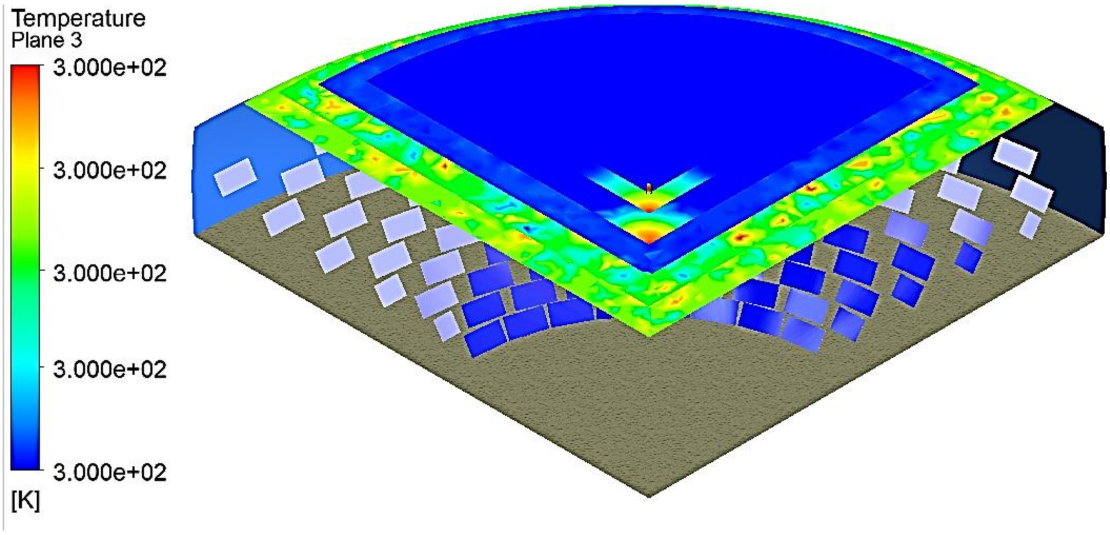

Figure 7.2 Temperature variation on Earth's surface.

In the solar tower collector system, the temperature distribution on the surface of the heliostat shows variations. As depicted in the provided image, there are significant temperature variations observed. As we move closer to the solar tower receiver, the temperature tends to increase, indicating higher thermal energy concentration. On the other hand, as we move farther away azimuthally (horizontally), the temperature variations reduce, indicating a decrease in thermal energy concentration. Therefore, the temperature distribution on the heliostat surface exhibits a pattern where temperatures are higher near the solar tower receiver and decrease as we move away from it in the horizontal direction.

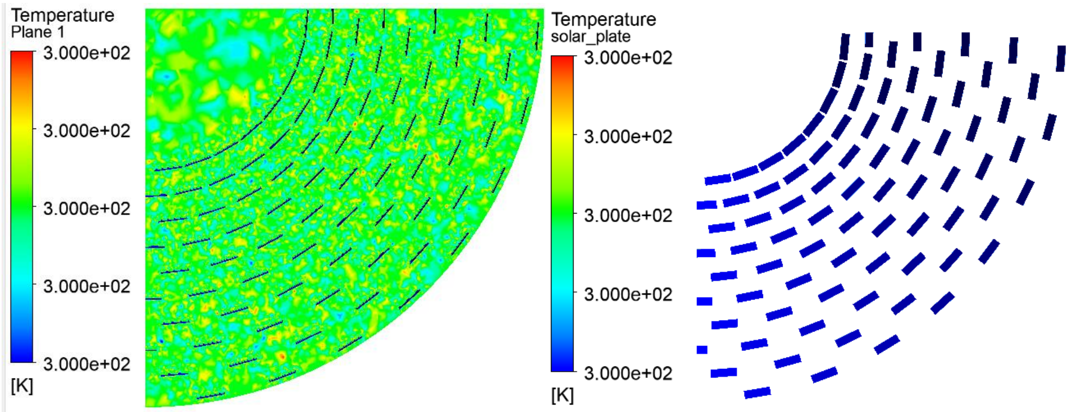

Figure 7.3 Temperature Distribution on the Plane and Solar Plate.

The temperature distribution on the surface of the heliostat is described as being ambiently distributed. This means that the temperature is relatively uniform or evenly spread across the surface of the heliostat mirror. There are no significant variations or gradients in temperature observed on the heliostat surface. Instead, the temperature remains relatively constant or consistent throughout the surface. This ambient temperature distribution implies that there is no concentrated or localized heating or cooling on the heliostat mirror, and the temperature remains relatively stable across its entire surface.

b. Reciever Temperature with each distrbuted Helostat

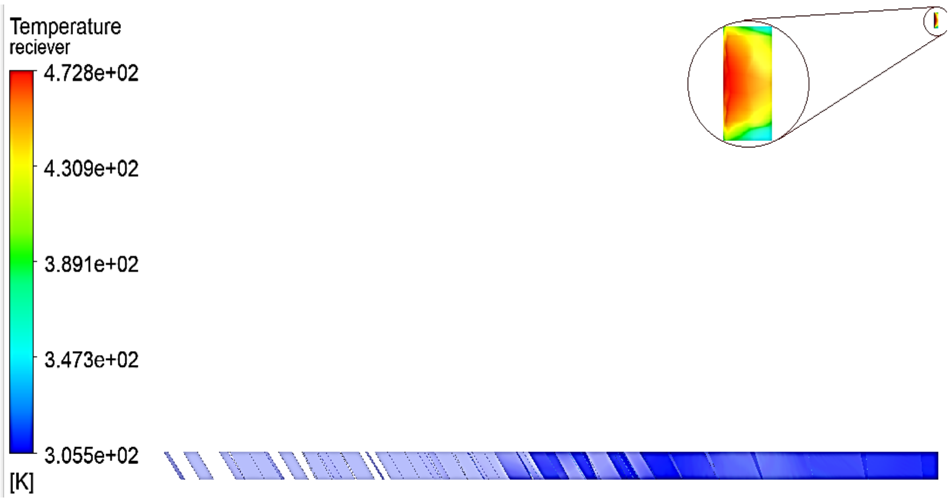

Figure 7.4 Receiver with Each Distributed Heliostat Glass.

Based on the simulation results, the temperature distribution on the surface of the heliostat with the receiver indicates that the maximum temperature reached is approximately 472.8 K. "Overily distributed" might imply that the temperature is distributed across the surface in a widespread manner.

This means that different areas or points on the heliostat surface experience varying temperatures, with the highest temperature recorded being 472.8 K. The distribution of temperature suggests that certain regions or sections of the heliostat surface receive more concentrated solar energy or heat, leading to higher temperatures in those areas.

c. Temperature Distribution on Reciever

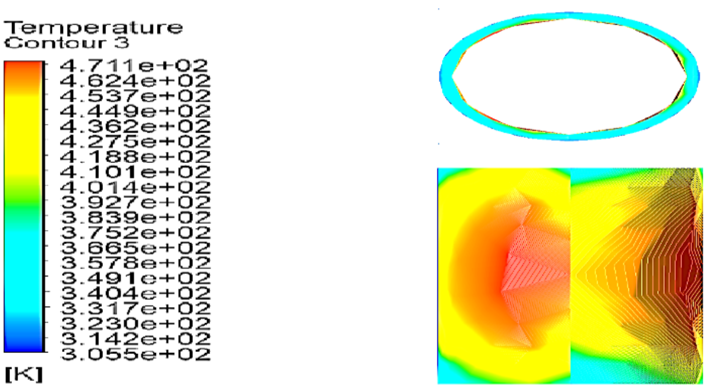

Figure 7.5 Distrbution of Temperature Variation on Receiver

In the observed temperature distribution on the receiver, it is evident that the maximum temperatures are concentrated at the center of the cylindrical part of the receiver. This implies that the highest thermal energy or heat is being absorbed or received at this specific location. The figure indicates that the temperature gradually decreases as we move away from the center of the cylindrical part towards the outer edges or surrounding regions of the receiver. Therefore, the temperature distribution highlights the central area as the region experiencing the highest temperatures, suggesting a focused heat absorption or concentration at that particular spot.

d. Turbulence Kinetic energy of receiver local air

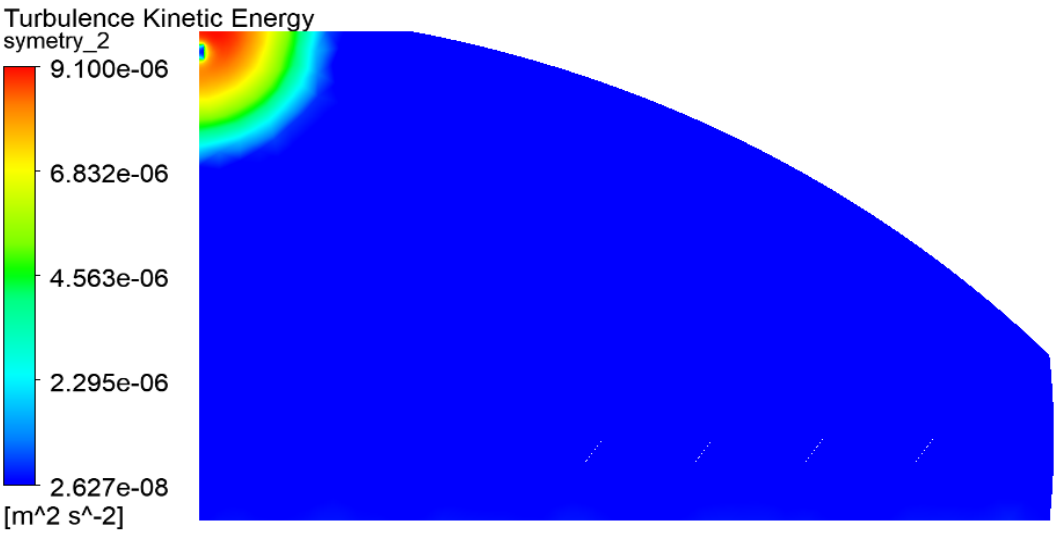

Figure 7.6 Turbulence Kinetic Energy of Receiver

In the described scenario, turbulence occurrence increases as we approach the center of the track, while it becomes rarer as we move farther away from the center. This indicates that the central region experiences a higher frequency or intensity of turbulent flow compared to the outer regions. Turbulence refers to the chaotic and irregular motion of fluid or air, often characterized by fluctuations in velocity, pressure, and flow direction. As we approach the center of the track, factors such as flow obstructions, uneven terrain, or other influencing factors might contribute to the generation of turbulent flow.

These conditions lead to increased turbulence occurrence in that area. Conversely, as we move away from the center towards the outer regions of the track, the factors causing turbulence may diminish or become less significant. As a result, the occurrence of turbulence becomes less frequent or rare in these areas. In summary, the description suggests that turbulence is more prevalent and intense near the center of the track, while it becomes increasingly frequent as we move away from the center towards the outer parts.

e. Average Temperature Distribution on Reciever

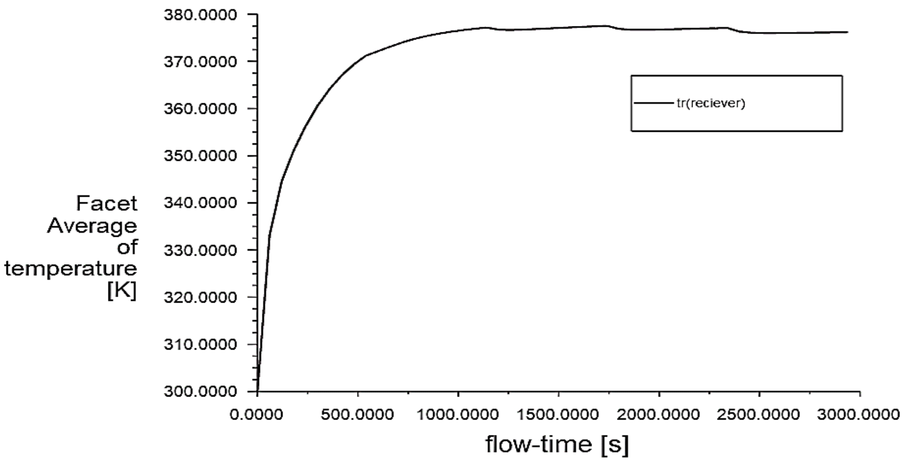

Figure 7.7 Average Temperature Distribution on Reciever

Average Temperature Circulation: The average temperature circulation, as mentioned, is around 375K. Temperature circulation typically refers to the movement or distribution of heat energy within a system or medium. In this context, the average temperature circulation indicates that the temperature tends to hover around 375K on average. It implies that the system or medium maintains a relatively steady temperature level, with deviations from this average being relatively small. It's important to note that without additional context or specific details, it is challenging to provide a comprehensive analysis or draw any specific conclusions. However, based on the information given, it seems that the temperature remains relatively stable for an extended period of time (around 50 hours) and has an average value of 375K.

f. Total Temperature of Mixture

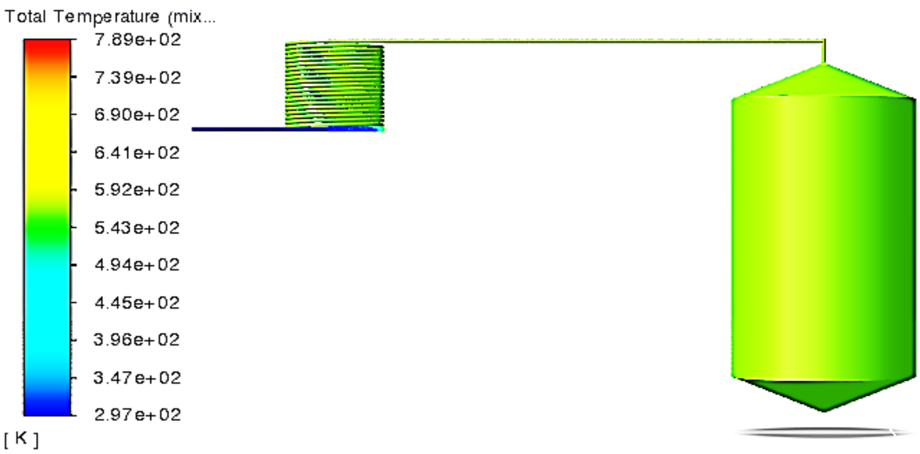

Figure 7.8 total temperature of steam water

The figure illustrates that the temperature of the tracked water is predominantly at the boiling point, reaching temperatures close to that of steamed water. This indicates that the tracked water has absorbed sufficient heat to reach its boiling point, where it undergoes a phase change and turns into steam. After the tracked water is transferred into the storage tank, further heating occurs, raising the temperature of the water even higher. Eventually, the water reaches a temperature of approximately 516 degrees Celsius, at which point it transforms into steam.

This process of heating the tracked water to the point of boiling and subsequently generating steam is commonly employed in various systems, such as power plants or industrial processes, to harness the energy of steam for power generation or other applications.

g. Total Pressure of the Mixture

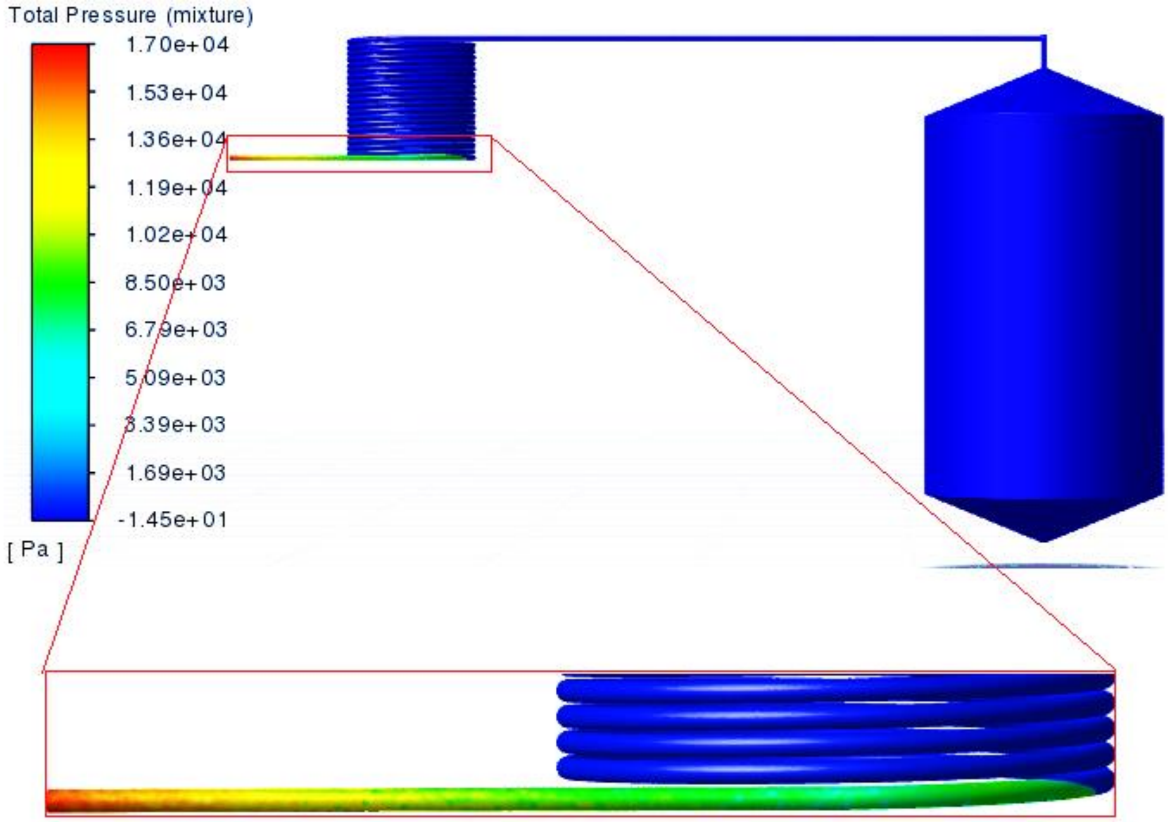

Figure 7.9 total pressure of steam water

Flow Rate and Velocity:- Higher pressure in the inlet pipe of the receiver tube can lead to an increased flow rate of the working fluid, such as steam or a heat transfer medium. This higher flow rate results in higher fluid velocity, which affects the overall system dynamics. Enhanced Heat Transfer: The increased pressure can facilitate better heat transfer between the working fluid and the receiver tube. Higher pressure often leads to improved convective heat transfer, allowing for more efficient energy absorption from the concentrated solar radiation.

System Efficiency:- With a higher pressure effect, the overall system efficiency can be improved. The increased pressure allows for a higher temperature and enthalpy of the working fluid, which contributes to enhanced power generation or thermal energy extraction. Structural Considerations: It's important to note that higher pressure in the inlet pipe places additional stress on the receiver tube and associated components. The system needs to be designed and engineered to withstand the increased pressure to ensure the integrity and safety of the receiver tube.

Control and Regulation:- The higher pressure effect requires effective control and regulation mechanisms to maintain the desired operating conditions. This may involve pressure relief valves, pressure sensors, and control systems to ensure optimal performance and prevent any pressure-related issues.

h. Mass Transfer Rate

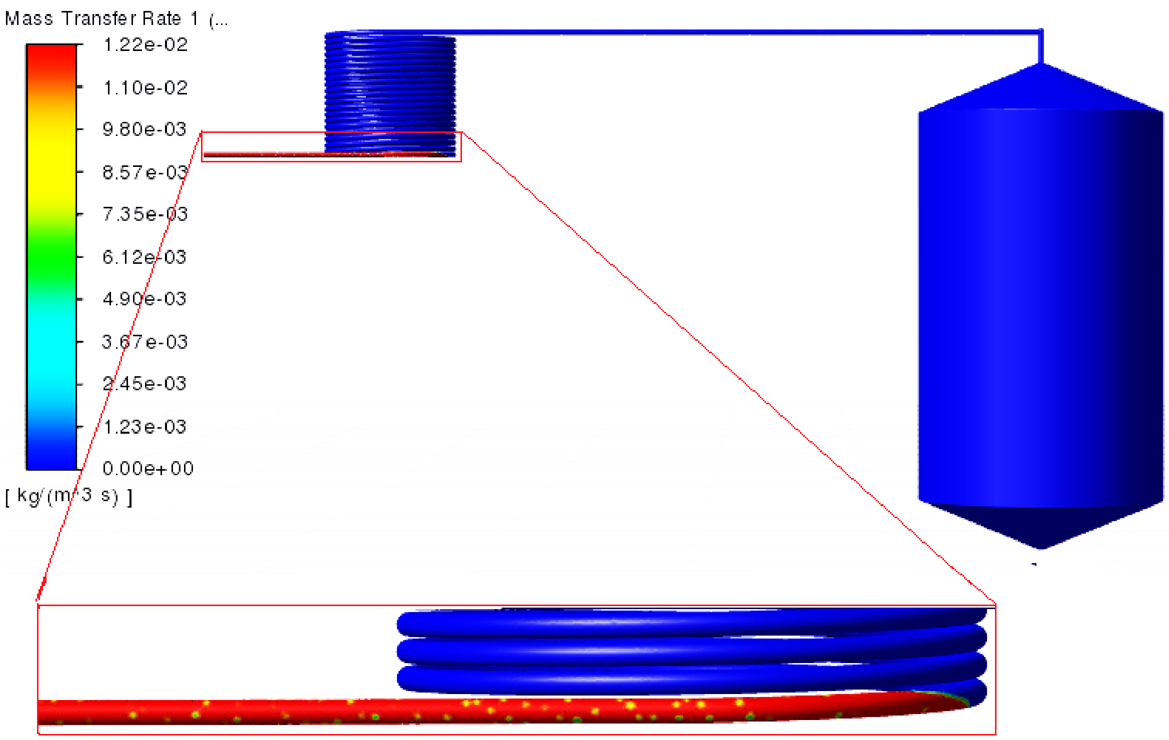

Figure 7.10 mass flow rate of steam water

A higher mass transfer rate at the inlet of a receiver tube, as visually observed in figures, indicates a larger amount of liquid substance passing through the tube per unit time. It represents the rate at which mass is transferred into the tube, typically measured in units such as kilograms per second or liters per minute. The precise determination of the mass transfer rate requires additional information, such as the density and volumetric flow rate of the liquid substance. By multiplying these values, the mass flow rate can be calculated, providing a quantitative measure of the mass of the liquid substance passing through the inlet per unit time.

i. Enthalpy formation

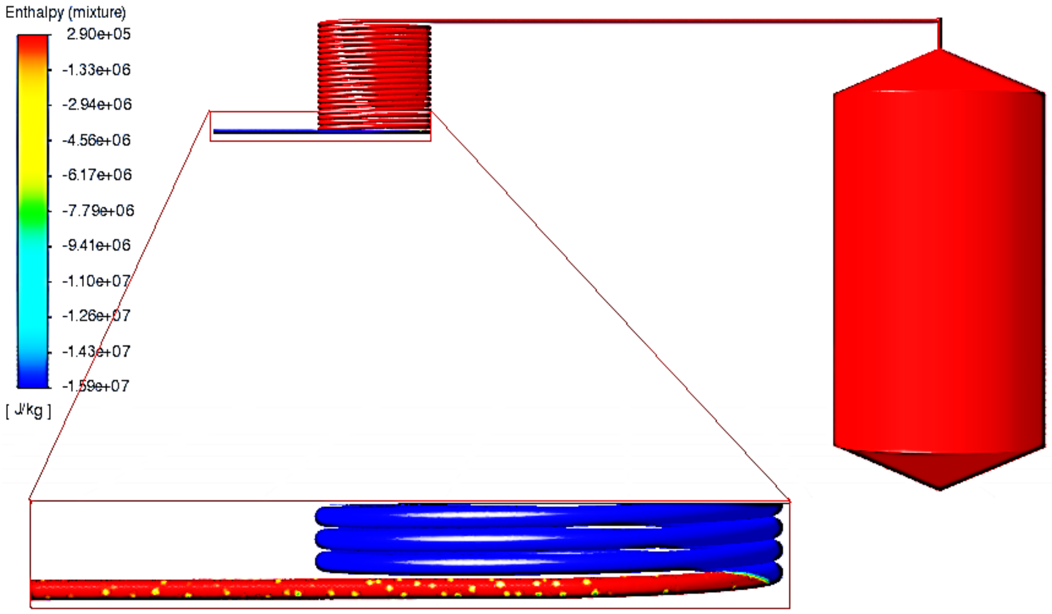

Figure 7.11 Enthalpy of steam water

During water heating, the enthalpy formation refers to the change in enthalpy that occurs as water undergoes a phase change or temperature increase. Enthalpy is a measure of the total energy of a system, including both its internal energy and the work it can do. When water is heated, its temperature increases, and at certain temperatures, phase changes may occur. The enthalpy formation during water heating depends on the initial and final states of the water. When water is heated from a lower temperature to its boiling point, it undergoes a phase change from a liquid to a gas, which is known as vaporization or boiling. The enthalpy change during this phase change is called the enthalpy of vaporization. It represents the energy required to convert one unit of liquid water into water vapor at a specific temperature and pressure.

If the water is already in the gaseous state, further heating will lead to an increase in temperature without a phase change. The enthalpy change during this process is called the sensible heat or enthalpy of the gas. It represents the energy required to raise the temperature of the gas without changing its phase.

In summary, the enthalpy formation during water heating involves the enthalpy changes associated with phase transitions (such as boiling) and sensible heat changes (temperature increase) of the water. The specific enthalpy values depend on the initial and final states of the water and can be determined experimentally or calculated using thermodynamic equations.

j. Density of the Mixture

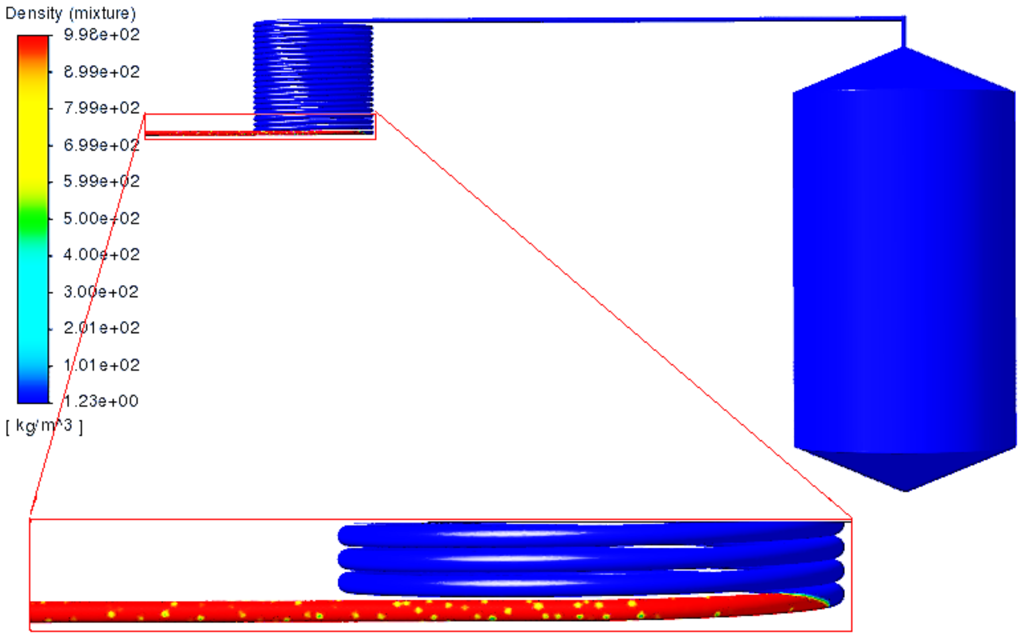

Figure 7.12 density of steam water

When water changes to steam, its density decreases. This is due to the change in the physical state of water from a liquid to a gas. In the liquid state, water molecules are closely packed together, resulting in higher density. However, during the phase transition from liquid to gas (vaporization or boiling), the water molecules gain sufficient energy to break the intermolecular forces and become gaseous water molecules (steam).

In the gaseous state, the water molecules have higher kinetic energy and are more spread out. They occupy a larger volume compared to the liquid state, leading to a decrease in density. This decrease in density is because the mass remains the same, but the volume increases significantly. The reduction in density when water changes to steam is significant. At standard atmospheric pressure and temperature, the density of liquid water is about 1000 kg/m³, while the density of steam is around 0.6 kg/m³. This means that steam is much less dense than liquid water.

7.2 Cost and Financial Analysis of the Solar Tower Power Plant

7.2.1 Economic Analysis of the Solar Tower Collector System

The primary concern that came up in customers' minds while using solar thermal applications is its cost point of view. High initial expenses and low operational costs are typical traits of solar processes. The fundamental economic challenge thus consists of contrasting an initial known investment with projected future running costs. The life cycle saving approach is the most widely used evaluation tool among economical evaluation methods, hence it was chosen for the current study.

7.2.2 Investment Cost

Investment expenses comprise all of the expenditures associated with purchasing and installing a solar system, including those for the tower, receiver, heliostat glass mirror collector, and storage tank that's hot and cold. A solar system's installed cost is the product of its cost per square foot of collector area and its installed cost differently.

The benefits of investing in solar energy technology include a pollution-free environment, a cost-free renewable energy source, great reliability, and little maintenance requirements. Although solar energy is free, the tools needed to transform it into a usable form are not. Therefore, a cost must be ascribed to solar thermal that reflects the cost of the conversion equipment, which is lower than the cost of other energy sources that can accomplish the same task, based on the number of kWh delivered by the solar energy(Chine et al., 2014).

Therefore, using solar energy has financial benefits. Solar processes are typically characterized by high initial costs and low ongoing costs. The cost of obtaining and installing solar energy equipment is a significant component of the economics of the solar process.

The primary objective of cost evaluation is to identify the most affordable way to provide the necessary energy, taking into account both solar and non-solar options, as well as solar energy equipment purchased now to lower fuel costs tomorrow. Solar water heaters (SWH) are gaining popularity in our nation as a sustainable development tool, and efforts are ongoing to bring down their price point and make them more accessible. An SWH is made to provide a certain amount of hot water per day at a certain temperature. As a result, the annual heating load for heating water becomes:

Thus, the annual heating load for water heating becomes:

$$Q_a = 365 * \rho_w * Cp_w * V_{st}(T_{hot} - T_{cold}) \tag{7.1}$$

While a solar fraction portion of this heating load is satisfied by solar energy, the remainder is supplied by an auxiliary energy system. hence, the system's annual contribution of solar energy;

$$Q_{a,solar} = sf * Q_a \tag{7.2}$$

7.2.3 The Price of Solar Process Systems

An essential component of solar process economics is the expenditures associated with purchasing and setting up solar energy equipment. These consist of the delivered cost of all the solar installation-related equipment, including pipelines, pumps, controllers, storage units, collectors, and other equipment.

Table 7.1 Estimated Cost of Solar Water Heating System

No	Items	Specification	Total Price [Birr]
1.	**Receiver**	Cylindrical and tube Latent Heat Storage Copper tube sheet	
	Height of the receiver, and thickness of the tube	H_{rec} =1.5315m, D_{rec}=1.021m D_{tube}=23mm, T_{thick}=1.5mm	27,000.00
2.	Heliostat	Glass Mirror	
	Mirror Thickness	4mm	1,269,824.00
3.	Tower (Supporting Structure)	Aluminum frame(18m and t=5mm)	21,500.00
4.	Storage Tank	Cylindrical	
	Inside material, Insulation, Insulation cover, and Manufacturing	2mm Thick Sheet Steel, Glass Fiber (t = 15 mm W = 1m, L=2m), 0.8 mm Thick Galvanized Pre Painted Steel (1m*1m), 25% of Material Cost	43,000.00
5.	Piping Material Tee, Elbow 90, and Fitting Pipe	Galvanized Steel Piping	
		1'' Galvanized Steel	5,500.00
		1 ½'' Galvanized Steel	7,500.00
		2'' Galvanized Steel	8,300.00
6.	Pump	Electrical Drive(2)	116,000.00
7.	System and accessory control	PRV, RTD, thermostat, pump controls, vacuum and air vent, check and block valves, safety	33,000.00
Total			**1,531,624.00**

Investment in solar energy technology is encouraged as the merits such as pollution free environment, free renewable and energy source, high reliability and low maintenance costs. When a consumer decides to buy a solar water heater system, economics is a major factor. The utilization of solar energy has financial benefits. Solar processes are often characterized by low operational costs and high initial costs. One of the main determinants of solar process economics is the amount of money spent on buying and installing solar energy equipment(Kalogirou, 2012).

If a customer or company knows that the main advantages of solar energy are for the environment, they are refusing to purchase a system. Any business thinking about producing solar energy will closely examine the economics to make sure that such a project will be profitable for them.

7.2.4 Operation Maintenance and Replacement Cost

The initial investment and installation costs associated with a solar energy project are important considerations. Additionally, the ongoing operating costs of the system must be factored in, which include: Energy costs for operating pumps, controllers, and other accessories the overall system operating costs for the duration of the project's operation

Carefully evaluating both the upfront capital expenditures and the long-term operational expenses is crucial when assessing the viability and total cost of ownership of a solar energy system.

The replacement and repair costs of a solar energy system can vary significantly depending on the manufacturer and specific components used. This makes accurate lifecycle costing challenging. for solar collectors, manufacturers generally estimate a lifespan of 20-25 years, but an exact average replacement age is difficult to pin down.

Similarly, for thermal energy storage tanks, companies typically recommend replacement every 8 to 12 years on average. the variability in component lifetimes and replacement costs is an important consideration when evaluating the total cost of ownership and long-term viability of a solar energy system. Careful research into manufacturer specifications and industry averages is required to best approximate the lifecycle costs.

- Operation, Maintenance and Replacement Cost of solar tower is 10% of the system cost which is 153,162. Investments in buying and installing solar energy equipment are important factors in solar process economics. These include the delivered price of equipment such as collectors, storage unit, pumps, controls, pipes, heat exchangers, and all other equipment associated with the solar installation.

$$CI = C_A A_C + C_E \tag{7.3}$$

Where, CI= total cost of installed solar energy equipment, C_A = total area of dependent cost, Ac = collector area, and C_E = total cost of equipment which is independent of collector area. When calculating the life cycle cost of a solar water heating system, various elements need to be taken into account, including the interest rate, inflation rate, unit cost of energy, operating and maintenance costs, and the service life of the solar water heater. Variations in the economy, governmental policy, and power tariffs have an impact on all these aspects.

7.2.5 Life Cycle Cost (LCC) :- the total cost of an energy delivery system during its lifespan, accounting for time value of money. This cost may also be determined for a specific time frame.

The life cycle cost of solar water heating system is determined from the investment cost and the present value of maintenance and pumping cost distributed over the life as follows;

$$\mathrm{LCC} = \mathrm{CI} + C_m \frac{1}{i}\left(1 - \frac{1}{(1+i)^n}\right) \tag{7.4}$$

Where, CI =Investment cost of solar water heating system

C_m= annual maintenance and pumping cost and n is years of economic analysis

7.2.6 Life Cycle Saving of Energy :- The energy cost savings from switching from electricity to solar power is known as the life cycle saving of a solar water heater. the distinction between the LCC of a solar and auxiliary system and the LCC of a conventional fuel-only system. This is the same as the benefits of the solar energy system above the fuel-only system, totaling their present value. The energy cost savings from switching from fuel or electricity to solar power are known as the solar water heater's life cycle savings.

The annual energy saving is calculated as:

$$ES = f_a Q_a \tag{7.5}$$

The life cycle saving of energy

$$LCS = P_e f_a Q_a \left(\frac{1+i_e}{i-i_e}\right)\left[1 - \left(\frac{1+i_e}{1+i}\right)^n\right] \tag{7.6}$$

Where, LCS is life cycle saving of solar water heating system $[kwh]$

Q_a is annual heating load $[kwh]$

f_a is an annual fraction of load supplied by solar energy

i is annual market discount rate

i_e is annual market rate if energy escalation

7.2.7 Unit price of solar energy

To determine the unit price of solar energy cost, the life cycle cost has to be equal to the life cycle savings of the solar water heater during its life time.

$$LCC = LCS \tag{7.7}$$

By substituting equation (7.4) and (7.6) into equation (7.7) P_e determined as follows:

$$\mathrm{CI} + C_m \frac{1}{i}\left(1 - \frac{1}{(1+i)^n}\right) = P_e f_a Q_a \left(\frac{1+i_e}{i-i_e}\right)\left[1 - \left(\frac{1+i_e}{1+i}\right)^n\right]$$

$$P_e = \frac{\mathrm{CI} + C_m \frac{1}{i}\left(1 - \frac{1}{(1+i)^n}\right)}{f_a Q_a \left(\frac{1+i_e}{i-i_e}\right)\left[1 - \left(\frac{1+i_e}{1+i}\right)^n\right]} \tag{7.8}$$

7.2.8 Payback Period :- is the duration of time required for the yearly solar savings to turn positive and the cumulative solar savings to turn zero, or the number of years required to precisely recover the original investment cost.

To determine the pay-back period, the maintenance cost is neglected. Hence the investment of the solar water heater has to be pay-backed by the life cycle saving of electric cost.

$$LCCS = C_f f_a Q_a \left(\frac{1+i_e}{i-i_e}\right)\left[1 - \left(\frac{1+i_e}{1+i}\right)^n\right] \tag{7.9}$$

Where, $LCCS = CI \quad at\ n = N_p$

$$C_f f_a Q_a \left(\frac{1+i_e}{i-i_e}\right)\left[1 - \left(\frac{1+i_e}{1+i}\right)^{N_p}\right] = CI$$

$$N_p = \frac{\ln\left[1 + CI\frac{\left(\frac{i_e - i}{1+i_e}\right)}{C_f f_a Q_a}\right]}{\ln\left[\frac{1+i_e}{1+i}\right]} \tag{7.10}$$

Where $LCCS$ is Life Cycle Saving of electric cost $[Birr]$

C_f is the unit cost of electricity for the first year of analysis $\left[{}^{Birr}/_{KWh}\right]$

7.2.9 An Overview of the Project Installation's Cost Estimation

COST SUMMARY OF THE PROJECT FOR INSTALLATION					
The project's whole starting cost(ETB) (Birr)	**Total Life Cycle cost(LCC) (Birr)**	**Total Life Cycle saving(LCS) (Birr)**	**Unit cost of Solar Energy Birr/Kwh**	**Unit cost of Electricity and fuel Birr/Kwh**	**Payback period Year**
1,531,624.00	**1,807,316.32**	**1,901,073.15**	**0.14**	**0.25**	**2.7**

7.3 Simulation Result using SOLAR PILOT Software

Chosen Metehara as the climate or location reference for a software simulation,

Metehara is a town in Ethiopia, located in the Oromia Region. It has a hot semi-arid climate, characterized by high temperatures and relatively low rainfall. The town experiences a short rainy season from March to May, while the rest of the year is mostly dry. During the dry season, which lasts from October to February, rainfall is minimal. In terms of temperature,

Metehara can get quite hot, with average temperatures ranging from 30°C (86°F) to 40°C (104°F) or even higher during the summer months. It is important to consider the high temperatures and low precipitation when simulating the climate conditions of Metehara.
Taking into account these climate characteristics, your software simulation can incorporate the hot semi-arid climate of Metehara by including features such as high temperatures, limited rainfall, and distinct dry and rainy seasons. This reference will help create a realistic representation of the climate for the intended simulation.

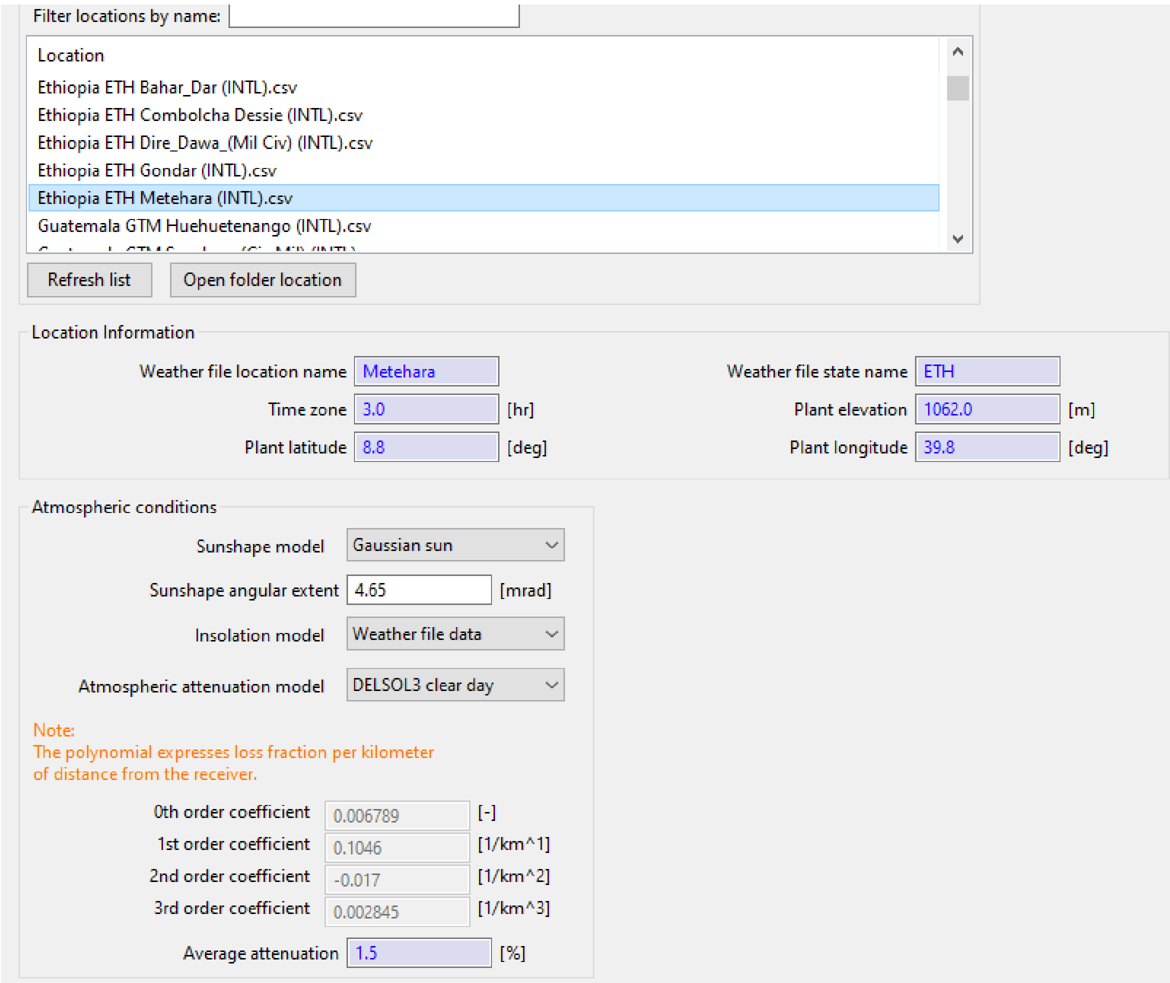

Figure 7.13 Selection of Location for Simulating SOLARPILOT

Inserting receiver data that get on solar tower receiver analysis

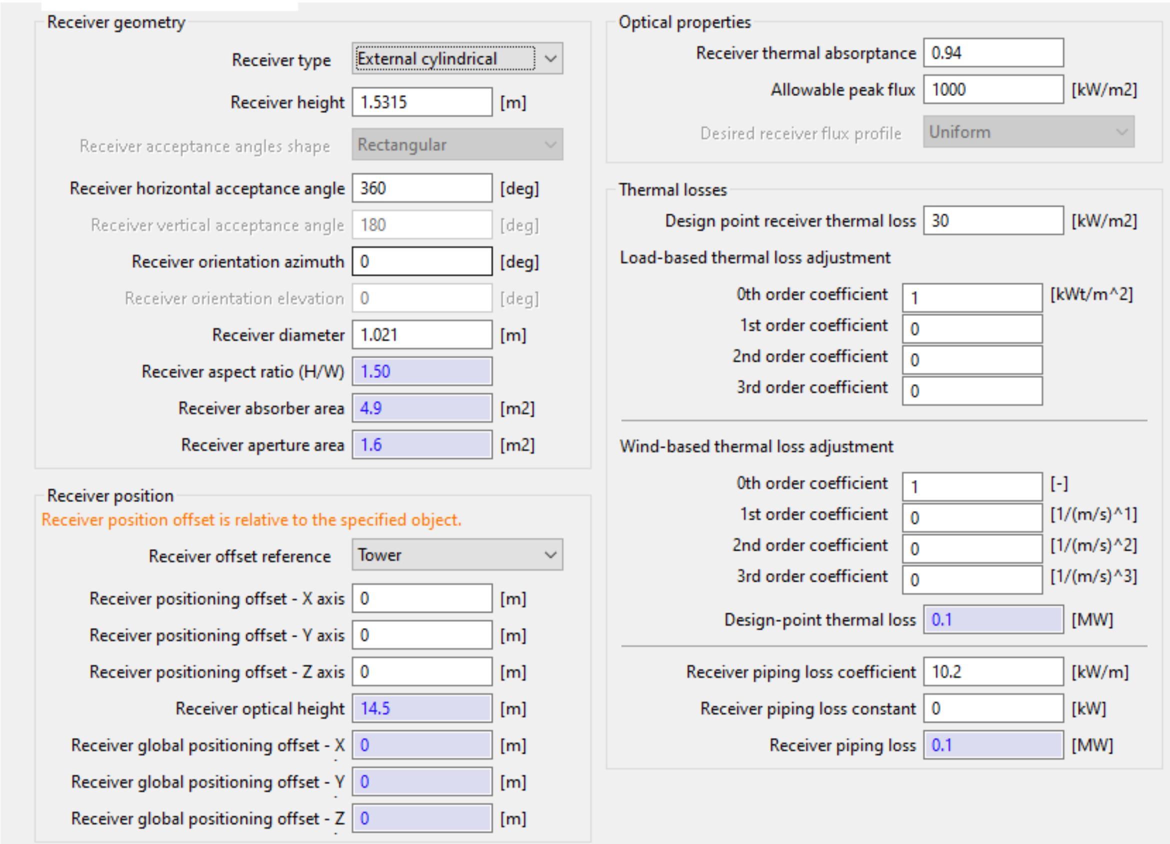

Figure 7.14 Receiver Geometry

Here is a summary of the flux simulation results for the table fields of cost, efficiency, and power:By analyzing the cost, efficiency, and power fields in the table, researchers and engineers can evaluate the performance and economic viability of the solar tower receiver. This information can guide design improvements, system optimization, and decision-making processes related to the deployment and operation of solar power tower systems.

Flux simulation results summary

Export to CSV   Copy to clipboard

	Units	Value	Mean	Minimum	Maximum	Std. dev
Total plant cost	$	8081784				
Simulated heliostat area	m^2	8206.2				
Simulated heliostat count	-	4230				
Power incident on field	kW	6159.2				
Power absorbed by the receiver	kW	2755.8				
Power absorbed by HTF	kW	2460.5				
Cloudiness efficiency	%	100.00	100.00	100.00	100.00	0.0000
Shading efficiency	%	100.00	100.00	100.00	100.00	0.0000
Cosine efficiency	%	78.36	78.36	67.36	97.80	6.2811
Reflection efficiency	%	90.25	90.25	90.25	90.25	0.0000
Blocking efficiency	%	96.89	96.91	55.77	100.00	7.7300
Attenuation efficiency	%	98.52	98.51	97.95	99.14	0.3546
Image intercept efficiency	%	70.51	69.43	36.01	99.57	22.0787
Absorption efficiency	%	94.00				
Solar field optical efficiency	%	47.60		17.54	86.78	18.1655
Optical efficiency incl. receiver	%	44.74		16.49	81.57	17.0756
Annualized heliostat efficiency	%	0.00		14.67	75.00	15.6312
Incident flux	kW/m2	596.80		151.81	880.47	241.4360

Figure 7.15 Summary of the flux simulation results for the table fields of cost, efficiency, and power

Heliostat distrbution on the plane surface of solarpilot simulation result is here.

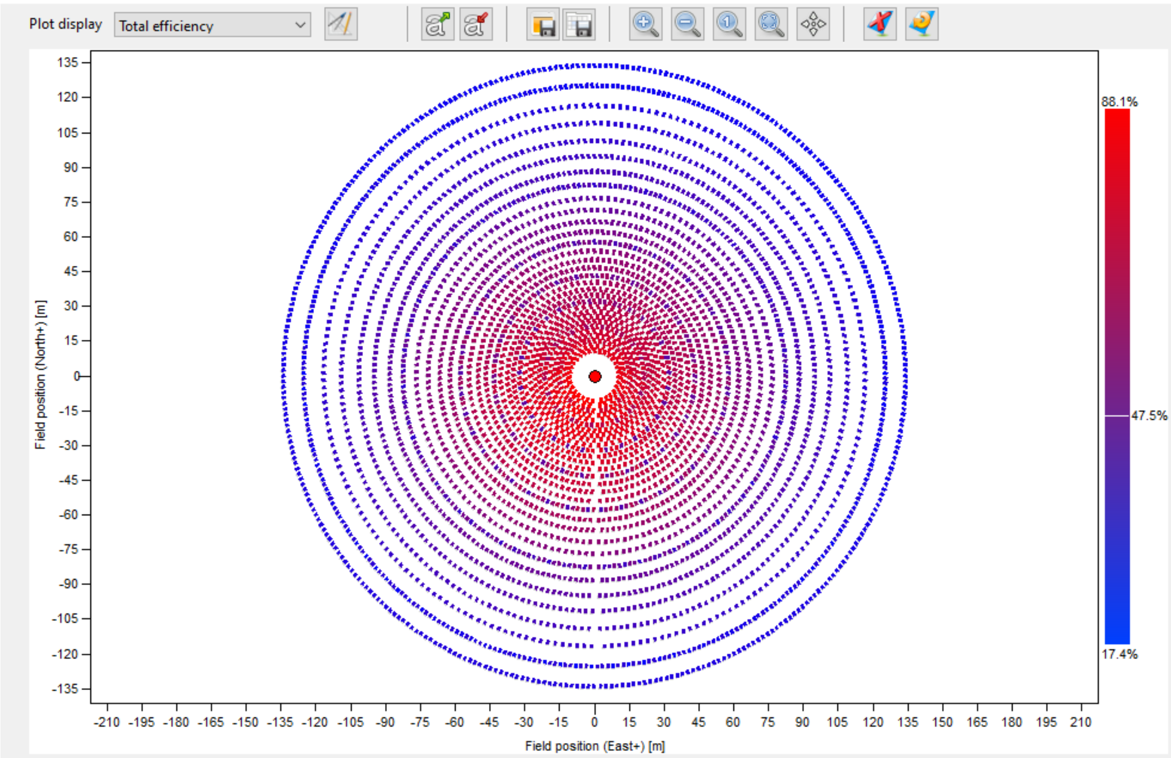

Figure 7.16 Heliostat plot display on the plane distribution

Receiver results display at this software data are simulated.

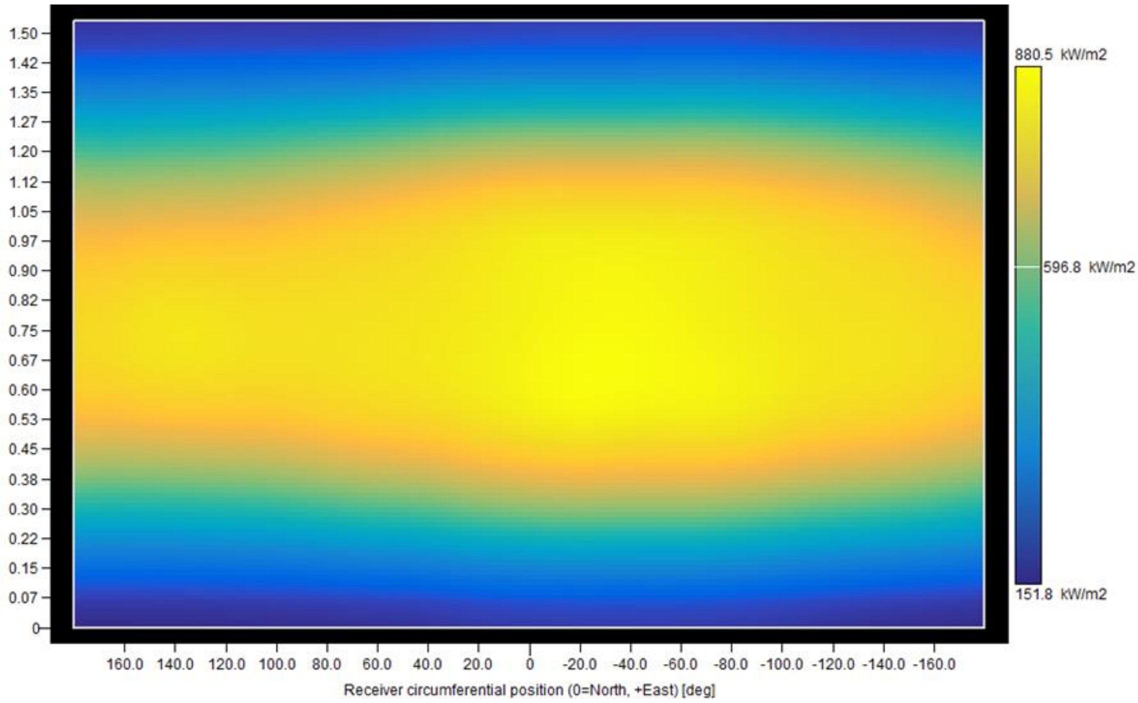

Figure 7.17 Receiver flux profile

CONCLUSION AND RECOMMENDATION

Based on the analytical and simulation results presented, the following conclusions can be drawn:

- Simulation results showed the maximum temperature reached on the surface of the heliostat with the receiver was approximately 472.8 K, indicating localized areas of higher thermal concentration. Temperature distribution measurements on the receiver found the highest temperatures concentrated at the center of the cylindrical part, reaching upwards of 525 K, demonstrating effective solar energy focusing in this region.
- The temperature distributions on the heliostat and receiver show that higher temperatures are achieved near the receiver tower where solar concentration is greatest. This demonstrates the system's ability to effectively focus sunlight and produce high heat levels.
- Analysis of turbulence kinetic energy indicated higher frequency turbulent flow near the center of tracks and receivers, enhancing local heat transfer but requiring structural considerations to prevent erosion at these locations over long term use.
- The average circulation temperature of the receiver was found to hover around 375K over extended operational periods, highlighting relatively stable and consistent thermal management within the system.
- Heating water to its boiling point of approximately 516 °C was achieved, allowing for high-quality steam generation suitable for power production or industrial processes.

RECOMMENDATION

Based on the findings of this study, the following recommendations are provided:

- Additional experimentation and modelling is recommended to test and evaluate new high-temperature heat transfer materials for use in central receivers. Their thermal properties, durability over long-term exposure to concentrated solar radiation, and economic viability should be analysed in detail.
- Developing dynamic algorithms to optimize heliostat positioning and aiming throughout the day based on real-time weather data has potential to improve thermal efficiencies. Simulation studies are suggested to test different field configurations and control approaches.

- Designing and prototype testing thermochemical or phase change storage systems tailored for integration with solar tower plants could help maximize the value of solar power generation. Both techno-economic and performance assessments should be conducted.
- Creating operational models of hybrid solar tower-PV or solar tower-wind plants could provide valuable insight into effective control logics and power scheduling algorithms to maximize renewable penetration on the grid.
- Carrying out detailed modelling of capital and costs under varied incentive structures and market rules through life cycle cost analysis would aid in benchmarking the Levelized cost of electricity outcomes against grid tariffs.
- Pilot-scale installations with integrated monitoring systems are recommended to collect performance data under real weather conditions over several years. This can help validate design improvements and identify reliability issues.

REFERENCES

Abdunnabi, M., Alakder, K., Alkishriwi, N., & Abughres, S. (2014). Experimental validation of forced circulation of solar water heating systems in TRNSYS. *Energy Procedia*, *57*, 2477-2486.

Al-Madani, H. (2006). The performance of a cylindrical solar water heater. *Renewable Energy*, *31*(11), 1751-1763.

Alemu, D. (1998). OPTIMAL DESIGN OF SOLAR WATER HEATING SYSTEMS. *Zede Journal*, *15*, 53-60.

Alexopoulos, S., & Hoffschmidt, B. (2017). Advances in solar tower technology. *Wiley Interdisciplinary Reviews: Energy and Environment*, *6*(1), e217.

Allouhi, A., Amine, M. B., Buker, M., Kousksou, T., & Jamil, A. (2019). Forced-circulation solar water heating system using heat pipe-flat plate collectors: Energy and exergy analysis. *Energy*, *180*, 429-443.

Arekete, A. (2013). Performance of solar water heater in Akure, Nigeria. *Journal of energy technologies and policy*, *3*(6), 1-8.

Arniac, A. (2016). «Because they die in our name»: responsabilité et engagement dans Party Time de Harold Pinter. *Études britanniques contemporaines. Revue de la Société d'études anglaises contemporaines*(50).

Ashour, A. I., Almitani, K. H., & Abu-Hamdeh, N. H. (2021). Developing and improving a prototype scale concentrating solar power tower-system. *Sustainable Energy Technologies and Assessments*, *45*, 101105.

Battleson, K. W. (1981). *Solar power tower design guide: Solar thermal central receiver power systems. A source of electricity and/or process heat*.

Bekele, A., Alemu, D., & Mishra, M. (2013). Large-scale solar water heating systems analysis in Ethiopia: A case study. *International Journal of Sustainable Energy*, *32*(4), 207-228.

Bellos, E., & Tzivanidis, C. (2018). Analytical expression of parabolic trough solar collector performance. *Designs*, *2*(1), 9.

Ben Taher, M., Kousksou, T., Zeraouli, Y., Ahachad, M., & Mahdaoui, M. (2021). Energetic, economic and environmental analysis of domestic solar water heating systems under the African continent. *International Journal of Environmental Science and Technology*, 1-16.

Bertranda, A., Mastruccia, A., Schülerb, N., Aggounec, R., & Maréchalb, F. (2017). Modelling of Domestic Hot Water End-Uses for Integrated Urban Thermal Energy Assessment and Optimisation. *Applied Energy*, *186*, P2.

Betseha, M. (2020). *DESIGN AND MODELLING OF SOLAR TOWER POWER PLANT WITH THERMAL ENERGY STORAGE SYSTEM*

Boretti, A., Nayfeh, J., & Al-Kouz, W. (2020). Validation of SAM modeling of concentrated solar power plants. *Energies*, *13*(8), 1949.

Boukelia, T. E., Mecibah, M.-S., & Meriche, I. E. (2014). General models for estimation of the monthly mean daily diffuse solar radiation (Case study: Algeria). *Energy conversion and management*, *81*, 211-219.

Cengel, Y., & Heat, T. M. (2003). A practical approach. *Heat and Mass Transfer*.

Chine, W., Mellit, A., Pavan, A. M., & Kalogirou, S. A. (2014). Fault detection method for grid-connected photovoltaic plants. *Renewable Energy*, *66*, 99-110.

Dimitrios, P. (2001). *Solar water heating systems study reliability, quantitative survey and life cycle cost method* Thesis (MSc). University of Strathclyde in Glasgow].

Duffie, J. A., & Beckman, W. A. (2013). *Solar engineering of thermal processes*. John Wiley & Sons.
Duffie, J. A., Beckman, W. A., & Blair, N. (2020). *Solar engineering of thermal processes, photovoltaics and wind*. John Wiley & Sons.
Elbeh, M. B., & Sleiti, A. K. (2021). Analysis and optimization of concentrated solar power plant for application in arid climate. *Energy Science & Engineering*, *9*(6), 784-797.
Endale, A. (2019). Analysis of status, potential and economic significance of solar water heating system in Ethiopia. *Renewable Energy*, *132*, 1167-1176.
Falcone, P. K. (1986). *A handbook for solar central receiver design*.
Gong, J., & Sumathy, K. (2016). Active solar water heating systems. In *Advances in Solar Heating and Cooling* (pp. 203-224). Elsevier.
Goswami, D. Y. (2022). *Principles of solar engineering*. CRC Press.
Grigoriev, V., Milidonis, K., Blanco, M., & Constantinou, M. (2021). Method to determine the tracking angles of heliostats. *MethodsX*, *8*, 101244.
H.E. Jacobs 1 , B. E. B., E.J.M. Blokker3. (2018). Household Hot Water Temperature – An Analysis at End-Use Level. *1 st International WDSA / CCWI 2018 Joint Conference, Kingston, Ontario, Canada*, *1 hejacobs@sun.ac.za*.
Hachicha, A. A., Yousef, B. A., Said, Z., & Rodríguez, I. (2019). A review study on the modeling of high-temperature solar thermal collector systems. *Renewable and Sustainable Energy Reviews*, *112*, 280-298.
Hailu, A. D., & Kumsa, D. K. (2021a). Ethiopia renewable energy potentials and current state. *Aims Energy*, *9*(1), 1-14.
Hailu, A. D., & Kumsa, D. K. (2021b). Ethiopia renewable energy potentials and current state. *Aims Energy*, *9*(1).
Hazami, M., Naili, N., Attar, I., & Farhat, A. (2013). Solar water heating systems feasibility for domestic requests in Tunisia: Thermal potential and economic analysis. *Energy conversion and management*, *76*, 599-608.
Homola, C. (2014). Solar domestic hot water heating systems design, installation and maintenance. In: Solar Rating and Certification Corporation.
Homola, C. (2018). Solar domestic hot water heating systems design, installation and maintenance. In.
Hunnewell, T. S., Walton, K. L., Sharma, S., Ghosh, T. K., Tompson, R. V., Viswanath, D. S., & Loyalka, S. K. (2017). Total hemispherical emissivity of SS 316L with simulated very high temperature reactor surface conditions. *Nuclear Technology*, *198*(3), 293-305.
Jamar, A., Majid, Z., Azmi, W., Norhafana, M., & Razak, A. (2016). A review of water heating system for solar energy applications. *International Communications in Heat and Mass Transfer*, *76*, 178-187.
JARED SAMUEL, S., & O THANGGARAJ, J. S. (2012). DESIGN OF CENTRAL SOLAR TOWER RECEIVER.
Kalogirou, S. A. (2012). A detailed thermal model of a parabolic trough collector receiver. *Energy*, *48*(1), 298-306.
Katsanis, J., Halaris, P., Tsarabaris, P., Malahias, G., & Bourkas, P. (2006). Estimation of energy consumption for domestic hot water in hospitals. *Series on Energy and Power Systems*, *2006*, 1-7.
King, J. L., Jo, H., Shahsafi, A., Blomstrand, K., Sridharan, K., & Kats, M. A. (2018). Impact of corrosion on the emissivity of advanced reactor structural alloys. *Journal of Nuclear Materials*, *508*, 465-471.

Lamrani, B., Khouya, A., Zeghmati, B., & Draoui, A. (2018). Mathematical modeling and numerical simulation of a parabolic trough collector: A case study in thermal engineering. *Thermal Science and Engineering Progress*, *8*, 47-54.

Liu, Z., Tao, G., Lu, L., & Wang, Q. (2014). A novel all-glass evacuated tubular solar steam generator with simplified CPC. *Energy conversion and Management*, *86*, 175-185.

Mahboob, K., Aslam, M. M., Qaddus, A., Ahmad, A., Mushtaq, U., & Khan, A. (2018). Design and analysis of tower structure for solar thermal power plant. 2018 2nd international conference on energy conservation and efficiency (ICECE),

Mahboob, K., Mushtaq, U., Khan, A., Awais, Q., Zahid, T., Ahmad, A., Aslam, M., & Qaddus, A. (2021). Design and Modeling of Tubular Receiver of a Solar Tower Power Plant. *Pakistan Journal of Engineering and Technology*, *4*(1), 201-206.

Mahdi, M. S., & Khudheyer, A. F. (2021). Central receivers design in concentrated solar thermal power plants: A review. IOP Conference Series: Materials Science and Engineering,

Masters, J. T. (2011). Tower-Tracking Heliostat Array.

Mongibello, L., Bianco, N., Caliano, M., de Luca, A., & Graditi, G. (2015). Transient analysis of a solar domestic hot water system using two different solvers. *Energy Procedia*, *81*, 89-99.

Murray, D. (2012). Small-scale solar central receiver system design and analysis.

N'Tsoukpoe, K. E., Azoumah, K. Y., Ramde, E., Fiagbe, A. Y., Neveu, P., Py, X., Gaye, M., & Jourdan, A. (2016). Integrated design and construction of a micro-central tower power plant. *Energy for Sustainable Development*, *31*, 1-13.

Naghavi, M., Ong, K., Badruddin, I., Mehrali, M., & Metselaar, H. (2017). Thermal performance of a compact design heat pipe solar collector with latent heat storage in charging/discharging modes. *Energy*, *127*, 101-115.

Ozturk, M., & Dincer, I. (2013). Thermodynamic assessment of an integrated solar power tower and coal gasification system for multi-generation purposes. *Energy conversion and management*, *76*, 1061-1072.

Padilla, R. V., Demirkaya, G., Goswami, D. Y., Stefanakos, E., & Rahman, M. M. (2011). Heat transfer analysis of parabolic trough solar receiver. *Applied Energy*, *88*(12), 5097-5110. https://doi.org/https://doi.org/10.1016/j.apenergy.2011.07.012

Panapakidis, D. (2009). Solar water heating systems study reliability, quantitative survey and life cycle cost method. *Master of Science Thesis, department of mechanical engineering, University of Strathclyde, Glasgow*.

Parab, A., Sakarwala, A., Paste, B., Patil, V., & Mangrulkar, A. (2014). Aerodynamic analysis of a car model using Fluent-Ansys 14.5. *International Journal on Recent Technologies in Mechanical and Electrical Engineering*, *1*(4), 7-13.

Pei, D., Meng, Y., Li, Y., Liu, J., & Lu, Y. (2019). Influence of nano-hydroxyapatite containing desensitizing toothpastes on the sealing ability of dentinal tubules and bonding performance of self-etch adhesives. *Journal of the mechanical behavior of biomedical materials*, *91*, 38-44.

Sadhishkumar, S., & Balusamy, T. (2014). Performance improvement in solar water heating systems—A review. *Renewable and Sustainable Energy Reviews*, *37*, 191-198.

Saleem, M. S., Abas, N., Kalair, A. R., Rauf, S., Haider, A., Tahir, M. S., & Sagir, M. (2020). Design and optimization of hybrid solar-hydrogen generation system using TRNSYS. *International Journal of Hydrogen Energy*, *45*(32), 15814-15830.

Shatnawi, H., Lim, C. W., Ismail, F. B., & Aldossary, A. (2021). An optimisation study of a solar tower receiver: the influence of geometry and material, heat flux, and heat transfer fluid on thermal and mechanical performance. *Heliyon*, *7*(7), e07489.

Srilakshmi, G., Suresh, N., Thirumalai, N., & Ramaswamy, M. (2017). Preliminary design of heliostat field and performance analysis of solar tower plants with thermal storage and hybridisation. *Sustainable Energy Technologies and Assessments*, *19*, 102-113.

Stalin Maria Jebamalai, J. (2016). Receiver Design Methodology for Solar Tower Power Plants. In.

Stine, W. (2001). Power from the Sun, Published online by William B. Stine and Michael Geyer. In.

Tian, Y., & Zhao, C.-Y. (2013). A review of solar collectors and thermal energy storage in solar thermal applications. *Applied energy*, *104*, 538-553.

Tiruye, G. A., Besha, A. T., Mekonnen, Y. S., Benti, N. E., Gebreslase, G. A., & Tufa, R. A. (2021). Opportunities and challenges of renewable energy production in Ethiopia. *Sustainability*, *13*(18), 10381.

Turchi, C. S., Ma, Z., Neises, T. W., & Wagner, M. J. (2013a). Thermodynamic study of advanced supercritical carbon dioxide power cycles for concentrating solar power systems. *Journal of Solar Energy Engineering*, *135*(4), 041007.

Turchi, C. S., Ma, Z., Neises, T. W., & Wagner, M. J. (2013b). Thermodynamic study of advanced supercritical carbon dioxide power cycles for concentrating solar power systems. *Journal of Solar Energy Engineering*, *135*(4).

Tzivanidis, C., Bellos, E., & Antonopoulos, K. A. (2016). Energetic and financial investigation of a stand-alone solar-thermal Organic Rankine Cycle power plant. *Energy conversion and management*, *126*, 421-433.

Wagner, M. J. (2008). Simulation and predictive performance modeling of utility-scale central receiver system power plants.

Wagner, M. J., Klein, S. A., & Reindl, D. T. (2009). Simulation of utility-scale central receiver system power plants. Energy Sustainability,

Wah, L. L., Swe, W., & Lwin, T. T. (2019). Analysis of Optical Efficiency in Heliostat Field Layout with Various Separation Distance.

Xue, Y., Diallo, I., Boone, A. A., Yao, T., Zhang, Y., Zeng, X., Neelin, J. D., Lau, W. K., Pan, Y., & Liu, Y. (2022). Spring Land Temperature in Tibetan Plateau and Global-Scale Summer Precipitation: Initialization and Improved Prediction. *Bulletin of the American Meteorological Society*, *103*(12), E2756-E2767.

Yang, B., Liu, J., Hao, M., & Gao, L. (2018). Study on performance of solar water heating system using TRNSYS software. *Chemical engineering transactions*, *70*, 2071-2076.

Yılmaz, İ. H., & Mwesigye, A. (2018). Modeling, simulation and performance analysis of parabolic trough solar collectors: A comprehensive review. *Applied Energy*, *225*, 135-174.

Zeghib, I., & Chaker, A. (2011). Simulation of a solar domestic water heating system. *Energy Procedia*, *6*, 292-301.

Zhang, L., Fang, J., Wei, J., & Yang, G. (2017). Numerical investigation on the thermal performance of molten salt cavity receivers with different structures. *Applied Energy*, *204*, 966-978.

Zhou, Y., & Zhao, Y. (2014). Heliostat field layout design for solar tower power plant based on GPU. *IFAC Proceedings Volumes*, *47*(3), 4953-4958.